# IDENTIFICATION OF MALARIA PARASITE-INFECTED RED BLOOD CELL APTAMERS BY INERTIAL MICROFLUIDICS SELEX

by

Christina M. Birch

B.S. Biochemistry & Molecular Biophysics and Mathematics (2008)
University of Arizona, Tucson, AZ

Submitted to the Department of Biological Engineering
in Partial Fulfillment of the Requirements for the Degree of

Doctor of Philosophy in Biological Engineering

at the

MASSACHUSETTS INSTITUTE OF TECHNOLOGY

June 2015



Author

.....

Christina M. Birch
Department of Biological Engineering, MIT

Certified by

.....

Jacquin C. Niles
Associate Professor, Department of Biological Engineering, MIT
Thesis Advisor

Approved by

.....

Forest M. White
Professor, Department of Biological Engineering, MIT
Course XX Graduate Program Committee

This doctoral thesis has been examined by a committee of the Department of Biological Engineering as follows:

Certified by

.....

Alan P. Jasanoff
Associate Professor, Department of Biological Engineering, MIT
Thesis Committee Chair

Certified by

.....

Barbara Imperiali
Class of 1922 Professor of Biology & Professor of Chemistry,
Department of Biology and Department of Chemistry, MIT
Thesis Committee Member

Certified by

.....

Jacquin C. Niles
Associate Professor, Department of Biological Engineering, MIT
Thesis Advisor

**IDENTIFICATION OF MALARIA PARASITE-INFECTED RED BLOOD CELL APTAMERS BY INERTIAL MICROFLUIDICS SELEX**

**by**

**Christina M. Birch**

Submitted to the Department of Biological Engineering on April 27, 2015 in Partial Fulfillment of the Requirements for the Degree of Doctor of Philosophy in Biological Engineering

## ABSTRACT

Malaria kills over 500,000 people annually, the majority of whom are children under five years old in sub-Saharan Africa. This disease is caused by several parasite species, of which *Plasmodium falciparum* is associated with the highest mortality. The clinical manifestations of malaria are associated with the phase of infection where parasites develop within red blood cells (RBCs). Infected RBCs can adhere to the host microvasculature, triggering inflammatory responses in affected organs that contribute to the pathophysiology of life threatening cerebral malaria and pregnancy-associated malaria. The expression of specific *Plasmodium falciparum* Erythrocyte Membrane Protein 1 (PfEMP1) variants on the RBC surface is associated with severe disease, such as VAR2CSA-mediated placental sequestration during pregnancy-associated malaria. While parasite proteins expressed on the surface of infected RBCs are linked to disease pathogenesis, this surface proteome is poorly characterized. Identifying parasite-derived antigens on the infected RBC surface could facilitate diagnosis, monitoring, and prevention of sequestration.

To interrogate the infected RBC surface proteome, we require a panel of affinity reagents that robustly distinguish the parasite-derived proteins from the elaborate RBC surface milieu. Nucleic acid aptamers are widely used in biological applications for their high specificity and affinity to targets and are highly suitable for malaria applications. Efficiently generating aptamers against complex targets–such as whole cells–remains a challenge. Here we develop a novel strategy (I-SELEX) that utilizes inertial focusing in spiral microfluidic channels to stringently partition cells from unbound oligonucleotides. We use I-SELEX to efficiently discover high affinity aptamers that selectively recognize distinct epitopes present on target cells. Using first an engineered RBC model displaying a non-native antigen and, second, live malaria parasite-infected RBCs as targets, we establish suitability of this strategy for *de novo* aptamer selections. We demonstrate recovery of a diverse set of aptamers that recognize distinct epitopes on parasite-infected RBCs with nanomolar affinity, including an aptamer against the protein responsible for placental sequestration, VAR2CSA. These findings validate I-SELEX as a broadly applicable aptamer discovery platform that enables identification of new reagents for mapping the parasite-infected RBC surface proteome at higher molecular resolution to potentially contribute to malaria diagnostics, therapeutics and vaccine efforts.

Advisor: Jacquin C. Niles
Title: Associate Professor of Biological Engineering

## ACKNOWLEDGEMENTS

I am incredibly grateful to each of the organizations and individuals that enabled me to pursue this challenging project culminating in my Ph.D. First and foremost, I am honored to have been offered the opportunity to conduct independent and original research at the Massachusetts Institute of Technology, where truly I have stood on the shoulders of giants to further both knowledge in the field of Biological Engineering and my own education and training as a scientist and engineer.

Specifically, the Department of Biological Engineering, under the incredible leadership of Prof. Doug Lauffenburger, has been a supportive, energetic community in which to perform research and to be continuously challenged to grow intellectually. The training I received within the BE program is second to none, and I am a firm believer in the power of approaching biological questions with an engineer's perspective.

I am grateful to Prof. Bob Sauer (Department of Biology, MIT) for a conversation he probably does not remember during my first year of graduate school when I was seeking advice on which lab to join. His question to me was simple: "Are you a risk taker?"

Eager to be at the forefront of biological engineering technologies and discoveries, I decided that I was. I joined the one-year-old Niles Lab and took on a solo project that had yet to be born, thus embarking on one of the most challenging and rewarding endeavors of my life. This milestone would not have been possible without the support of my advisor, Prof. Jacquin Niles, who also took a risk by accepting me, someone who had done significantly more computational modeling than pipetting prior to joining his lab. Prof. Niles has instilled in me a commitment to be unwaveringly rigorous in my experiments and critical thinking.

I have also had incredible support from other great minds at MIT, including Prof. Alan Jasanoff (Department of Biological Engineering), my committee chair, and Prof. Barbara Imperiali (Departments of Biology and Chemistry). Barbara was an incredible role model for me, beginning my scientific training as part of the inaugural Chemistry-Biology Interface Training Program. I am also grateful to Prof. Forest White (Department of Biological Engineering) for his light-hearted and motivational chats, and Aran Parillo for his support and encouragement (and technical/IT skills).

I am honored to have had the support of the National Science Foundation through the Graduate Research Fellowship Program, which provided significant funding for my Ph.D. research. I'm happy and somewhat surprised to report that I indeed completed what I originally proposed to do (with some minor tweaks, of course).

A large part of my growth as a scientist is a direct result of the "older" members of the Niles Lab: Stephen Goldfless, Brian Belmont, and Jeff Wagner. Brian, in particular, worked with me during my brief rotation in the lab and helped me hit the ground running when I began my own experiments. I am forever grateful for his warm personality and Socratic mentoring style. I'm not sure whether to thank or to blame Steve, who taught me how to culture the malaria parasite, which as a result meant I was in the lab most weekends to feed the little buggers. This drudgery would have been less tolerable if it wasn't for the sometimes predictable but always appropriate humor that Jeff brought to the lab. I respect these three immensely, not only for their incredible scientific talent and their invaluable mentoring, but also because they are wonderful human beings.

I am so happy that my classmates Jim Abshire and Bridget Wall also joined the Niles Lab. I owe Jim so much gratitude for sharing the ups and downs that the paths of our research took, and always believing in my project even when yet another assay development step failed to prove fruitful. I also cannot express my thanks enough to Erika Bechtold, who was such an important mentor to me, who had unwavering confidence in my scientific abilities and potential. I have also immensely enjoyed sharing my time in lab with Karen Wong, Daiying Xu, Aleja Falla, Sebastian Nasamu, Sumanta Dey, and Suresh Ganesan. I also thank our administrative assistant Denise MacPhail for her dedication to keeping the lab running smoothly for us all.

My path through graduate school would not have been the same without sharing the ride with my BE classmates of 2008: Brandon Russell, David Hagan, Tim Curran, Chris Ng, Miles Miller, Pete DeMuth, Tiffany Chen, Yvonne Yamanaka, Xiaosai Yao, Amneet Gulati, Nathan Klapoetke, Yang Li, Nicole Casasnovas, and, a particular inspiration, LTC F. John Burpo. I fondly remember our camaraderie during the late night implementation sessions in the Dungeon.

One of the most rewarding experiences I had as a graduate student was working with Jaime Goldstein and the other BE Communication Lab Fellows to get the new coaching program off the ground. Jaime has been an incredible mentor to me and is an inspiration in how she is unafraid of innovation and iteration and her dedication to build something that works. As a BE Communication Fellow I was able to work closely with other students and postdocs in the department, coaching them on best practices for communicating (writing, speaking, presenting) technical scientific material. Mentoring students one-on-one has been one of my favorite activities in grad school and I'm so grateful for the opportunity.

I am indebted to all the great educators I have had throughout my life who have set me on the path of lifelong learning. I believe it is incredibly important to explicitly recognize the impact of the following educators: Mrs. Dorothy, Mrs. Nilo, Mrs. Paula, Mrs. Theresa, and Mrs. Irma for teaching me to love learning at the Tempe Montessori School (Tempe, AZ); Mrs. Chilton at Burk Elementary School (Gilbert, AZ); Mrs. Jennifer Sifuentes for making AP Biology so much fun we came in on the weekends to study, Mr. Brendan Keyes for using AP Government and AP European History as an excuse to teach us about being critical thinking, independent, confident adults (and how to survive a zombie apocalypse), and Coach Jeff Corn, my varsity cross-country coach, for teaching me how to challenge myself compassionately at Gilbert High School (Gilbert, AZ).

I am proud to have been educated and mentored at the University of Arizona (Tucson, AZ) by some incredible scientists. Profs. Thomas Baldwin and Miriam Ziegler (now at UC Riverside) were compassionate and invaluable guides during my later years at the U of A, and are the reasons I fell in love with biochemistry. Prof. Baldwin always had an open door and would listen patiently as I outlined all the things I wanted to study and passions I wanted to pursue, knowing full well I'd have to make some tough choices to narrow down that list. I owe my undergraduate mentor, Prof. Anderw Hausrath, immense thanks for always treating me like a colleague and not just a naive undergrad, and being unafraid of sharing with me his scientific creativity and humor (including a one-of-a-kind journal article on why Leucine is the best amino acid). To him, I owe my convictions that science should be fun. I received incredible laboratory training by James

Hazzard, whose instruction of experimental biochemistry (with minimal resources) was a superb foundation on which to build my Ph.D. research. I am grateful to the Department of Mathematics for encouraging and supporting my continued pursuit of mathematics, in particular my Theory of Probability instructor, Prof. Thomas Kennedy, and my Theory of Statistics instructor, Prof. Joseph Watkins. I also want to thank Prof. Oliver Monti for hands-down the most thrilling class I have ever had (second semester Physical Chemistry, which seemed more like an intro quantum mechanics class). If I had taken his course any sooner than my final semester of undergrad, I likely would have become a particle physicist. It is his passion for science and teaching I hope to emulate in my own future classes.

I wish to thank my many close friends and supporters who have shared my graduate school adventures with me. MIT Cycling members past and present, Carston Kroll, Mike Busa, John DeTore, John Laupheimer, Jennifer Ellwood, Geoff Williams, Virginia White, Erin Faccone, and Erin Blass are but a few. I particularly want to thank Kate Wymbs, for sharing her unfiltered enthusiasm for life with me, and my best friend at MIT, Zach LaBry, for always being the cheerleader when I needed it most.

Finally, I want to thank my family for helping me every step of the way: my father, Bill Birch, for teaching me to make learning and challenges fun; my sister, Becky, who I think is the most talented, compassionate, hilarious person in the world; Andrew Lysaght for his unmatched love and support during this part of my life; my aunts Lisbeth, Nancy, Candace, and Laurie; my grandma Jeanne Chapin; and my late grandparents, Don Chapin, for showing me you can excel at all your passions, Margaret Birch for sharing with me her love of reading, and Oliver Kenneth Birch, whose advice to me when things got tough was to always “Give ‘em hell, kid.” I hope I have.

I want to dedicate this work to the memory of my mother, Joanne Lynn Birch. An educator herself, she was always the biggest advocate for my education and ensured that I had whatever resources and support I needed to succeed. While she did not get to see me complete my Ph.D., she never doubted that I would and I know she would be proud.

Christina Birch
April 20, 1015
Cambridge, MA

## ATTRIBUTIONS

One of the most rewarding and powerful aspects of research is being able to collaborate with other scientists across multiple disciplines. This work represents the achievements of such a partnership. The microfluidics work (Chapter 2) was performed in collaboration with Han Wei Hou, Ph.D., (BioSystems and Micromechanics IRG, Singapore-MIT Alliance for Research and Technology Centre) and Professor Jongyoon Han (Departments of Biological Engineering and Electrical Engineering and Computer Science, MIT).

Furthermore, this research was possible because of the many resources available both at MIT and from colleagues in the field. Quantitative PCR was performed at the MIT BioMicroCenter supported by NIEHS Center Grant P30-ES002109. We thank Joseph Donnenhoffer (Roche Diagnostics) for his consultation on qPCR, and Dr. Ali Asgar S. Bhagat for helpful discussions during the early phase of this work. Confocal microscopy images were obtained at the W.M. Keck Biological Imaging Facility in Whitehead Institute, and the authors thank Dr. Hiongyap Gan for assistance. The following reagent was obtained through the MR4 as part of the BEI Resources Repository, NIAID, NIH: *Plasmodium falciparum* CS2, MRA-96, deposited by SJ Rogerson. The DC-J parasite line was a kind gift from Ron Dzikowski and Kirk Deitsch. This work was carried out, in part, through the use of MIT's Microsystems Technology Laboratories.

## TABLE OF CONTENTS

# CHAPTER 1: INTRODUCTION

## 1.1 Malaria is a major global burden

Malaria is one of the world's most common infectious diseases endemic to poor tropical and sub-tropical areas. Approximately half of the global population is at risk for contracting malaria. Over 200 million new infections are estimated to occur each year, more than 600,000 of which are fatal, with most deaths occurring in young children in sub-Saharan Africa [1]. Malaria is caused by the apicomplexan parasite *Plasmodium* and is transmitted to the human host by *Anopheles* mosquito vectors. Of the five *Plasmodium* species that are able to infect humans (*P. falciparum, P. vivax, P. ovale, P. malariae,* and *P. knowlesi*), *P. falciparum* is responsible for most of the morbidity and mortality of the disease. The economic burden of malaria is massive: the costs of direct disease prevention, diagnosis and treatment, plus macroeconomic repercussions on trade and tourism, as well as social and human capital consequences, reach well into the billions of dollars per year [2]. Global malaria control and eradication will require a long-term commitment to research and development, an estimated $5.1 billion, and a multipronged attack on disease prevention, control, and treatment[1], which necessitates an increased understanding of the parasite, disease, and transmission.

## 1.2 The malaria parasite life cycle

The malaria parasite has a complex life cycle that requires two organisms: the *Anopheles* mosquito vector, where parasite sexual reproduction occurs, and the human host where asexual replication occurs *(Figure 1).* When an infected mosquito bites a

human host, malaria sporozoites carried in the mosquito saliva are released into the bloodstream and travel to the liver.

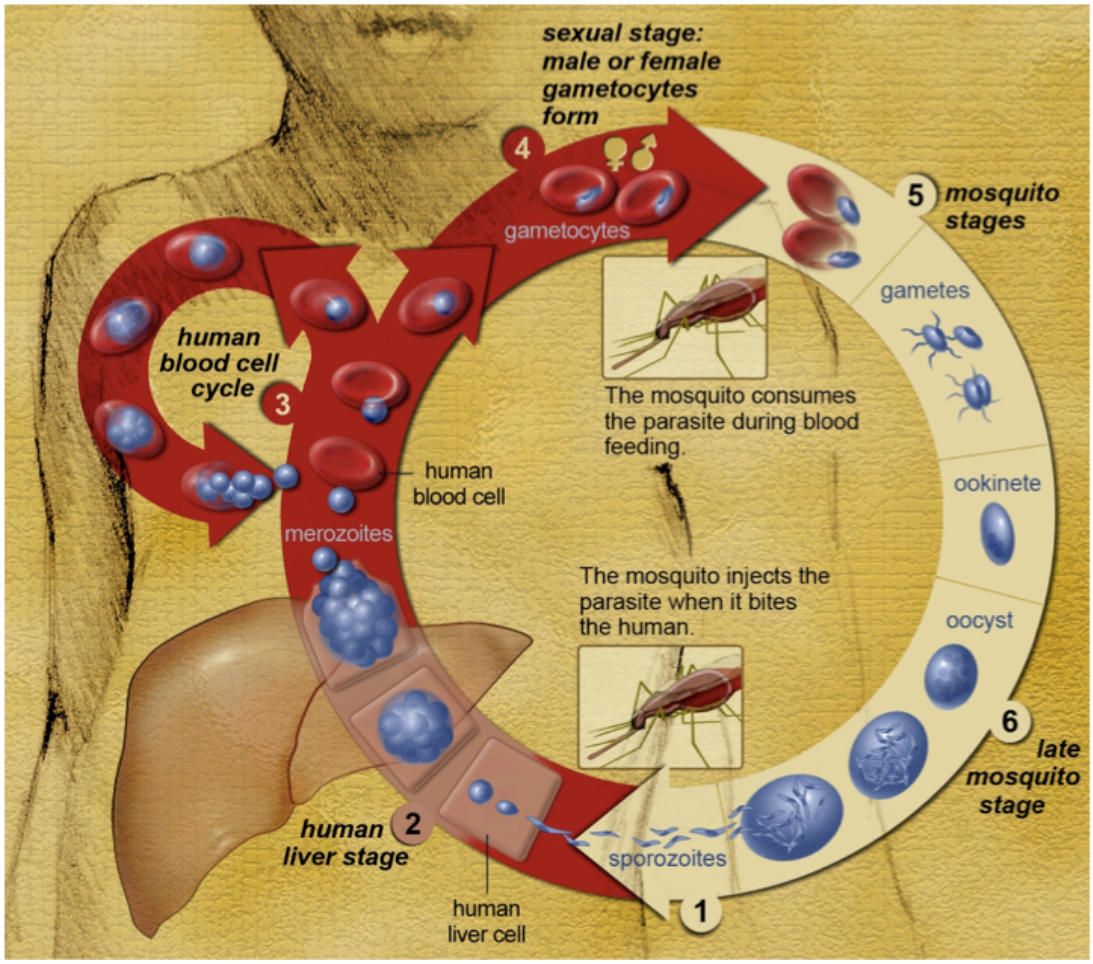


*Figure 1. The life cycle of the human malaria parasite,* Plasmodium falciparum. The transmission cycle begins when an infected female mosquito releases malaria sporozoites into the bloodstream during a blood meal (1). The sporozoites travel to the liver where they invade hepatocytes and develop over a period of ~2 weeks (2) into merozoites that are released into circulation. These merozoites invade host red blood cells to begin the asexual intraerythrocytic development cycle (3), the phase associated with clinical manifestations of the disease. Occasionally, intra-erythrocytic parasites will differentiate into male or female gametocytes (4), which can be taken up by mosquitoes during a blood meal. These undergo fertilization in the mosquito's midgut (5). Further differentiation ultimately produces sporozoites (6) present in the mosquito's salivary gland are ready to complete the transmission cycle when then mosquito bites the next human host. Figure by National Institute of Allergy and Infectious Diseases (2007)[3].

There, they invade and mature within hepatocytes for approximately two weeks, before releasing merozoites that can invade red blood cells (RBCs). Once inside the RBC, the parasite begins its 48-hour asexual replication phase (the intraerythrocitic development cycle, IDC) maturing from early ring stage parasites to trophozoites and schizonts with high metabolic activity. A single schizont parasite may release 16-32 merozoites that are capable of invading fresh erythrocytes. In response to some as-yet unknown stimuli, blood stage parasites will differentiate into male and female gametocytes. These forms, when taken up by the female mosquito during a blood meal, will travel to the mosquito midgut where parasite sexual development occurs. Oocysts develop within the mosquito's midgut before the parasites are released and to the salivary glands as sporozoites, capable of infecting a new human host, thus completing the transmission cycle.[4]

### 1.3 Disease prevention and vaccine efforts

Insecticide-treated bednets and long-lasting insecticidal nets are incredibly effective at reducing mortality rates in endemic areas, but are insufficient as a sole effort to interrupt malaria transmission. Therefore, the development of a multi-faceted approach to malaria eradication is essential and will need to include vector control and transmission interruption (bednets) as well as disease treatment (anti-malarial drugs) and prevention (vaccines).[5] Unfortunately, the list of effective anti-malarias is quite short (with the standard treatment being artemisinin-based combination therapies) and drug resistance is rapidly evolving in endemic areas.[6] There is currently no approved malaria vaccine, although the most advanced vaccine in development, the RTS,S candidate

vaccine against the pre-erythrocytic parasite, provides moderate protection against the disease.[7] In Phase II clinical trials, ~30-50% of malaria-naïve adults immunized with RTS,S were protected when challenged with malaria infection.[8,9]However, the mechanism of how the vaccine confers protection is poorly understood.[10] Relatively few antigens from blood-stage forms of the parasite are in clinical development for vaccines, the most advanced blood-stage candidates being apical membrane protein 1 (AMA1) and merozoite surface protein 2 (MSP2).[7] The extensive genetic diversity of parasitic proteins, for example AMA1, presents a major hurtle for blood-stage vaccine development, as antibodies against certain haplotypes may not be effective against other haplotypes.[11] Unfortunately, recent Phase II clinical trials did not demonstrate any protection for patients immunized with either AMA1 or MSP2 vaccines.[12,13] Additionally, vaccine efforts that aim to block transmission of the disease by infecting humans with irradiated or genetically attenuated sporozoites has been challenging, as the vaccine protected only a small number of individuals.[14] Ideally, vaccines that block multiple stages of the parasite lifecycle simultaneously, for example by using blood-stage and sporozoite targeting vaccines or by targeting multiple extracellularly exposed blood-stage proteins, could be combined to give broader coverage of polymorphic epitopes and improve the total protection conferred to patients. Vaccine development against has been hindered by incomplete knowledge of how the intraerythrocytic forms interact with the host, and especially how the highly polymorphic parasite proteins on the infected RBC contribute to disease. [15] Therefore, a more complete understanding of the blood-stage surface proteins would be helpful in guiding vaccine development efforts.

## 1.4 Malaria pathophysiology

Patients are initially asymptomatic after being bitten by an infected mosquito while the parasites incubate within the liver. However, once the parasite begins its intraerythrocytic development cycle, patients will manifest with flu-like symptoms, a 48-hour fever cycle, and splenomegaly.[16] During its development within the erythrocyte, the parasite must direct the remodeling of the infected red blood cell (iRBC) in order to survive within the human host.[17,18] As the RBC lacks the endogenous cellular machinery necessary to contribute to protein trafficking, the parasite must coordinate the expression and transport of proteins and other cellular materials to the iRBC plasma membrane that are essential for parasite survival. These cellular modifications enable parasite and host interactions that ultimately contribute to the clinical manifestations of the disease.[19]

*P. falciparum* iRBCs are able to adhere to other cells through specific parasite ligand and host-cell receptor interactions that lead to parasite sequestration.[20] Binding to cells of the microvasculature allows the mature parasite to sequester in the deep vascular beds of multiple organs and tissues (such as the brain, lungs, kidney, liver, placenta, and subcutaneous tissue) thereby avoiding clearance by the spleen.[21] As a result, only early-stage (ring) iRBCs are observed circulating in the blood stream. Sequestration and associated local and systemic cytokine release contribute to severe malaria phenotypes.[22-24] Severe malaria patients present with hyperparasitemia and serious systemic complications such as severe anemia, thrombocytopenia (decrease in blood platelets), shock, and organ failure.[25] Major complications such as cerebral malaria (CM) and pregnancy-associated malaria (PAM)[26] often arise during *P. falciparum* infection, causing tremendous health problems for two of the most at-risk populations. The majority

of CM cases and subsequent fatalities are among children less than 10 years old[27], and PAM causes maternal anemia, low infant birth weight, and higher mortality for both.[28]

### *1.4.1 Parasite proteins that contribute to sequestration and severe disease*

Parasite proteins exported to the iRBC membrane are exposed to the extracellular environment and interact with surface receptors of the endothelial cells of deep tissue microvasculature.[29] Similar to leukocyte adhesion, iRBCs roll along the vascular epithelium making nonspecific interactions that help to slow down the iRBC and orient parasite ligands for binding to specific host-cell receptors.[29,30] One well-studied group of parasite ligands involved in host-cell binding is the *Plasmodium falciparum* Erythrocyte Membrane Protein 1 (PfEMP1) adhesion proteins family.

The PfEMP1 family of variant surface proteins is at least partially responsible for iRBC adhesion to a number of different host cells. PfEMP1 proteins are encoded by ~60 *var* genes and are exported to "knob" structures on the surface of the iRBC. Only one PfEMP1 variant is expressed at a time on the surface of the iRBC during an intraerythrocytic development cycle, and can be detected starting 16 hours post-RBC invasion.[21] While PfEMP1 expression is homogeneous on a single iRBC, the expression across a population is quite heterogeneous and may affect tissue distribution and pathogenesis.[31] PfEMP1 variants have specific host-cell receptors that determine to which cell types they may bind and with what affinity, such as CD36 and ICAM-1 in CM,[32] or chondroitin sulfate (CSA) in PAM.[33]

While all mature *P. falciparum* iRBCs can sequester, not all infections lead to severe disease.[34] To what extent each PfEMP1 variant and its contribution to the iRBC

population sequestration affects the development of severe malaria complications has yet to be determined and could greatly influence drug design and vaccine development efforts.

### *1.4.2 Cerebral malaria*

CM is a potentially fatal malaria complication that severely impairs neurological function to the point of causing a coma, most frequently in children.[35] As iRBCs sequester in the microvasculature of the brain, they block RBC passage and disrupt gas exchange, causing localized acidosis, hemorrhaging, and inflammation which impair patient behavior as a result of increasing neurological damage, often culminating in seizure, coma, and death. [31,36-39] In CM, iRBCs bind ICAM-1 and CD36 scavenger receptors present on the surface of endothelial cells lining the microvasculature. CM is a particularly devastating disease complication as it is responsible for most malaria deaths worldwide, most often in young children during their first exposure to *P. falciparum.*[34] Patients who develop CM have mortality rates of 15-20%. Survivors are often are left with varying degrees of irreversible neurological impairment.[40]

Standard of care for CM patients does not differ significantly from uncomplicated malaria treatment: antimalarial drugs (arteminisin, quinine, and their derivatives) are administered parenterally to control overall parasite load and supportive care is given.[41] Adjunctive therapies for CM or severe malaria have been targeted at reducing secondary effects of parasite sequestration but most have had inconclusive, contradictory, and sometimes adverse results. Past clinical trials have attempted to reduce systemic inflammation and intracranial pressure (using steroids such as dexamethasone[42]), lower

proinflammatory cytokine levels (using anti-TNF-α antibodies[30]), reduce iron burden (using chelation agents such as desferrioxamine[37] or deferipone[43]), reduce oxidative stress (administration of *N*-acetylcysteine[44]), or expand plasma volume to improve microcirculation (using albumin[9]). Of all adjunctive therapies studied, only albumin was associated with reduced mortality (3.6% versus 18% in patients who received saline). However, larger-scale efficacy trials are still underway.[45]

Despite efforts to improve the effectiveness of antimalarial and adjunctive treatments for CM patients, there has not been a significant reduction in mortality, in part because the biochemical mechanisms leading to neurological dysfunction are poorly understood.[1] Determining the extent of how PfEMP1-mediated cytoadhesion to brain endothelial cells contributes to severe disease outcome should inform new mechanism-based approaches for patient treatments.

### *1.4.3 Pregnancy-associated malaria*

PAM risk decreases with parity and first time mothers are especially susceptible to massive iRBC sequestration in the placenta.[38] Placental sequestration restricts nutrient flow to the developing fetus and removes a large percentage of circulating RBCs from the blood, resulting[31] in anemia. Sequestration in the placenta vasculature occurs when the PfEMP1 variant VAR2CSA binds the glycosaminoglycan CSA present on syncytiotrophoblasts.[31] PAM is more likely to occur during the first few pregnancies and women often achieve immunity with increasing parity. Antibodies from malaria-exposed multigravid women have been shown to disrupt *P. falciparum* binding to CSA and interfere with cytoadhesion *in vitro,*[26] supporting the hypothesis that physical

sequestration is essential for PAM development. As women in endemic areas can acquire protection against PAM by generating a panel of VAR2CSA-blocking antibodies from multiple exposures to VAR2CSA-expressing parasites, this suggests potential for a therapeutic intervention for placental sequestration if we can effectively target VAR2CSA-expressing iRBCs.

### 1.5 Studying and targeted disruption of sequestration

Novel treatments that target iRBC cytoadhesion are needed to improve standard of care and prognosis of severe malaria patients. No approved therapies exist to target the underlying mechanisms of iRBC sequestration, in part because they remain so poorly understood. The major drawback that all clinical trials face for anti-sequestration vaccines or adjunctive therapies is the lack of technologies that allow quantitatively correlating sequestration burden and clinical outcome. Classically, analysis of sequestered parasites from CM patients has only been available from autopsies[46]; sequestration burden cannot be monitored as a function of drug treatment protocol.

Current methods to study iRBC sequestration and severe malaria pathogenesis are desperately lacking. Neuroimaging of CM patients with either computed tomography[25**Error! Bookmark not defined.**] (CT) or magnetic resonance imaging[39,47,48] (MRI) has only been able to capture images of CM complications: brain swelling, cortical infarcts, and hyperintense or lesion areas in white matter. While visualization of these symptoms may provide important information regarding patient prognosis, they are not diagnostic of CM itself, nor do they provide readouts of the actual sequestration mechanisms that may underlie CM pathogenesis. Early mouse model studies have attempted to monitor iRBC

sequestration in a more targeted manner. Von zur Muhlen and colleagues conjugated an antibody fragment against activated platelet proteins to microparticles of iron oxide (MPIOs) and were able to resolve platelet aggregation within brains of mice infected with the murine parasite *Plasmodium berghei.*[48] However, platelet activation and aggregation are involved in multiple other disease states, such as stroke, thrombosis, and cardiovascular disease and are not specific to malaria sequestration.[49]

In order to avoid such indirect monitoring methods of severe malaria progression, we first need to be able to specifically monitor iRBC sequestration *in vivo* in real time in an noninvasive manner. Such imaging studies would require a bioprobe against late-stage iRBCs that would enable specific targeting of contrast-enhancing agents to areas of sequestration. This tool would allow clinicians to ask important questions about sequestration and severe disease pathophysiology over the course of infection, or in response to different treatment protocols.

### 1.6 Conclusion

To understand the mechanisms of parasite sequestration and disease progression, one would like to monitor the distribution of iRBC load across multiple organ systems prior to patient death and in response to treatment protocols, ultimately to establish an improved standard of care for severe malaria patients. Furthermore, while parasite-induced changes in the variety of ligands displayed on the surface of infected RBCs are recognized as an important mechanism mediating severe malaria, our knowledge of their expression, localization, and function is incomplete. A detailed characterization has been impeded by limitations in the technologies available for identifying, targeting, and

interrogating the infected RBC surface proteome. If we can better identify and characterize these parasite proteins (and their binding partners), we will be able to better understand and potentially modulate severe malaria.

### 1.7 Preview of thesis research

We propose to develop affinity probes against iRBCs using RNA aptamers in order to enable monitoring and manipulating mechanisms of iRBC sequestration and its contribution to severe malaria progression. First, we address a current limitation in aptamer selection technologies available for targeting of whole cells like iRBCs using inertial microfluidics in a selection method we call I-SELEX. Second, we conduct a proof of concept I-SELEX experiment using an engineered model cell system that mimics the challenges of the malaria iRBC target. Finally, we apply I-SELEX to live iRBCs and recover a panel of iRBC-binding aptamers that recognize a variety of surface targets. Further development of these iRBC aptamer probes has the potential to enable surface characterization studies, parasite strain typing, and *in vivo* tracking or modulation of cytoadhesion in the disease process. Such advanced studies of severe malaria pathogenesis, with particular emphasis on the mechanisms of sequestration, will facilitate development of novel adjunctive interventions for severe malaria and augment our understanding of the disease.

# CHAPTER 2: CREATION AND CHARACTERIZATION OF AN EFFICIENT APTAMER SELECTION STRATEGY USING INERTIAL MICROFLUIDICS (I-SELEX)

## 2.1 Introduction

### *2.1.1 Aptamer bioprobes and SELEX technology*

Aptamers are small oligonucleotides, usually <100 bases in length, whose sequence-dependent tertiary structures enable them to bind with high specificity and affinity to a variety of targets. Target binding aptamers are enriched from a highly diverse library of diverse ~$10^{14}$-$10^{15}$ unique sequences through iterative cycles of a selection process called Systematic Evolution of Ligands by Exponential Enrichment (SELEX).[50,51]

While aptamers are most analogous to antibodies, they have several distinct advantages that make them more appealing for downstream malaria applications. While antibody production requires biological systems to produce, aptamers are produced chemically in a manner that is easy to scale up. Unlike antibodies, aptamers can be reversibly denatured and have long shelf lives, especially when chemically modified to protect from nuclease degradation. Additionally, aptamers thus far reported are non-immunogenic, an important consideration when developing possible adjunctive therapies.[52]

Many aptamers also inhibit the function of the target they bind. Currently, there is an FDA approved aptamer treatment for wet macular degeneration that utilizes the inhibitory function of an anti-VEGF aptamer.[53]

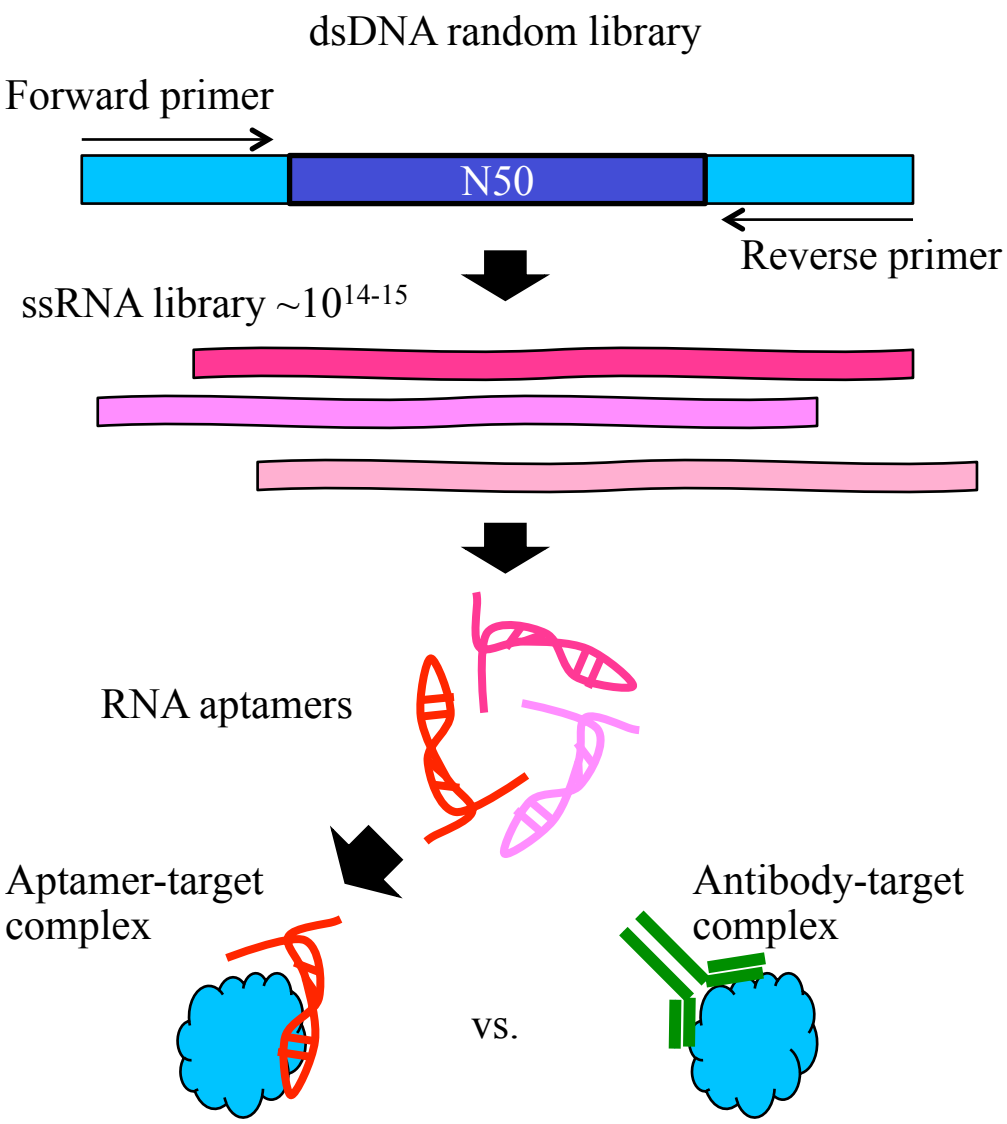


*Figure 2. A random library for RNA aptamer discovery.* A double stranded DNA (dsDNA) library is commercially synthesized with two constant primer binding regions flanking a central 50-base random region. The dsDNA template is transcribed into a single-stranded RNA (ssRNA) library with ~$10^{14\text{-}15}$ unique species. Each sequence (deemed "aptamers") folds into a unique tertiary structure that may bind to a specific target with affinity and specificity similar to an antibody.

Aptamers (*Figure 2*) are generated through an iterative selection process called SELEX, independently developed in the 1990s by two groups.[50,51] In a typical SELEX experiment (*Figure 3*), a random ssDNA or ssRNA library, 20-100 nucleotides in length, is synthesized, with 5' and 3' constant primer binding regions flanking a central random region. Usually, an aptamer selection begins with synthesis of a dsDNA library containing $10^{14}$-$10^{15}$ sequences; the size of the random region determines the diversity and coverage of the sequence space. In the case of RNA aptamer selections, the dsDNA is first *in vitro* transcribed into the RNA aptamer library. For downstream applications where aptamer stability in complex biological fluids is desired, base modifications can be introduced at the transcription step; for instance, substitution of pyrimidines for 2'-fluoro-modified nucleotides increases RNA stability and half-life. The RNA library is first exposed to a decoy target in a negative selection step where decoy target-binding sequences are removed. Nonbinding sequences are then exposed to the target of interest in the positive selection step. Critically, nonspecific binding sequences are removed via a washing or "partitioning" step. Finally, specific binders are recovered and amplified using their 5' and 3' constant regions, before re-entering the selection process.

SELEX typically produces RNA or DNA aptamers with nanomolar affinities to a broad array of targets: from small molecules[54] to proteins[55] and whole cells.[56] Traditional methods of partitioning the aptamer target from the nonbinding sequence pool have been shown to be quite effective with uniform, purified targets, such as bead-immobilized recombinantly expressed proteins.[57] Standard techniques include nitrocellulose filtration,[58] column immobilization, capillary electrophoresis,[59] and magnetic-bead based washing (M-SELEX).[60]

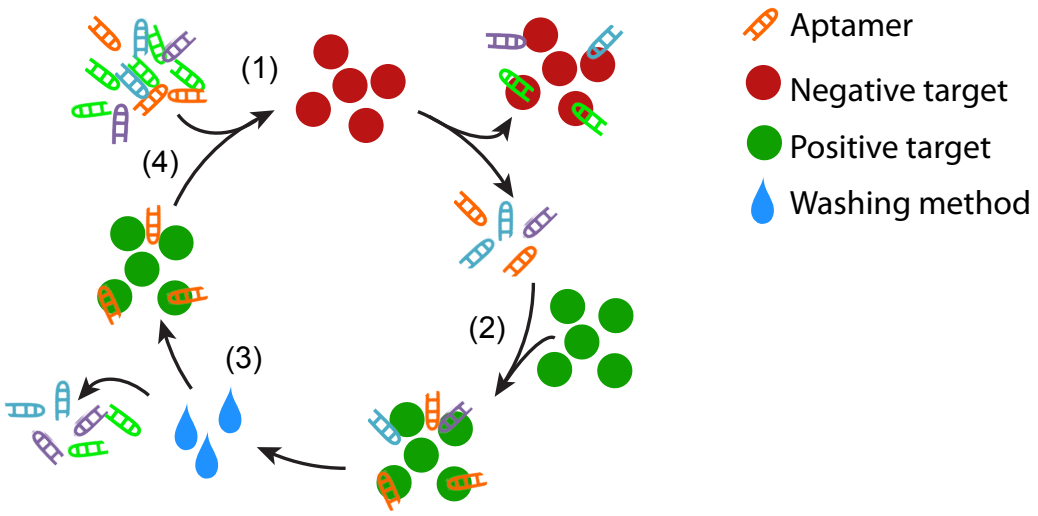


*Figure 3. A standard aptamer selection.* SELEX is commonly performed with a negative selection step (1) against "background" targets, for instance an affinity column with no target present. Sequences that do no interact with the negative target are incubated with the target, such as a protein immobilized on a bead, in a positive selection step (2). After incubation, nonspecifically bound sequences are washed away during the critical partitioning step (3). The remaining sequences are eluted from targets and amplified (4) before another round of selection begins.

### *2.1.2 Partitioning methods and partitioning efficiency*

The efficiency of separating target-bound aptamers from a large background of non-binding sequences is critical for a successful SELEX.[46] Inefficiency at this step significantly increases the number of selection rounds needed to isolate aptamers or leads to SELEX failure when amplification efficiency, rather than target affinity, dictates composition of the selected library.[61] Therefore, improved partitioning efficiency, achieved in a standardized and broadly applicable manner, using targets in their most biologically native state, should facilitate successful SELEX more consistently.

Microfluidic strategies, such as capillary electrophoresis (CE)[62,63] and microfluidic (M-SELEX)[64], consistently attain high (~$10^6$) partitioning efficiencies. The overall SELEX efficiency achieved using these approaches increases significantly, and high affinity aptamers can be isolated in 1–3 rounds compared to the typical 8–15 rounds when using traditional affinity column/microbead centrifugation approaches[65]. CE- and M-SELEX strategies offer standardization during the SELEX partitioning step, but each has an important set of considerations that can limit applicability as solutions to the SELEX partitioning challenge. In addition to the need for specialized equipment, CE-SELEX requires that the aptamer-target complex remains intact during CE and exhibits differential electrophoretic mobility relative to the free nucleic acid library. In M-SELEX, the target is immobilized on magnetic particles and exposed to the nucleic acid library in specially designed microfluidic devices. An externally applied magnetic field traps the aptamer-target complex bound to the magnetic beads, allowing the non-binding library fraction to be stringently eliminated under continuous flow. While more broadly applicable than CE-SELEX, the requirement for attaching the target to magnetic beads is limiting, especially when performing selections against native targets displayed on whole cells, for example.

### *2.1.3 Whole cell-SELEX*

Interest in whole cell-SELEX is rapidly growing. Aptamers discovered in this manner can be used for applications such as cancer diagnostic profiling[65], circulating tumor cell (CTC) enrichment for prognostics[66], cell type profiling[67], and as antiparasitic agents[68,69]. Cell membranes provide a complex mixture of potential targets, and cell-

SELEX essentially becomes a set of multiple, simultaneous selections. In cell-SELEX, fewer rounds of selection preserve library diversity of aptamers to a broad spectrum of surface targets, while greater rounds of selection become narrower in scope but higher in apatamer affinity[70]. Using whole cells as SELEX targets challenges the effectiveness of the chosen partitioning strategy and negative selection step(s). However, using whole cells as targets preserve the native context, frequency, and distribution of potential surface targets of interest, facilitating downstream development and translation in diagnostic or treatment applications.

Presently, few straightforward yet highly efficient strategies are available for identifying aptamers by whole cell-SELEX. The partitioning step is most commonly accomplished by centrifugation[71,72] or less frequently by fluorescence activated cell sorting (FACS)[73]. The former approach, though simple, is inefficient and aptamers are typically identified in ≥12 rounds of selection[71,74,75]. While FACS offers high throughput sorting with single cell sensitivity, major technical drawbacks include clogging, cross-contamination of sorted cells, and decreased cell viability. Additionally, the aptamer library tagging modifications required for FACS pre-biases the selection toward sequences that can tolerate fluorophore coupling, and require the cell surface target to be sufficiently abundant and positioned such that fluorescently labeled aptamer signal can be observed under sorting conditions. Empirically, SELEX typically produces RNA or DNA aptamers with nanomolar affinities in as few as five rounds[76] (typically 8-12 rounds for purified targets such as small molecules or proteins[77]) or in as many as 25 rounds in the case of RBC ghosts[70] (typically 12-20 rounds for whole-cell targets[78]). Whole-cell SELEX on intact RBCs has not been previously reported. The observed disparity

between the number of required rounds between purified and whole-cell targets is supported by theoretical work suggesting the selection efficiency (here, the fraction of binding aptamer within a selected library pool) is proportional to the partitioning efficiency multiplied by target concentration,[46] which is often low or difficult to control in whole-cell systems. Additionally, current methods of cell partitioning are inherently variable from round to round or between users.

An important challenge inherent to the cell-SELEX approach, however, is that many distinct targets will be present on the cell surface during selection, and these will drive enrichment of diverse aptamer solutions. To prevent high false discovery rates that would compromise efficient recovery of high affinity aptamers, this strategy demands a sufficiently stringent selection process to minimize enrichment of non-binding sequences from unmodified aptamer libraries. Therefore, the need exists for a general, widely accessible and inexpensive SELEX partitioning strategy that takes advantage of the high efficiency achieved with microfluidic device, and is suitable for use with both bead-immobilized targets and unmodified whole cells. We have addressed this need by developing a continuous partitioning device based on inertial microfluidics in curvilinear channels, which we call inertial SELEX or I-SELEX.

## 2.2 Overview

Inertial microfluidics is a powerful technique for high throughput particle/cell separation, as previously demonstrated in applications such as blood fractionation[79], CTC enrichment from blood[80], and stem cell synchronization[81]. In this work, a spiral device that imparts differential inertial and Dean migratory effects on micron-sized particles

(e.g. beads and cells) versus macromolecules (e.g. nucleic acid libraries) within a mixture is used to stringently separate these components. To validate this strategy, we present a model system in which thrombin is displayed from the surface of intact human red blood cells. This permits characterization of the high partitioning efficiency achievable with the device, and the ability to selectively enrich a known aptamer from mock libraries. Finally, we demonstrate successful *de novo* SELEX using a library containing ~$10^{14}$ unique sequences. With the device, we discover high affinity ($K_d$ ~ 1 nM) aptamers containing a conserved motif distinct from previously described thrombin aptamers. We identify these novel aptamers by the third round of selection, and observe that they are dominant by the fifth round of selection. Overall, I-SELEX uses a simple and inexpensive microfluidics strategy to allow the efficient discovery of new aptamers.

## 2.3 Results

### *2.3.1 I-SELEX microfluidic device overview*

The device used for I-SELEX is shown schematically in *Figure 4a*. The user interface is simple, requiring only a pair of syringe pumps for routine operation. Importantly, the current device is used strictly as a generic strategy for achieving the partitioning step in SELEX (*Figure 4b*), and so it is easily integrated with existing sample and library preparation, manipulation and deconvolution procedures.

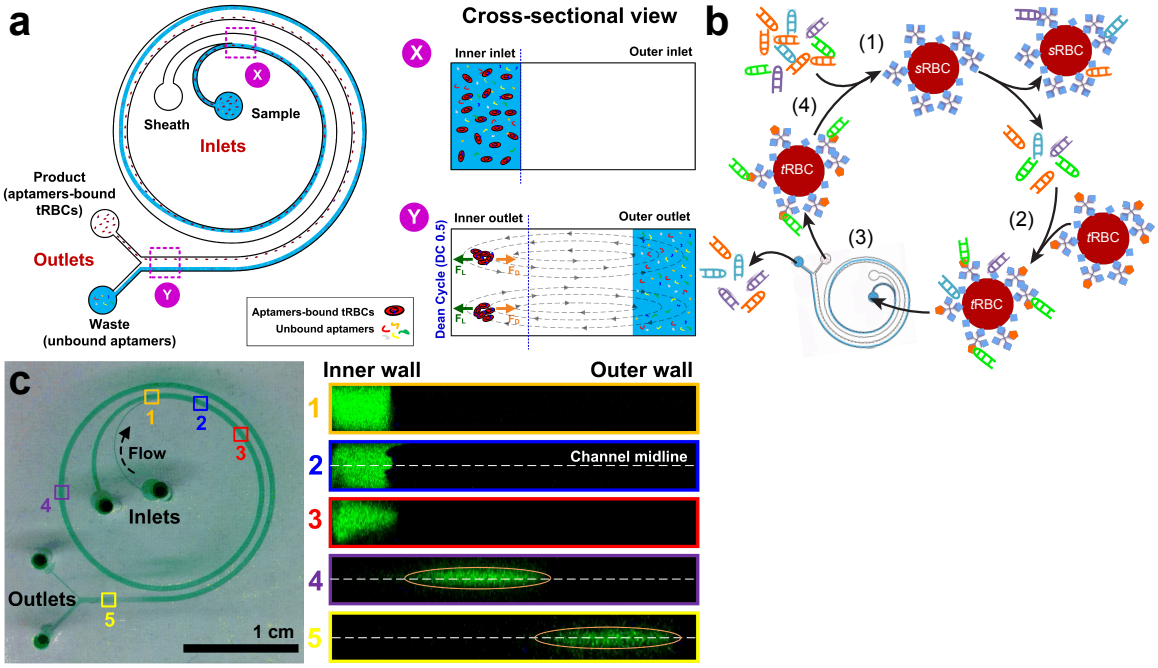


*Figure 4. The I-SELEX microfluidic device and its use in aptamer selection.* **(a)** The microchannel design consists of a bi-loop spiral of radius ~1 cm with dual inlets and outlets. Pre-incubated bead/cell target-aptamer library mixtures and sheath buffer are pumped through the right and left inlets of the device, respectively. Under the influence of Dean drag forces ($F_D$), unbound aptamers migrate along Dean vortices towards the outer wall and are diverted to the waste (bottom) outlet. Target beads/cells (and any bound aptamers) experience additional strong inertial lift forces ($F_L$) and are focused along the inner microchannel wall and collected in the product (top) outlet. **(b)** A schematic of the I-SELEX procedure showing: (1) negative selection of random library against scaffold RBCs (*s*RBCs); (2) positive selection of surviving library on thrombin-presenting RBCs (*t*RBCs); (3) partitioning of *t*RBC-bound aptamers from unbound library in the I-SELEX device; (4) recovery, RT-PCR amplification and in vitro transcription to enrich tRBC-bound aptamers. **(c)** Optical cross sections through the device were taken at positions 1-5 along the length of the channel using high-speed confocal microscopy. Fluorescently labeled CRP aptamers injected via the sample inlet (right) enter the microchannel nearest the inner wall (positions 1 and 2). Dean forces focus free aptamers along the channel midline (position 3). Once focused along the midline (position 4), the aptamer stream migrates toward the outer wall (positions 4 and 5) before exiting the device.

Operationally, the nucleic acid library-target mixture and a sheath buffer are introduced via the right and left inlets of the device, respectively, at an empirically determined appropriate flow rate. After a brief period during which inertial forces within the device stabilize (< 90 seconds), particles (and any bound aptamers) are recovered at the product (top) outlet, while the non-binding fraction of the nucleic acid library is diverted to the waste (bottom) outlet (*Figure 4a and Figure 5*). This flow pattern in the device is stable indefinitely once established, and permits continuous input mixture fractionation and sampling of complex libraries. Under typical operating conditions, a library size of ~$10^{14}$ can be sampled and partitioned in ~10 minutes at a sample flow rate of 150 μL $min^{-1}$ and ~ $2\times10^{6}$ cells $min^{-1}$.

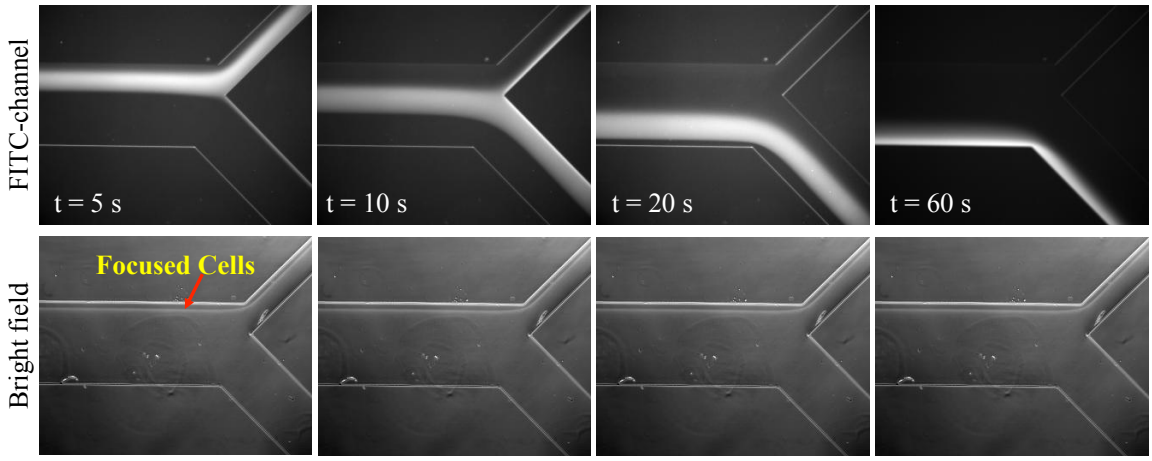


*Figure 5. Establishing Dean's vortices along the channel length as a function of time.* The fluorescently labeled unbound aptamer stream moves from the sample outlet (top) to the waste outlet (bottom) as Dean's vortices are established along the channel length during the initial flow establishment period. Cells (large particles) remain focused at the inner channel wall and are collected in the sample outlet.

### *2.3.2 Fluid mechanics principles governing the design and operation of the I-SELEX device.*

Due to centrifugal acceleration in curvilinear channels, faster-moving fluid at the channel center moves towards the outer wall in a radial direction from the channel midline. Conservation of mass principles dictate that fluid near the channel walls circulates inwardly. Consequently, two symmetrical and counter-rotating Dean vortices perpendicular to the main axial flow in the channel are established[82] (*Figure 4a*). The magnitude of these Dean vortices is determined by the dimensionless Dean number parameter (*De*), which relates channel dimensions, curvature, and flow rate as described in Equation (1)[83]:

$$De = \frac{\rho U_f D_h}{\mu}\sqrt{\frac{D_h}{2R}} = Re\sqrt{\frac{D_h}{2R}} \quad (1)$$

where $\rho$ is fluid density (kg $m^{-3}$), $U_f$ is the average primary channel velocity (m $s^{-1}$), $D_h$ is the microchannel hydraulic diameter defined as $2w \times h/(w + h)$, $\mu$ is fluid viscosity (kg $m^{-1}s^{-1}$), $R$ is the radius of curvature, and $Re$ is the Reynolds number. Ookawara *et al.* formulate an empirical expression for the average Dean velocity ($U_{De}$) for a given *De* as[84]:

$$U_{De} = 1.84 \times 10^{-4}\ De^{1.63} \quad (\text{m s}^{-1}) \quad (2)$$

Due to transverse Dean flows, particles flowing in a curvilinear channel experience lateral drag forces ($F_D$), which allow them to migrate across streamlines. Dean drag increases in magnitude with particle size and channel width[85]. We can define the lateral distance traversed by a particle due to Dean flow in terms of Dean Cycle (DC). A particle that travels across the entire channel width (*x*-axis) has completed half a Dean Cycle (DC

0.5), and a full Dean cycle (DC 1) upon returning to its starting *x*-coordinate relative to the channel midline. The path length of a full Dean Cycle ($L_{DC}$) is approximated by:

$$L_{DC} \approx 2w + h \tag{3}$$

where $w$ and $h$ are the channel width and height, respectively. Particles may undergo multiple Dean Cycle migrations, the number of which increases with increasing channel length, L, and flow rate ($U_f$). In addition to Dean drag forces, particles in curvilinear microchannels experience an appreciable inertial lift force ($F_L$), which is the combination of a shear gradient lift force (directed toward the channel walls) and a wall-induced lift force (directed away from the channel walls). The superposition of competing inertial lift ($F_L$) and Dean drag ($F_D$) forces results in particle focusing at two equilibrium positions – one within each Dean vortex – provided the particle size ($a_p$) and channel height ($h$) satisfy the following criterion[79,86]:

$$a_p/h \geq 0.07 \tag{4}$$

With optimized channel dimensions and flow conditions, these hydrodynamic forces act differentially on particles to achieve highly efficient size-based separation. If the force ratio ($R_f = F_L/F_D$) is ≥ 1, lift forces dominate, and inertial focusing at distinct equilibrium positions near the inner channel wall, based on particle size, is attained. As the equilibrium position of a particle is strongly dependent on $R_f$, which varies with the third power of particle diameter[87], this phenomenon has been used to stringently separate mixtures of micron-sized particles[86-88] or cells[80]. Interestingly, we observed that cells are able to tumble and rotate (while remaining at an equilibrium point within a Dean's vortex) as they move down the length of the channel, which may contribute to the shear forces acting on the surface of the cells/particles during buffer exchange (*Figure 6)*.

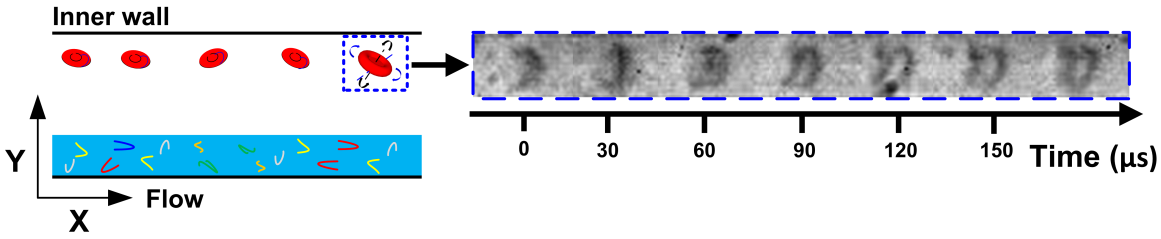


*Figure 6. Rotation and tumbling of red blood cells in the inertial microfluidic device.* Cells move along the inner device wall as they traverse the length of the channel toward the inner outlet. They remain focused at the inner wall due to Dean's forces; however, they retain the ability to rotate and tumble in response to shear and other fluid forces in the channel.

However, inertial focusing of sub-micron sized particles and macromolecules is not possible in these devices due to the negligible inertial forces exerted on nanoscale species ($R_f < 1$). Instead, Dean drag forces dominate, and continuously drive these small species along circulating secondary flows to induce homogeneous mixing. This phenomenon would be undesirable in a SELEX application, as it severely reduces partitioning of the free nucleic acid library away from aptamers bound to the micron-sized bead/cell target. Currently, inertial focusing of molecules is not possible due to difficulties in fabricating sufficiently small microchannels to satisfy the focusing criterion ($a_p/h \geq 0.07$), while tolerating the large pressure drop inherent at high flow conditions in these devices.

We have addressed this limitation by using a two-inlet, spiral channel design (*Figure 4*) in which the sample stream is introduced via the inner inlet while a sheath buffer is pumped via the outer inlet at a higher flow rate to form a tight sample stream at the inner wall. If the channel is truncated at $L = n \times$ (DC 0.5) for $n \in \mathrm{N}$, circulating macromolecules migrate along the midline (dictated by Dean flow) as a focused band

towards the outer channel wall, and are thereby maximally spatially resolved from inertially-focused particles migrating near the inner channel wall (*Figure 4c*). Additionally, we built our microchannel with a low aspect ratio ($h/w << 1$), as Dean drag forces become stronger with increasing channel width[85]. The device measures 9 cm ($l$) × 500 μm ($w$) × 60 μm ($h$) with a dual-inlet and asymmetric dual-outlet spiral microchannel. The product and waste outlet diameters are 150 μm and 350 μm, respectively. We selected the channel height such that particles ≥ 6 μm in diameter (e.g. human RBCs) predominantly experience inertial forces ($a_p/h \sim 0.1$) and focus to the inner channel wall, while macromolecules (e.g. nucleic acid SELEX libraries) experience Dean drag forces ($a_p/h << 1$) and are transported to the outer channel wall by the time they reach the device outlet (DC 0.5). This allows tightly focused particles/cells (and any bound macromolecules) to be efficiently collected at the product outlet, while unbound macromolecules are diverted to the waste outlet. Primarily, channel height determines particle focusing, and this parameter can easily be varied to accommodate beads/cells of different sizes.

### *2.3.3 Whole-cell target system used to quantitatively validate the I-SELEX device*

We used a synthetic whole cell model to quantitatively characterize the performance of our device during SELEX. We selected human RBCs as a model cell type, as they present two extreme yet realistic challenges faced in whole cell-SELEX. First, the cell surface is dominated by a single glycoprotein, glycophorin A, which is present at ~0.5-1× $10^6$ molecules per cell[89]. This can be used to recapitulate the scenario in complex target whole cell-SELEX where relatively rare surface targets may be

occluded by proteins of significantly higher abundance. Second, RBCs have very high cell surface glycan content, and the majority of these terminate in negatively charged sialic acid residues[89]. Thus, RBCs naturally display abundant glycan targets that favor recovery of low affinity ($K_d$ ~ μM affinity) aptamers[90]. While preserving the above characteristics, we modified the RBC surface to display human α-thrombin as a target protein. This allowed us to take advantage of the previously described Toggle-25 thrombin aptamer[91] to characterize the I-SELEX device, and to stringently exclude unfavorable target characteristics as the primary reason for potential failure of a *de novo* SELEX experiment.

We first lightly biotinylated RBCs using NHS ester chemistry and coated them with streptavidin to generate "scaffold" RBCs (*s*RBCs) (*Figure 7a*). We then attached biotinylated thrombin to the cell surface to produce "thrombin-displaying" RBCs (*t*RBCs). The remaining biotin-binding sites on streptavidin were capped using an excess of free biotin. We determined the final amount of thrombin displayed on *t*RBCs for each new batch prepared, and controlled this parameter by titrating the concentration of biotinylated thrombin used (*Figure 7b*). *t*RBCs used in our experiments typically displayed ~$10^3$–$10^4$ molecules/cell, which is ~50- to 1000-fold lower than glycophorin A. Using 3′-FITC-labeled Toggle-25 aptamer, we confirmed that high-affinity and specific binding to *t*RBCs occurs (apparent $K_d$ ~ 34 nM), while no binding to *s*RBCs is observed, as expected (*Figure 7c*). This established that the displayed thrombin is accessible and selectively recognized by a cognate nucleic acid aptamer, confirming the suitability of our model system for device characterization.

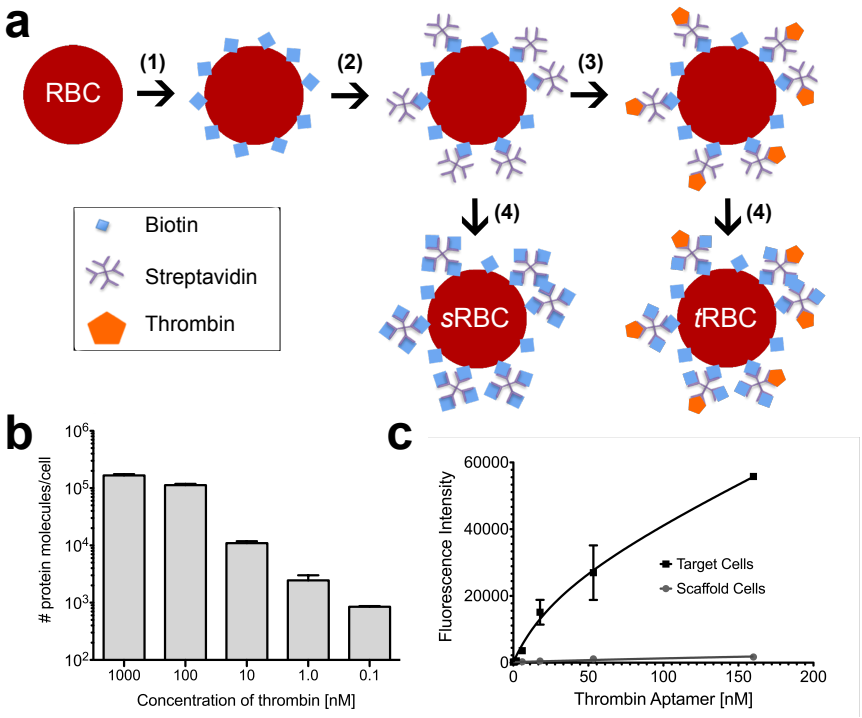


*Figure 7. The synthesis and quantitative characterization of a thrombin-displaying model system are summarized.* (**a**) Human red blood cells (RBCs) are surface biotinylated then coated with streptavidin to produce scaffold RBCs (*s*RBCs). Biotinylated human α-thrombin is added to sRBCs in titrated quantities to create thrombin-displaying RBCs (*t*RBCs). Excess biotin is added to both sRBCs and tRBCs to cap residual open sites on streptavidin. (**b**) Quantitative control over the amount of thrombin displayed from tRBCs can be achieved by titrating the concentration of biotinylated human α-thrombin used is step 3 above. tRBCs used in our experiments typically displayed ~$10^3$-$10^4$ thrombin molecules/cell. (**c**) Fluorescently-labeled Toggle-25 aptamer selectively binds tRBCs with an apparent $K_d$ ~ 34 nM. No significant binding to sRBCs is detected.

### *2.3.4 The I-SELEX device facilitates resolution of tRBCs and aptamers into distinct streams*

We used *t*RBCs and the 5′-FITC-labeled C-reactive protein (CRP) DNA aptamer[92] (no binding to *t*RBCs) to empirically determine the optimal input flow rates needed to simultaneously: *(i)* focus the *t*RBC stream at the inner wall of the device and

ultimately into the product outlet; *(ii)* stringently divert the non-interacting CRP aptamer to the outer wall of the device and into the waste outlet; while *(iii)* minimizing *t*RBCs entering the waste outlet. In the limit, these boundary criteria define perfect stringency in the ideal I-SELEX experiment, where the non-interacting nucleic acid library is completely excluded from the product outlet, and all *t*RBCs with aptamer bound are collected at the product outlet.

We monitored focusing of the fluorescently labeled aptamer stream by fluorescent microscopy and empirically determined that predictable control over the free aptamer stream occurs when the sheath buffer flow rate is ten-fold greater than the sample input flow rate. A minimum overall flow rate (sheath buffer + sample) must be maintained ($Re > 50$ or $U_f \approx 900$ μL min$^{-1}$) to ensure inertial focusing. Simultaneously, the flow rate-induced increase in $F_L$ from the sheath stream results in better partitioning of the unbound nucleic acid library to the outer channel wall. At input sample flow rates of 50 μL min$^{-1}$ (total flow rate = 550 μL min$^{-1}$), unbound aptamers are collected in the product outlet with the *t*RBCs. As the sample input flow rate is progressively increased to the 180 μL min$^{-1}$ maximum tested (total flow rate = 1980 μL min$^{-1}$), the unbound aptamer is increasingly recovered in the waste outlet (*Figure 8a*).

Since the diameter of the waste outlet is greater than that of the product outlet, near-complete collection of unbound aptamers in the waste channel can be achieved while inertially focused RBCs remain at the inner wall during their short (~ 0.1 s) passage through the device (*Figure 8b and 8c*). *t*RBC recovery at the product outlet is inversely dependent on sample input flow rate (*Figure 8d*), as increased channel velocity $U_f$ increases the magnitude of Dean drag. Based on these data, we selected a sample input

flow rate = 150 µL min$^{-1}$ and sheath buffer flow rate = 1500 µL min$^{-1}$ as standard operating conditions for achieving high partitioning between *t*RBCs and unbound aptamer while maintaining high (~85%) *t*RBC recovery at the product outlet (*Figure 8d*).

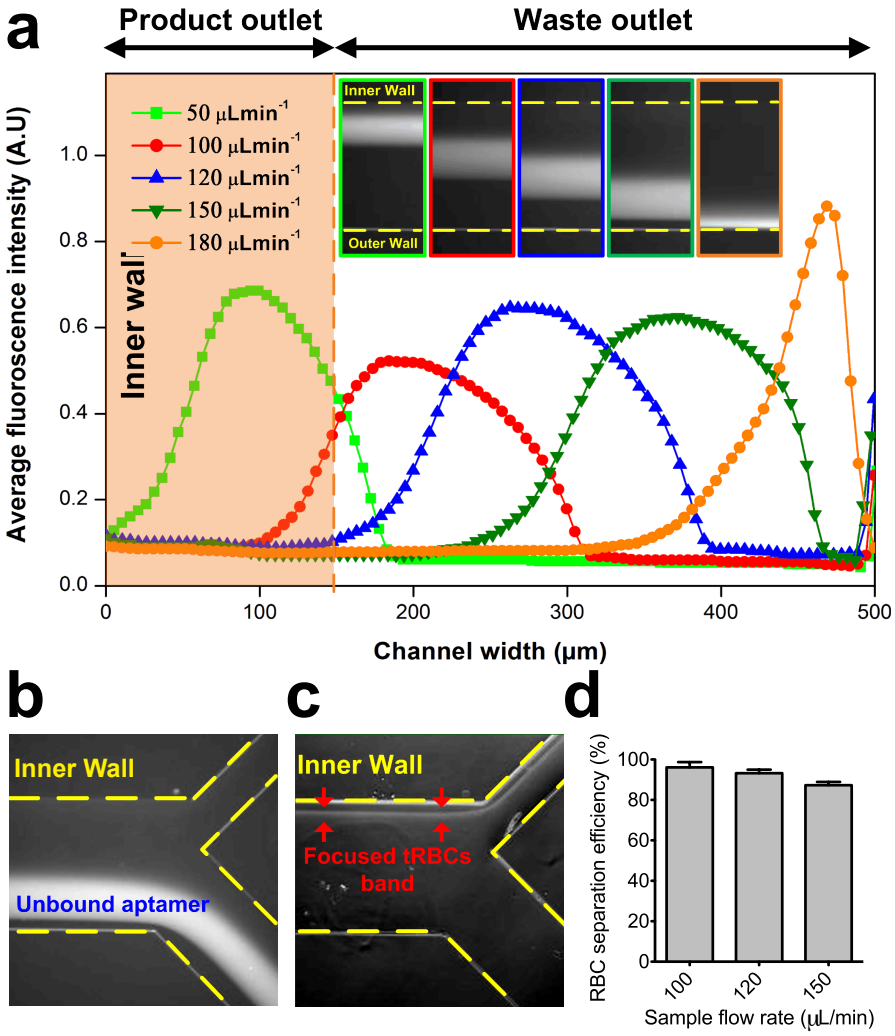


*Figure 8. Optimization of the operating flow rates within the I-SELEX device to achieve stringent separation of a model non-interacting aptamer from tRBCs while maximizing tRBC recovery.* (**a**) Average fluorescence intensity line scans showing the normalized distribution of unbound FITC-labeled CRP aptamers (200 nM) across the channel width at increasing flow rates. Approximate positions of the product and waste outlets are indicated. Corresponding fluorescence images illustrating flow positions of unbound aptamers are also shown as an inset (yellow dashed lines indicate the approximate position of the

microchannel walls). (**b**) Average composite images indicate unbound aptamers move to the outer wall and are diverted into the waste (bottom) outlet. (**c**) Average composite images indicate efficient *t*RBC focusing to the inner microchannel wall and diversion into the product (top) outlet. In both (**b**) and (**c**), the sample input and sheath buffer flow rates are 150 μL $min^{-1}$ and 1500 μL $min^{-1}$, respectively, and the yellow dashed lines indicate approximate positions of the microchannel walls and bifurcation. (**d**) Recovery of *t*RBCs at the product outlet as a percentage of the cells loaded into the device when operated at different sample input flow rates. In all cases, the sheath buffer flow rate is 10-fold higher than the sample input flow rate.

### *2.3.5 The I-SELEX device has a high partition efficiency and permits selective enrichment of aptamers from a mock library*

We first tested whether selective recovery of aptamers bound to *t*RBCs can be achieved in our device. We used the Toggle-25 thrombin aptamer and a scrambled version (*scr*Toggle-25) with no affinity for thrombin or *t*RBCs. These were incubated separately at 100 nM with *t*RBCs collectively presenting an ~10-fold excess of thrombin binding sites prior to partitioning on the I-SELEX device. Using quantitative RT-PCR, we determined Toggle-25 and *scr*Toggle-25 levels at the sample input and product outlet (*t*RBC-bound fraction). As shown in *Figure 9a*, Toggle-25 was quantitatively recovered, while the amount of *scr*Toggle-25 collected at the product outlet was below the limit of detection.

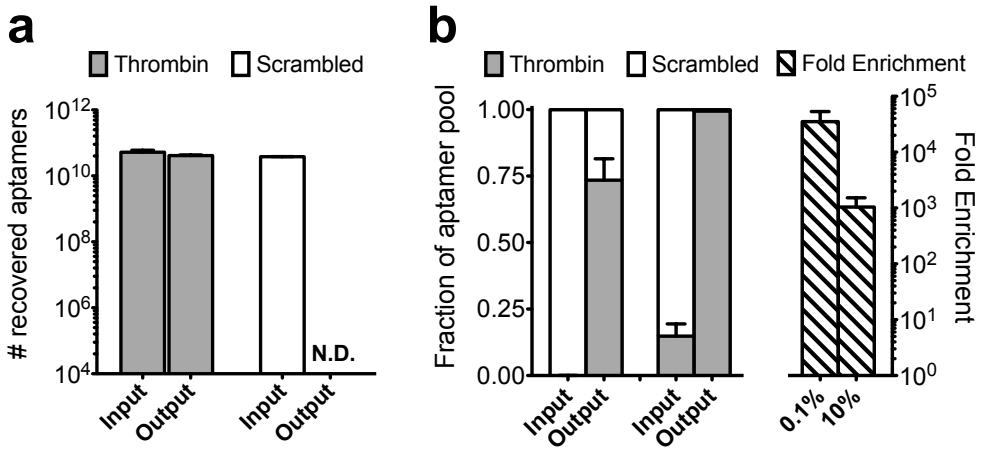


*Figure 9. The I-SELEX device exhibits high partitioning efficiency and can be used to selectively recover and enrich target aptamers from mock libraries.* (**a**) Near complete recovery of Toggle-25 bound to *t*RBCs is reproducibly achieved, whereas scrToggle-25 recovery using *t*RBC targets is below the limit of detection. These data are consistent with a device partitioning efficiency that is $\geq 10^6$. (**b**) Mock SELEX libraries containing Toggle-25:*scr*Toggle-25 in 1:10 and 1:1000 ratios, respectively, were incubated with *t*RBCs and partitioned in a single pass through the I-SELEX device. Toggle-25 is selectively enriched and becomes the dominant species post-selection as determined by quantitative RT-PCR.

From these data, we determined the partition efficiency (PE) attainable with the I-SELEX device. PE is a measure of the device's ability to reject non-binding sequences from the recovered pool containing true aptamers and is a common metric used to evaluate SELEX washing methods[57,64]. It is defined by the ratio of the number of input sequences to the number of non-binding sequences recovered in the product output after partitioning. A single pass through our device reproducibly removed $\geq 10^6$ non-binding sequences (*Figure 9a*), establishing this as the lower limit of PE for the I-SELEX device. This PE is similar to or exceeds that attained in NECEEM[57] and M-SELEX[64] methods, and is consistent with the reproducibly high PEs accessible using microfluidics.

In preparation for conducting a *de novo* I-SELEX experiment, we empirically tested whether *t*RBC targets could significantly enrich Toggle-25 thrombin aptamers from a mock library containing excess *scr*Toggle-25. Two artificial SELEX libraries were prepared, each containing ~$10^{14}$ total molecules with either 0.1% or 10% Toggle-25. Each library was incubated with *t*RBCs ($10^7$ cells; $10^4$ thrombin molecules/cell) and this mixture was subjected to a single partitioning step through the I-SELEX device. As shown in *Figure 9b*, significant and preferential enrichment of Toggle-25 was achieved, and the recovered pools from both mock libraries were dominated by Toggle-25.

### *2.3.6 Successful* de novo *selection using the I-SELEX device*

Using a randomized library containing ~$10^{14}$ sequences, we conducted *de novo* SELEX using *t*RBCs as a whole cell target. For each round, the partitioning step was achieved in a single pass of the *t*RBC-library mixture through the I-SELEX device. *t*RBCs were collected at the product outlet, and the bound RNA recovered, amplified by RT-PCR, then transcribed *in vitro* by standard procedures in preparation for the next round. A total of five rounds of selection were completed. The bulk initial library and the Rounds 1–5 selected pools were evaluated for thrombin binding using bio-layer interferometry with thrombin-coated probes. The Round 5 selected pool exhibited thrombin binding ($K_d$ ~ 4 nM) similar to Toggle-25 (*Figure 10a*).

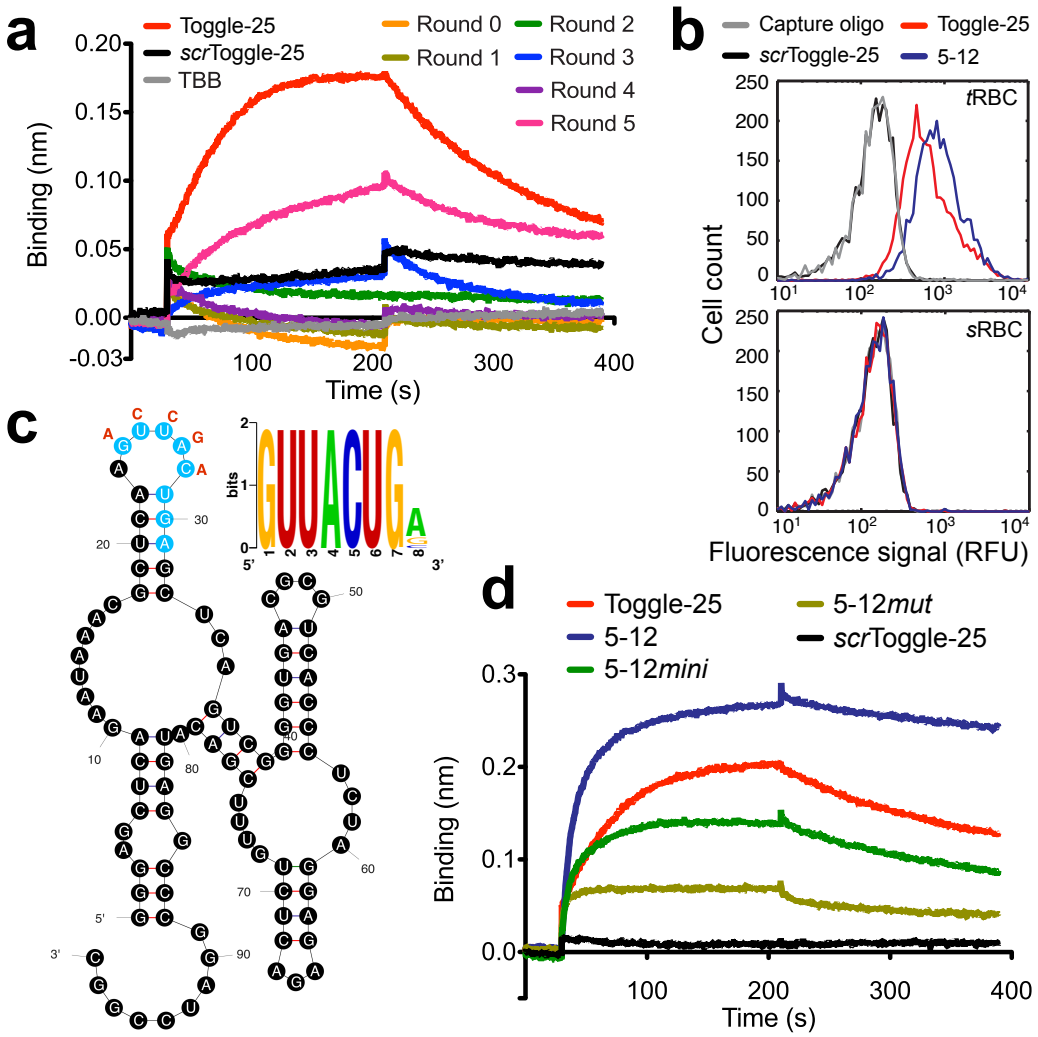


*Figure 10. The I-SELEX device can be used for* de novo *discovery of high affinity aptamers.* (**a**) Bio-layer interferometry kinetic binding data on the interaction between probe-immobilized thrombin and the selected RNA pools from each round are shown. Toggle-25 and *scr*Toggle-25 were included as positive and negative controls, respectively. High affinity (Kd ~ 40 nM) binding of the pool from the fifth selection round was observed. (**b**) **5-12** and Toggle-25 show enhanced binding to *t*RBCs but not sRBCs. *scr*Toggle-25 and the capture oligonucleotide used for aptamer fluorescent labeling do not exhibit binding to either cell type. (**c**) Clones sequenced from the Rounds 3 and 5 selected pools were collectively analyzed using MEME[93]. A conserved heptanucleotide motif (Motif 1), distinct from that present in Toggle-25, was detected in 12/38 unique clones (Cluster I sequences). By mfold[94], Motif 1 is predicted to be part of a stem-loop secondary structure element, as shown for **5-12**. (**d**) Using **5-12** as an example, the conserved motif was shown to contribute significantly to high affinity binding to thrombin. Truncated **5-12** (**5-12mini**), in which the conserved motif is retained in the predicted parental stem-loop arrangement, bound thrombin with a $K_d$ ~ 5 nM, similar to

**5-12** ($K_d$ ~ 2 nM). However, **5-12mut**, which is the full-length aptamer containing mutations to the motif indicated in red in (**b**), bound thrombin with significantly lowered thrombin affinity ($K_d \geq 3$ μM).

We sequenced 26 and 17 clones from the Rounds 3 and 5 selected pools, respectively (*Table 1*), and analyzed these sequences with MEME[93]. The majority (86%) of the sequences were unique. One clone (**3-19**) was duplicated, and another was represented four times (**3-7**, **5-3**, **5-9** and **5-16**). Clones could be broadly grouped into three clusters based on the presence of a MEME-identified motif or lack thereof. Cluster I sequences contained a conserved *GUUACUG*(*A*/*G*/*C*) motif (Motif 1), and 2/25 and 10/13 (31% overall) of the unique clones recovered from rounds 3 and 5, respectively, fell into this group. Clones **5-5** and **5-12,** arbitrarily chosen as representatives from this cluster, were identified as high affinity thrombin aptamers by bio-layer interferometry ($K_d$ ~ 2 nM for both). We selected **5-12** to test its binding to *t*RBCs and *s*RBCs. Similar to Toggle-25, **5-12** exhibited significant binding to *t*RBCs but not to *s*RBCs as expected based on its thrombin-specific binding properties (*Figure 10b*). To understand whether Motif 1 is involved in binding, we used mfold[94]-predicted secondary structures to guide the design of truncated or mutated versions of **5-12**. Motif 1 is predicted to lie within a stem-loop region of these aptamers. (*Figure 10c*). We generated **5-12*mini*** by truncating the parent aptamer while preserving the predicted stem-loop structure containing the conserved motif, and determined that high-affinity thrombin binding was retained ($K_d$ ~ 5 nM). In the context of the full-length aptamer, we mutated the motif while preserving the stem-loop element to produce **5-12*mut*** (*Figure 10d*). This mutated aptamer exhibited significantly reduced thrombin binding ($K_d \geq 3$ μM). Taken together, these data establish

that the conserved Motif 1 present in Cluster I aptamers may be required for high affinity binding to thrombin.

| Clone ID | $K_d$ (nM) | Sequence of variable region |
|---|---|---|
| **Cluster I** | | |
| 3-25 | | **GUUACUG** AUCUUCCUGCAGCGCGAAUCACAUGUAUGAAGCCGGAUCGACG |
| 3-30 | | A **GUUACUG** CGCUCUUACGAGGUAACUACUUAGUUGGCAUUACGUAGUACU |
| 5-1 | | A **GUUACUG** AGCUCUUGUGUGUUACAGUUGAGAAUCACAACGAUUCCCUG |
| 5-2 | | A **GUUACUG** GGUUCCCCUUCCCACACGCCAUCAUCGUAUGCCGGCAAACGA |
| **5-5** | 2 | A **GUUACUG** AGUUCCGGGGAGAGGGGUAGAGCUCUACCGCCCAAAUAGCGA |
| 5-8 | | **GUUACUG** GGUUCCGCACAAAUGAGAUUUAUGUUUUUCUAAUCUGCCUCA |
| 5-10 | | **GUUACUG** AGAGCCCUUGACCUCUGGAGCCCACGACGUCGUGAAUAUGAGG |
| 5-11 | | **GUUACUG** ACACUCCCCGUUGGUGCGAAGCACCAAGUAACGACAGACUCAG |
| **5-12** | 2 | **GUUACUG** AGCUCAGUCGGGGUGACGCGUCACCCUCUAGGAGAGACUCUGU |
| 5-14 | | A **GUUACUG** AUGUCCCCGAACUGGUGUGGCAAUGGCAGACAUUGCAGCAGG |
| 5-15 | | A **GUUACUG** CGCUCCUAUACUGGCUCAUUGUGCCCGGCAUCGAGGACAUUG |
| 5-17 | | **GUUACUG** AACUCUCGCCGUGGCGCCACGUUGAUAUGCAGUCGACUUCAAG |
| **Cluster II** | | |
| **Toggle-25** | 40 | GAACAAAGCUGAAGUAC **UUACCCAAG** AUCAUCCCGA |
| 3-4 | | UGAUGUAAGACUGUUACUUGUGUGUUA **UUGCCCAAG** UUUGGUCUGUAUUG |
| 3-10 | | UGGUGACUGGGUGAGAAUAGCAUU **UUGCCCUAG** UCAUUCGAGUCUACAAC |
| **3-19** (2) | > 1000 | CUGCCUGAGACUGCACUUUUUCGCUCC **UUCCCCAAG** UCUUUUUGCGAGUU |
| 5-6 | | CGAAUGCCGAAAUUAGAGCGUG **UUCUCCAAG** CCCGACUCGUACGGCUCGA |
| **Cluster III** | | |
| 3-1 | | UCAAAUUAGUGCGCGAGGACUAUUAGGACGUCCAGUACAUAAUAUCAGAA |
| 3-2 | | CGAAAAACAGUAUUACGAUGCAUCCUUCGUAAUCCACCUUGAAAUAAAAC |
| 3-5 | | UAAGUUGCAGUAAUGGAGUUCCUGAAAUGGACGUACGGUCCUAUU |
| 3-6 | | UAGUCAUUGGUUAAAAACCAGUCUCCAAUCGAAUAUUACCGGUUAUGUUU |
| **3-7** (4) | > 1000 | CAACGGAUCACACGCAAGCGAAUCUAUGUCCUUCGGGUCUAAGGGUCGCU |
| 3-8 | | UCCAUUUCUUCUGAAACGAUGAGCAC |
| **3-9** | 4 | ACGAACGUACAAGUUAUGAGAACUGACCUCCCUAUUGUCAUCCACACUCA |
| 3-11 | | ACUUAAGAAUCGACCUGGGGUGACAAUUAAUCCUUCUUUGUUUUGUUAAC |
| **3-12** | 200 | GAUCAAAUUUAAUAUAUCCGAUCUGGAGAUCUAAUAUCAUAUUGUAGUGG |
| 3-13 | | ACAGGUUUAUAAAGUUUUCGUUUCGAUGGAUUUUAAAACAAUCUAGAUCC |
| 3-14 | | AUAAGCUGAUUUGUUCAGAACAUCUUAAUAUACAGUCACACAGGCUGCAG |
| 3-15 | | CCAUUUUAAGGAAUCACGCUGCCCCUACCCUGCGGUUCAGCCGACCUUU |
| 3-16 | | GGUUUUAAUUUAGUACUUCUCUAUAGUUUUACUAGCCUUGAACAUUGGGA |
| 3-17 | | CUUUGCCUUACAUCAAUAUAGGUCAACAUAAGUAGUGUAACGUUUGGUCA |
| 3-18 | | UACCUGUUAAGAAUGAGUUCAAGAGUAAAAGUUAUGUCCUGCAUGUCUAG |
| 3-24 | | UGGGAGACCGAUAUAAGCAAUGUAUCACCUGUGCGCAUUGAAGUCGGACU |
| 3-26 | | CAUUUGCGCGAAUCAGGCUUGCUUGUGUUAACACUGCAACGGUUUUAUCG |
| 3-27 | | CCGCGGACUUGCACUGUACCGCGUACCUUGCCUAAUUGUUCUGUAAAGAA |
| 3-28 | | AAGGUUGAUGGCGUUGAUUCUUAGUCAUUAAUCGUUGUCGUUAAAGACGU |
| 3-29 | | AUGAUUGAUUAUCAUGAAAAUGGCUGGUGGUAAACAUCACCUGAUAUUG |
| 5-7 | | UUGCACCAAGGUUCGGAAAUUGAGCGGGCGACGCGUCGAAUGCCGCUAAU |

*Table 1. The sequence of variable regions from clones isolated after three and five rounds of* t*RBC I-SELEX are shown.* By MEME analysis, these are grouped into three clusters based on the presence of a GUUACUG motif (Cluster I), a UUACCCAAG motif also present in Toggle-25 (Cluster II) or absence of a recognizable conserved motif (Cluster III). The number of times a clone was represented in the sequenced pool is indicated in parentheses following the clone ID. Dissociation constants for binding to thrombin are shown for tested clones (Clone ID in bold text).

A sequence identical to Toggle-25 was not present amongst the clones sampled, and Motif 1 is distinct from a motif implicated in Toggle-25 binding to thrombin[91]. However, Cluster II clones contained a *UU[G/C/A]YCC[A/U]AG* motif (Motif 2) that is shared between Toggle-25, **3-4**, **3-10**, **3-19** and **5-6**. The representative **3-19** exhibited very low binding affinity to thrombin (≥ 1 μM). Thus, while this conserved feature may confer some degree of binding to thrombin, it appears insufficient for mediating the high affinity binding observed for Toggle-25. Cluster III consists of sequences that do not contain the above motifs or any other primary sequence feature that is strongly conserved amongst the group. We tested **3-7**, **3-9** and **3-12** for thrombin binding. Although **3-7** was represented by four separate clones, it did not detectably bind thrombin. It is possible that this sequence persisted due to a replication advantage rather than target-binding affinity. Clone **3-12** bound thrombin with modest ($K_d$ ~ 200 nM) affinity, while **3-9** bound more strongly ($K_d$ ~ 4 nM).

Altogether, using I-SELEX with a complex whole cell target, we have identified a new class of high-affinity binding thrombin aptamers that are sufficiently enriched from a starting library of ~$10^{14}$ sequences within three rounds of selection. It is also worth noting that, while the I-SELEX partitioning step is stringent, aptamers with affinities varying by 100 fold (~2 nM–200 nM) can be recovered. Thus, without having to devise alternative partitioning protocols, I-SELEX may be broadly useful in recovering both high and modest affinity aptamers to a given target, thus expanding the option space for identifying the most suitable aptamer for the intended application.

## 2.4 Discussion

We have demonstrated the application of inertial microfluidics principles in a spiral device capable of rapidly and stringently resolving micron-sized particles (RBCs) from macromolecules (a nucleic acid library) to successfully perform whole-cell SELEX. Our device functions with very high partition efficiency ($\geq 10^6$) and efficiently yields high affinity aptamers in as few as three rounds of selection. We believe this device provides a generic strategy for effectively completing the critical partitioning step in SELEX, and has the advantage of being equally applicable to bead-immobilized targets and directly to whole cells without the need for modification. The theoretical principles guiding device design and operation are sufficiently well understood such that new designs to accommodate particles of different sizes can be easily achieved. Alternatively, standardization of the partitioning step using a single device design is also feasible under optimal operating conditions, as the device has sufficient tolerance to accommodate a range of particle sizes with no adverse impact on the resolution of particles and macromolecules into distinct output streams.

The microfluidics partitioning strategy we describe takes advantage of the combined effects of inertial focusing of *t*RBCs and well-controlled Dean migration of unbound nucleic acid library along the channel midline in spiral microchannels. By choosing a low-aspect ratio channel design, we can significantly enhance the resolving power of our device such that highly efficient separation of micron-sized particles (*t*RBCs) from macromolecules (nucleic acid library) is attainable. Remarkably, such stringent partitioning occurs extremely rapidly, as a particle or cell only spends ~0.1 s within the device under our standard operating conditions. We hypothesize that additional

particle/cell rotation due to high-shear gradients and secondary Dean flow near the channel wall might play a role in enhancing removal of weakly-bound aptamers from target cells. While *t*RBCs remained focused near the inner wall, Dean vortices establish a lateral shear gradient at their focusing positions, which may cause *t*RBCs to rotate as they flow along the channel. This hypothesis is supported by a recent study showing that the combination of cell rotation and transverse motion in a spiral channel enhanced transfection efficiency via more homogenous electroporation of individual cells[95]. Assuming cell rotation occurs laterally and is caused solely by Dean vortices, inertially-focused *t*RBCs would undergo ~20 rotations (shear rate of ~400 $s^{-1}$) with a residence time of ~0.1 second in our device. Dean velocity varies with flow rate, radius of curvature, and channel dimensions (Equations 1 and 2). By varying these parameters, we can potentially tune the degree of Dean flow-induced target cell/particle surface "washing" achieved during I-SELEX. This could allow selection stringency to be modulated with greater flexibility than is typical in other microfluidics-based aptamer selection devices.

We have emphasized attaining a generally applicable and highly efficient partitioning strategy. This step can be readily integrated with other recent advances aimed at improving the efficiency, reproducibility, and likelihood of routinely discovering target aptamers with the desired target-interaction profiles. For example, improvements in library design[96,97] and chemical diversity[52,98] can enhance the discovery of high affinity aptamers to a more diverse set of targets[99]. Similarly, high throughput DNA sequencing holds promise for more comprehensively deconvoluting selected libraries "in real time." Through systematic round-by-round analysis of selected libraries, it has been observed that high affinity aptamers are frequently sequences exhibiting the highest enrichment

between consecutive rounds[57,99,100]. The option to deep-sequence a selected library may be viewed as a simple solution to circumvent the development of highly efficient partitioning strategies for SELEX[100,101]. However, as observed by Kupakwana *et al*., when partitioning was achieved using a low-efficiency resin-based strategy, a substantial number of recovered sequences reflected inefficiency during the partitioning step. Furthermore, deep sequencing and follow-up characterization of putative aptamers require investing significant resources. Therefore, a highly efficient partitioning strategy significantly increases the probability that identified sequences are indeed aptamers. This strongly favors integrating high-efficiency partitioning with deep sequencing to improve the success rate achieved in *de novo* aptamer discovery.

In our proof of concept demonstration of using I-SELEX for successful *de novo* whole cell aptamer discovery, we have also generated a new class of anti-thrombin RNA aptamers. Thrombin is a serine protease that catalyzes the activation of a number of important factors in the coagulation cascade. Thrombin acts as a potent vasoconstrictor and is implicated in cellular proliferation post vascular injury, and tight regulation of its activity is essential for therapeutic applications such as regulating hemostasis[102]. In large part due to its extensive characterization, thrombin has been used in early SELEX experiments[103,104]. More recently, the RNA aptamer Toggle-25, used in this research as a positive control for thrombin binding, was developed for its ability to bind both porcine and human thrombin, a necessary feature for clinical development of anti-thrombin aptamer therapies. Our thrombin selection was performed using the human RBC as a scaffolding platform and thrombin-less RBCs were used as negative selection targets, thereby eliminating RBC-binding sequences from our selected library. This design could

prove a major advantage for downstream therapeutic applications where the aptamer would come into contact with RBCs and other blood components while in circulation. The thrombin aptamers discovered in this work contain motifs distinct from any reported in other 2'-fluoro-pyrimidine RNA aptamer selections[91]. Additionally, several aptamers from Round 5 of selection, particularly **5-12**, demonstrated higher affinities (faster $k_{on}$ and slower $k_{off}$) than Toggle-25 (*Figure 10d*), which may prove to be more desirable binding kinetics for particular applications.

## 2.5 Summary

We have designed and validated a simple, reusable, and broadly applicable inertial microfluidics device as an efficient way of achieving stringent, single pass library partitioning during SELEX. The device can be inexpensively fabricated and routine operation is straightforward. While we have demonstrated the use of a single device for a single target here, the approach is amenable to both automation and multiplexing. Combined with improvements in library synthesis and deconvolution methods, this could facilitate more robust and higher-throughput selections in the future.

## 2.6 Methods

### *2.6.1 Device Fabrication and Flow Conditions*

Microfluidic devices were fabricated in polydimethylsiloxane polymer (PDMS, Sylgard 184, Dow Corning) using the double molding process reported previously[105]. Briefly, patterned silicon wafers were silanized with trichloro(1H,1H,2H,2H-perfluorooctyl)silane (Sigma-Aldrich) for 1 hour and PDMS prepolymer mixed in 10:1

(w/w) ratio with curing agent was poured onto the silanized wafer and baked at 80°C for 1 hr. The cured PDMS mold then acted as a template for subsequent PDMS casting (negative replica). The PDMS master template was silanized for 1 hour before use to aid release of subsequent PDMS microchannels. Finally, holes (1.5 mm) for inlets and outlets were punched and the PDMS microchannels were irreversibly bonded to microscopic glass slides using an air plasma machine (Harrick Plasma Cleaner) and left for 2 hours at 70°C to complete the bonding.

Fluid flow through the microfluidic device was modulated with two NE-300 Just Infusion™ Syringe Pumps, one for sample input (inner inlet) and one for sheath buffer input (outer inlet) (syringepump.com). Micro-tubing (0.86 mm ID (inner diameter) by 1.52 mm OD (outer diameter)) (Scientific Commodities, Inc.) was used to move fluid from the syringes into the device inlets. Using slightly oversized tubing (OD 1.52 mm > device input/exit punch diameter of 1.5 mm) creates enough friction to hold the tubing in place during routine use at the relevant flow rates. Each sample mixture was pumped into the inner inlet at 150 μL $min^{-1}$ while sheath buffer (Thrombin Binding Buffer or TBB = 20 mM HEPES pH 7.4, 150 mM NaCl, 2 mM $CaCl_2$) was pumped through the outer inlet at 1500 μL $min^{-1}$. Sample at the product outlet (cells and aptamers) was collected after 1.5 minutes of run time to allow for establishment of Dean vortices along the channel length.

### *2.6.2 Microscopy*

Samples ($10^7$ cells/mL) and sheath buffer (TBB) were pumped through the microfluidic device using two syringe pumps (NE-1000, New Era Pump Systems) and

the ratio between the sample and sheath buffer flow rates was fixed at 1:10. For image acquisition, the microchannels were mounted on an inverted phase contrast microscope (Olympus IX71) equipped with a Hamamatsu Model C4742-80-12AG CCD camera (Hamamatsu Photonics, Japan). IPLab software (Scanalytics) was used for video acquisition and captured videos were analyzed using ImageJ software. A high speed CCD camera (Phantom v9, Vision Research) was used to capture additional rotational motions of individual focused RBCs within the channels using 1 μs exposure time (~70,000 fps).

### *2.6.3 Cell Synthesis and Quality Control*

Human RBCs were washed twice with 10 mL PBS, pH 8, and $2 \times 10^9$ were resuspended to 5% hematocrit in 4 mL PBS, pH 8 with 1 mg EZLink Sulfo-NHS-Biotin (Thermo Scientific). Cells were incubated for 30 minutes rotating at room temperature (25°C) then washed twice with 10 mL PBS, pH 7.4. Biotinylated RBCs were resuspended to 5% hematocrit in PBS, pH 7.4 and incubated with 200 μg streptavidin (Thermo Scientific) for 30 minutes at room temperature. Half of this cell suspension was directly transferred to a fresh tube and incubated with 100 μL of biotin-saturated PBS, pH 7.4 for 15 minutes at room temperature to cap free biotin-binding sites and create *s*RBCs. The other half of the cell suspension was incubated with thrombin-BFPRck (Haematologic Technologies) for 30 minutes prior to biotin capping to create *t*RBCs. *t*RBCs were synthesized with surface thrombin concentrations spanning 4-logs. All cells were stored between use at 4°C in Gibco RPMI-1640 media (Life Technologies) supplemented with 0.25% Albumax (Invitrogen), 24 mM HEPES, 0.1 mM hypoxanthine, 50 mg/L gentamicin, and 2 g/L sodium bicarbonate. Effective surface thrombin

concentrations were determined by nonlinear regression analysis of titrated monoclonal anti-thrombin antibody (Haematologic Technologies ) labeled with a 1:1000 dilution of Alexa Fluor 488 goat anti-mouse secondary antibody (Invitrogen) before being analyzed by flow cytometry (Accuri C6 flow cytometer, FL1-H channel). Binding was fit to the following model: $Y = B_{max}*X/(X + K_d) + \mathrm{NS}*X + Y_0$, where $Y$ is fluorescence signal (RFU), $B_{max}$ is the total number of antibody-accessible binding sites, $X$ is the number of antibody molecules added to the solution, NS is the non-specific binding component, and $Y_0$ is the background fluorescence.

### *2.6.4 Aptamer Design and Synthesis*

The DNA template for the thrombin-binding Toggle-25 aptamer[91] was assembled by PCR using primers CMB49, CMB50, CMB51 and CMB56 (*Table 2*). *scr*Toggle-25, a non-binding variant, was prepared by scrambling the thrombin-binding region of Toggle-25 and installing unique primer binding sites while retaining overall length and (G+C) content. The *scr*Toggle-25 DNA template was PCR assembled using primers CMB95, CMB96, CMB97 and CMB98. Four aptamer clones from Round 3 were assembled with the SELEX Forward Primer and the following sequence-specific primers: **3-7** (identical to **5-3**), CMB112, CMB113, CMB114; **3-9**, CMB107, CMB108, CMB109; **3-12**, CMB133, CMB119, CMB120; and **3-19**, CMB134, CMB122, CMB123. Three aptamer clones from Round 5 were PCR assembled with the SELEX Forward Primer and the following sequence-specific primers: **5-3** (see above); **5-5**, CMB142, CMB125, CMB141; **5-12**, CMB126, CMB116, CMB117. Mutant **5-12** (**5-12*mut***) templates were synthesized with SELEX Forward Primer and sequence-specific primers CMB130,

CMB131 and CMB132. The minimized aptamer (**5-12*mini***) was synthesized from the DNA template assembled from the SELEX Forward and CMB127 primers. All PCR reactions were performed identically with Phusion High-Fidelity PCR polymerase (New England BioLabs) according to manufacturer's instructions, with the exception that internal primer concentrations were 10-fold lower than the external primers.

### *2.6.5 Partition Efficiency and Enrichment Experiments*

For partition efficiency experiments, 100 nM of either Toggle-25 or *scr*Toggle-25 was incubated in 1 mL TBB with $10^7$ *t*RBCs for 20 minutes at room temperature with continuous gentle inversion before being passed through the I-SELEX device. *t*RBCs were recovered directly from the sample outlet onto a vacuum filter plate membrane (Millipore MSHVS4510). Bound aptamers were eluted (off-vacuum) by a 5 minute incubation with 1 mM EDTA in PBS, pH 7.4 followed by plate centrifugation. Quantitative polymerase chain reaction (qPCR) with SYBR Green was used to determine absolute levels of Toggle-25 and *scr*Toggle-25 recovered after device partitioning. Recovered aptamers were ethanol precipitated and reverse transcribed using SuperScript III Reverse Transcriptase (Life Technologies) with either Toggle-25 reverse primer CMB94 or *scr*Toggle-25 reverse primer CMB104. The partner forward primers (CMB77 and CMB106, respectively) were added with 1× SYBR Green for qPCR quantitation using 40 cycles of amplification on a Light Cycler 480 (Roche Applied Science). For enrichment experiments, 100 nM total aptamer library (either 90% or 99% *scr*Toggle-25) was incubated with $10^7$ *t*RBCs for 20 minutes at room temperature with continuous gentle inversion before being passed through the device. In these enrichment

experiments, where the recovered aptamer sample contained two species, samples were divided in half after recovery and precipitation, followed by aptamer-specific reverse transcription and qPCR, as described above.

### *2.6.6 I-SELEX with tRBCs*

The DNA template for the random library (containing a 50-nt randomized region) was chemically synthesized (Integrated DNA Technologies). The primers used for RT and PCR amplification of the library are summarized in *Table 2*. A 2′-fluoro-pyrimidine RNA library containing approximately $3 \times 10^{14}$ unique sequences was synthesized using the DuraScribe T7 Transcription Kit (Epicentre). RNA was denatured at 65°C for 5 minutes, followed by refolding for 10 minutes at room temperature. The aptamer library was then incubated with $10^8$ *s*RBCs in 1 mL TBB for 30 minutes at room temperature with continuous gentle mixing. *s*RBCs and the aptamers bound to them were removed by centrifugation. The supernatant was incubated with $10^6$ *t*RBCs for 60 minutes at room temperature with continuous gentle mixing. After incubation, the entire binding reaction was partitioned in a single pass through the I-SELEX device at a flow rate of 150 μL $min^{-1}$ with sheath buffer (TBB) pumped at 1500 μL $min^{-1}$. Cells were recovered and aptamers eluted as described above for enrichment experiments. The recovered aptamers were RT-PCR amplified using an empirically determined minimum number of PCR cycles, minimized to prevent formation of truncation or PCR giant products (14 cycles on average). Half of the recovered PCR product (~1 μg) was stored, and the remainder used for *in vitro* transcription (37°C for 6-15 hours) to prepare RNA library for the subsequent round. Remaining template DNA was removed by Turbo DNase (Life Technologies).

RNA was purified by phenol-chloroform extraction and ethanol precipitation, then re-dissolved in dd$H_2O$. Five rounds of selection were performed.

A new device was used for each I-SELEX experiment, however, the inertial devices can be reused up to 20 times if properly washed. Prior to reuse, devices were washed extensively with 10 mL TBB, then 10 mL water, then 2 mL isopropyl alcohol, after which air was pumped into the device to remove all remaining liquid. The device was set on a hot plate (85°C) for 6-12 hours to solidify the PDMS-glass bond. Before subsequent each subsequent use, the device was washed again with 10 mL TBB, a fraction of which (100 μL) was periodically captured and analyzed by qPCR to ensure no sequences were carried over from a prior partitioning.

### *2.6.7 Flow Cytometry*

To test binding of Toggle-25 to *t*RBCs versus *s*RBCs, Toggle-25 was fluorescently labeled by addition of a single 3′-amino-2′,3′-ddATP (TriLink Biotechnologies) by Poly(A) Polymerase (New England BioLabs) followed by incubation with DyLight 488 NHS ester (Pierce). Varying amounts of Toggle-25 were incubated with $10^6$ cells in 200 μL TBB containing 0.1% BSA for 3.5 hours at room temperature. Cells were washed twice with TBB + 0.1% BSA prior to resuspension in 90 μL TBB, followed by analysis by flow cytometry (FL1-H channel).

To test binding of I-SELEX aptamer **5-12** to *t*RBCs, Toggle-25, *scr*Toggle-25 and **5-12** were synthesized with a 3’ 24-nt extension (5′-GAAUUAAAUGCCCGCCAUGACCAG-3′)[106] using PCR extension oligos CMB153, CMB154 and CMB152, respectively. A Capture Oligo (CO) (5′-Biotin-

CTGGTCATGGCGGGCATTTAATTC-3′) complementary to the aptamer extension was synthesized and fluorescently labeled with streptavidin-phycoerythrin (SA-PE). Aptamers were incubated with equimolar concentrations of CO for 5 minutes at 75°C then cooled slowly to 4°C. SA-PE was incubated in a 1:2 molar ratio of aptamer-CO:SA-PE for 15 minutes at room temperature. Importantly, free biotin-binding sites were capped with >10-fold molar excess of free biotin by incubation with 20 µL biotin-saturated PBS, pH 7.4 for 15 minutes at room temperature. 100 nM CO/SA-PE labeled aptamer (or 100 nM CO/SA-PE alone) was incubated with either $10^6$ *t*RBCs or *s*RBCs in 100 µL TBB with 1 µg BSA and 0.25 µg yeast tRNA for 1 hour at room temperature. Cells were washed with TBB and resuspended in 50 µL TBB prior to flow cytometry (FL2-H channel).

### *2.6.8 Bio-layer interferometry binding studies*

Aptamer binding kinetics were determined using a BLItz device and Streptavidin (SA) Dip and Read biosensors (ForteBio). TBB was used for probe hydration (10 minutes) and all baseline readings, aptamer dilutions, and dissociation steps. Thrombin-BFPRck (Haematologic Technologies) at 10 nM was immobilized on a SA biosensor via a 300 second loading incubation. Aptamers were *in vitro* transcribed, DNase treated, and refolded as described above, then incubated with thrombin-loaded SA biosensors (association: 180 seconds; dissociation: 180 seconds) at various concentrations. Probes were regenerated using the following protocol: 3 × {60 second incubation in regeneration buffer (1 M NaCl, 1 mM NaOH) followed by 60 second incubations in TBB}. The probe was regenerated at least once prior to collection of binding data using BLItz software for analysis.

### *2.6.9 List of primers used in this work*

| | |
|---|---|
| CMB49 | CCGCTCGAGTAATACGACTCACTATAGGGAGAGGAA |
| CMB50 | CTTCAGCTTTGTTCCCCATCCCTCTTCCTCTCCCTATAGTGAGTC |
| CMB51 | GATGGGGAACAAAGCTGAAGTACTTACCCAAGATCATCCCGAACGA |
| CMB56 | TCGACCTCTGGGTTATGTCGTTCGGGATGATCTTGGG |
| CMB77 | GGGAGAGAGGAAGAGGGATGGG |
| CMB94 | TCGACCTCTGGGTTATGTCGTTC |
| CMB95 | CCGCTCGAGTAATACGACTCACTATAGGGAGACAAGAT |
| CMB96 | GCAGCGTTCCTCGATGGCCTTGATCTTGTCTCCCTATAGTGAGTCG |
| CMB97 | CATCGAGGAACGCTGCCTACACACATGGACATAAAACAAGAGCCGA) |
| CMB98 | CCATTTTCTCGCCCTCTTCGGCTCTTGTTTATGTCCATG |
| CMB104 | TTCTCGCCCTCTTCGGCTCTTGTTTA |
| CMB106 | GAGACAAGATCAAGGCCATCGAGGAA |
| CMB107 | CACTATAGGGAGCTCAGAATAAACGCTCAAACGAACGTACAAGTTATGAGAACTG |
| CMB108 | CGAATGAGTGTGGATGACAATAGGGAGGTCAGTTCTCATAACTTGTACGTTCGT |
| CMB109 | GCCGGATCCGGGCCTCATGTCGAATGAGTGTGGATGACAATAGG |
| CMB112 | CACTATAGGGAGCTCAGAATAAACGCTCAACAACGGATCACACGCAAGCGAA |
| CMB113 | GCGACCCTTAGACCCGAAGGACATAGATTCGCTTGCGTGTGATCCGTTGTTG |
| CMB114 | GCCGGATCCGGGCCTCATGTCGAAAGCGACCCTTAGACCCGAAGGACATAGA |
| CMB116 | AGTCTCTCCTAGAGGGTGACCGCGTCACCCCGACTGAGCTCAGTAACTTGA |
| CMB117 | GCCGGATCCGGGCCTCATGTCGAAACAGAGTCTCTCCTAGAGGGTGACGCGT |
| CMB119 | CGAACCACTACAATATGATATTAGATCTCCAGATCGGATATATTAAATTTGATCTTG |
| CMB120 | GCCGGATCCGGGCCTCATGTCGAACCACTACAATATGATATTAGATCT |
| CMB122 | CTCGCAAAAAGACTTGGGGAAGGAGCGAAAAAGTGCAGTCTCAGGC |
| CMB123 | GCCGGATCCGGGCCTCATGTCGAAAACTCGCAAAAAAGACTTGGGGAAGGA |
| CMB125 | TCGCTATTTGGCGGTAGAGCTCTACCCCTCTCCCCGGAACTCAGTAACTTTGAG |
| CMB126 | CACTATAGGGAGCTCAGAATAAACGCTCAAGTTACTGAGCTCAGTCGGGGT |
| CMB127 | GCCGGATCCGGGCCTCATGCTGAGCTCAGTAACTTGAGCGTTTATTCTGAGCTCCCTAT |
| CMB130 | CACTATAGGGAGCTCAGAATAAACGCTCAAACCGATGAGCTCAGTCGGGGT |
| CMB131 | AGTCTCTCCTAGAGGGTGACGCGTCACCCCGACTGAGCTCATCGGTTTGA |
| CMB132 | GCCGGATCCGGGCCTCATGTCGAAACAGAGTCTCTCCTAGAGGGTGACGCGT |
| CMB133 | ATAGGGAGCTCAGAATAAACGCTCAAGATCAAATTTAATATATCCGATCTGGAGATCTAA |
| CMB134 | CTATAGGGAGCTCAGAATAAACGCTCAACTGCCTGAGACTGCACTTTTTCG |
| CMB139 | CTCTCCCCGGAACTCATCGGTTTTGAGCGTTTATTCTGAGCTCCCTATAGTG |
| CMB140 | TCGCTATTTGGGCGGTAGAGCTCTACCCCTCTCCCCGGAACTCATCGGTTTTGAG |
| CMB141 | GCCGGATCCGGGCCTCATGTCGAATCGCTATTTGGGCGGTAGAGCTC |
| CMB142 | CACTATAGGGAGCTCAGAATAAACGCTCAAAGTTACTGAGTTCCGGGGAGAG |
| CMB152 | CTGGTCATGGCGGGCATTTAATTCGGGCCTCATGTCGAAACAGAG |
| CMB153 | CTGGTCATGGCGGGCATTTAATTCTCGACCTCTGGGTTATGTCGTT |
| CMB154 | CTGGTCATGGCGGGCATTTAATTCCCATTTTCTCGCCCTCTTCG |
| SELEX Library template | CCGAAGCTTAATACGACTCACTATAGGGAGCTCAGAATAAACGCTCAA-[$N_{50}$]-TTCGACATGAGGCCCGGATCCGGC |
| SELEX Forward Primer | CCGAAGCTTAATACGACTCACTATAGGGAGCTCAGAATAAACGCTCAA |
| SELEX Reverse Primer | GCCGGATCCGGGCCTCATGTCGAA |
| Capture Oligo | Biotin-CTGGTCATGGCGGGCATTTAATTC |

*Table 2. Primers used in Chapter 2.*

# CHAPTER 3: GENERATION AND CHARACTERIZATION OF APTAMERS AGAINST MALARIA-INFECTED RED BLOOD CELLS

## 3.1 Introduction

### *3.1.1* Plasmodium falciparum *parasite directs changes to the infected red blood cell*

The human malaria parasite *Plasmodium falciparum* spends the majority of its asexual life cycle within the host red blood cell (RBC). Without endogenous RBC cellular machinery necessary for protein or membrane production and export, the parasite must direct the remodeling of the infected RBC (iRBC) for its survival (*Figure 11*).

When a merozoite invades an uninfected RBC, it creates a parasitophorous vacuole that separates it from the RBC cytosol. In order to interact with the extracellular environment, the parasite must synthesize proteins in its own cytosol and selectively traffic them across multiple membranes into the iRBC. In mature, late stage trophozoite- and schizont iRBCs, both the internal and external surfaces of the erythrocyte membrane are structurally and biochemically modified. Major virulence proteins, such as the PfEMP1 family, are synthesized in the parasite cytosol or endoplasmic reticulum and must be transported to the parasite plasma membrane, across the parasitophorous vacuole to the outer parasitophorous vacuole membrane, into the iRBC cytosol. Many parasite proteins are targeted to Golgi-esque membranous structures known as Maurer's Clefts, and others are ultimately directed to knob-like structures on the iRBC plasma membrane.

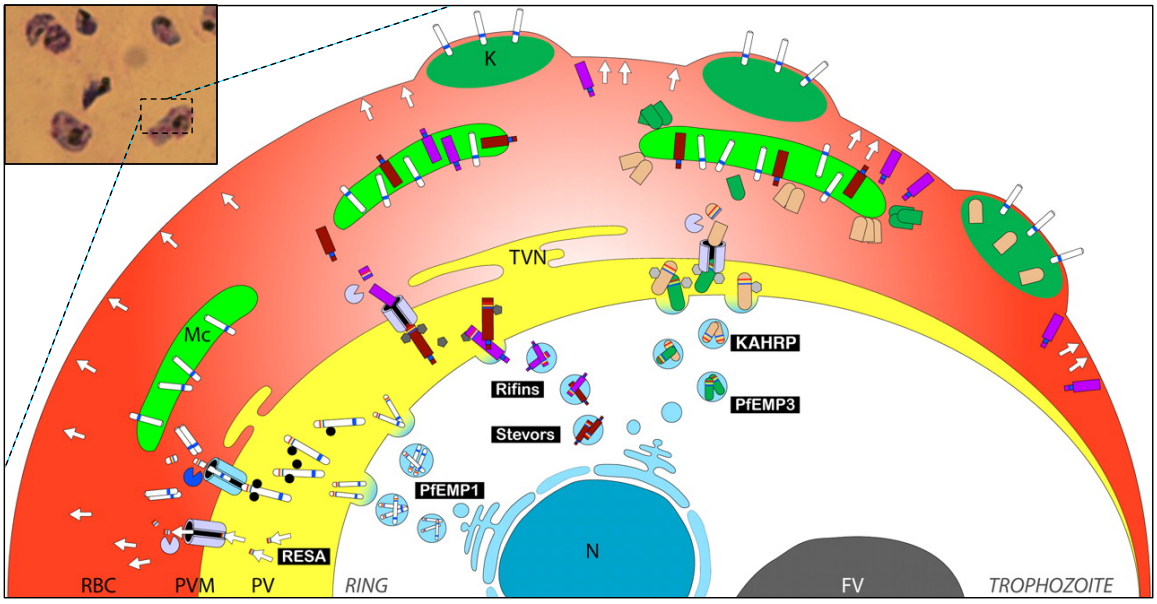


*Figure 11. Extensive parasite-driven modifications to the infected red blood cell.* Late stage trophozoite and schizont parasite-iRBCs are visualized under a light microscope using Giemsa staining (top left). The food vacuole (FV) can be seen as a dark black spot due to the presence of large quantities of malaria pigment, or hemozoin. The parasite creates many cytosolic and surface membrane modifications to enable late-stage iRBCs to interact with their environment for survival and replication. Beginning in the early ring stage, the parasite exports a variety of structural (KAHRP, PfEMP3), variant (Stevors, Rifins), or surface-exposed (RESA, PfEMP1) proteins that are encoded in the nucleus (N). These proteins must be transported across the parasitophorous vacuole (PV) to Maurer's Clefts (Mc) in the iRBC cytosol via the tubulovesicular network (TVN). Adhesion and potentially other antigenically variant proteins are then exported to knob (K) structures at the iRBC surface. Figure adapted from Marti *et al.*[107].

Some parasite proteins destined for the iRBC plasma membrane are primarily structural, such as the Knob-Associated Histidine Rich Protein (KAHRP) responsible for giving iRBCs their characteristic "knobby" appearance and significantly decreased overall membrane deformability.[17,19,108] Other select proteins are presented to the extracellular environment for nutrient acquisition, waste export, cytoadhesion, and immune evasion.[109] Many adherence proteins are localized at these knobs and create

concentrated cell-cell contacts important for iRBC cytoadhesion. These biochemical and morphological membrane alterations enable iRBC sequestration and are consistently observed in severe malaria cases, and are the basis of aptamer-based differentiation between infected and uninfected RBCs.

### *3.1.2 Molecular mechanisms of iRBC sequestration*

In *P. falciparum* infection, parasite proteins on the iRBC membrane are exposed to the extracellular environment and interact with surface receptors of the endothelial cells of tissue microvasculature. Similar to leukocyte adhesion, iRBCs roll along the vascular epithelium making nonspecific interactions that help to slow down the iRBC and orient parasite ligands for binding to specific host-cell receptors[20,29]. These specific, high-affinity binding events are understood to be the primary mechanism in iRBC sequestration. The degree of sequestration can be increased via three distinct mechanisms: auto-agglutination (iRBCs binding to iRBCs); rosetting (iRBCs binding to uninfected RBCs); and platelet-mediated adhesion of both iRBCs and RBCs, all of which involve PfEMP1 protein binding[17,29,110].

*P. falciparum* proteins documented in sequestration events include: *Plasmodium falciparum* Erythrocyte Membrane Protein 1 (PfEMP1);[45] RIFINS (of the Repetitive Interspersed Family, or *rif*, genes);[111] and STEVOR (of the Subtelomeric Variable Open Reading Frame, or *stevor,* genes) variable surface protein families[112]; cytoadherence-linked asexual gene 9 (CLAG9), a helper protein that interacts with PfEMP1 variant VAR2CSA in a way that at least a portion of CLAG9 is surface-exposed[113]; sequestrin, a CD36 recognizing protein[114]; and TF, a putative transferrin receptor[115]. Undoubtedly,

many more parasite-derived proteins that are trafficked to the iRBC plasma membrane remain to be identified and functionally characterized.

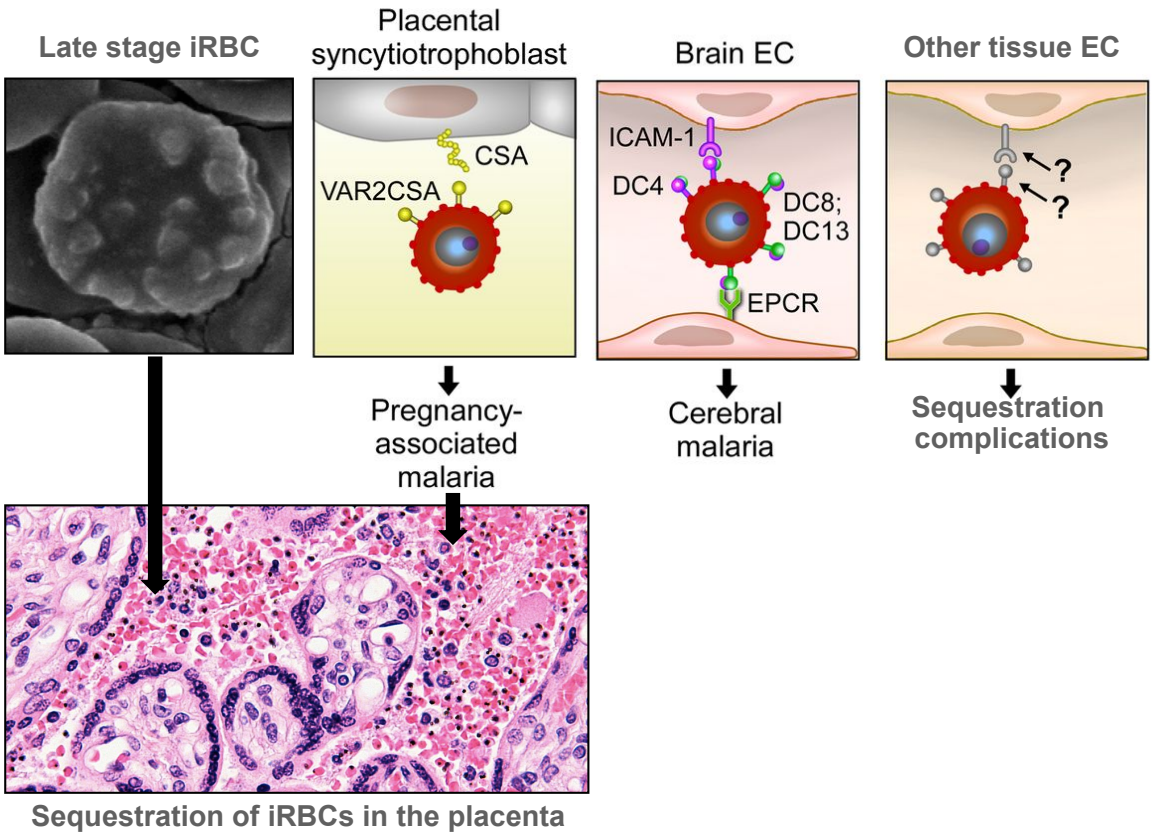


*Figure 12. Molecular mechanisms of sequestration.* Late stage iRBCs express adhesion ligands from the surface of knob structures produced by the parasite. The molecular identity of these adhesion molecules determines which receptor is targeted on host endothelial cells (EC) and how that binding event contributes to severe disease. When the PfEMP1 family protein VAR2CSA is expressed, the iRBC is able to bind CSA on placental syncytiotrophoblasts, causing sequestration in the placenta and pregnancy associated malaria. Similarly, iRBCs expressing PfEMP1 proteins with specific domain cassettes (e.g. DC4, DC8, or DC13) may bind to receptors like ICAM-1 and EPCR on brain EC and are associated with severe disease such as cerebral malaria. Other tissue-specific parasite ligand-host receptor interactions have yet to be fully identified. Figure credits: SEM image by Geoff Williams (Brown University). Illustration partially adapted from Aird *et al.*[116] Placenta sequestration image from Wikimedia Commons[117].

The PfEMP1 family of variant surface proteins interacts with specific receptors that determine which host cell types they may bind and with what affinity (*Figure 12*). The endothelial class II scavenger receptor CD36 mediates iRBC attachment through specific interactions with PfEMP1 proteins.[118] Sequestration in brain microvasculature is mediated by both CD36 and intercellular adhesion molecule 1 (ICAM-1). [118] Chondroitin-4-sulfate (CSA),[26] a sulfated glycosaminoglycan highly expressed in the placental microvasculature, is also able to mediate iRBC sequestration through interactions with PfEMP1 variant VAR2CSA.[119] CD36 and CSA are the only host-cell receptors shown to provide stable adherence points for iRBCs[120]; however, other cell factors such as Vascular Cell Adhesion Molecule 1 (VCAM-1) and P-selectin may promote rolling adhesion.[121] In addition, thrombospondin, Platelet Endothelial Cell Adhesion Molecule 1 (PECAM1/CD31), E-selectin, complement receptor 1, immunoglobulin M, and heparin sulfate have all been implicated in sequestration or rosetting events.[122] Other tissue-specific receptors may exist and have yet to be identified.

### *3.1.3 PfEMP1 expression, regulation, and organization*

Only one PfEMP1 protein, encoded by any one of ~60 *var* genes, is expressed on the surface of the iRBC during the 48-hour intraerythrocytic development cycle (IDC), detectable starting 16 hours post-invasion.[21] *Var* genes are regulated at the transcription level[123] using epigenetic modifications, including histone acetylation of inactive *var* genes,[124] subnuclear localization with chromatin,[125] interactions between the upstream and intronic *var* promoters,[126,127] and activation by anti-sense long noncoding RNAs.[128]

Such tight transcriptional control ensures that only a single *var* gene produces protein-coding RNA at a time.

At schizogeny, the daughter parasites have at most a 2%[110] (but more commonly <1%[129]) probability of switching variants that may increase chances of immune system evasion but also may change the parasite's adhesion phenotype. All mature *falciparum*-iRBCs sequester, but not all *falciparum* infections lead to severe malaria complications.[34] While parasite variant surface antigen expression on a single iRBC is homogenous for one PfEMP1 type, the expression across a population of sequestered iRBCs is quite heterogeneous and may affect tissue distribution and pathogenesis. To what extent each PfEMP1 variant and its contribution to iRBC population sequestration phenotype affects the development of severe malaria has yet to be determined and could greatly influence therapeutic drug design. Progress in this area of study awaits development of robust methods to monitor iRBC sequestration *in vivo* in real time that could be used in animal models of human *P. falciparum* infection that are currently being developed and ultimately in humans to establish drug efficacy and patient standard of care.

*Var* genes are grouped using sequence analysis upstream non-coding regions into three major subfamilies, subtelomeric UpsA and UpsB genes and centrally located UpsC genes, and three unusual variants, *var1csa, var2csa,* and type 3 *var*[131]. The extracellular PfEMP1 adhesion domains are encoded in the first exon of a two-exon *var* gene; the second exon encodes for a small transmembrane sequence and a cytosolic acidic terminal sequence that contains *cis*-information for protein trafficking to the RBC plasma membrane.[115] The extracellularly exposed PfEMP1 protein domains form together the 200-350 kDa "ligand" that is bound by host-endothelial cell receptors, an interaction that

is in turn responsible for iRBC sequestration within tissue microvasculature[132] (*Figure* 13).

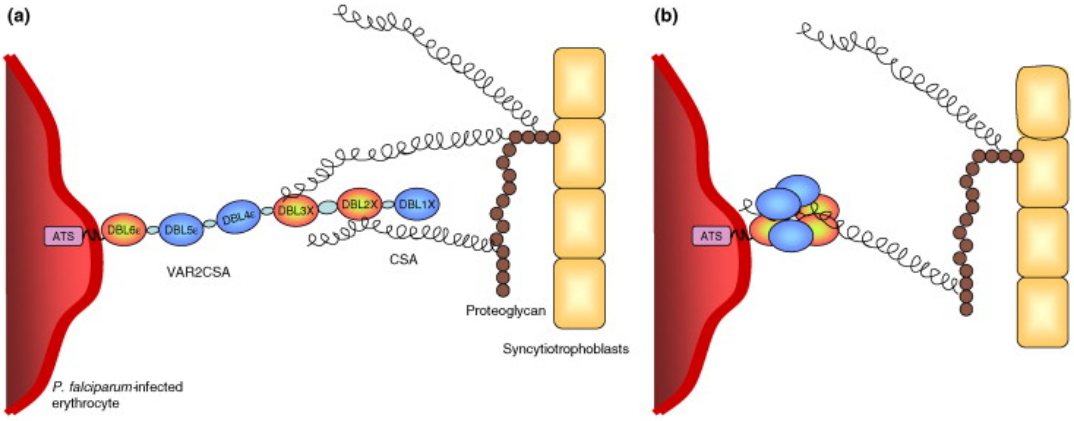


*Figure 13. Folding of PfEMP1 adhesion proteins is unknown and likely affects binding to host receptors.* PfEMP1 proteins are large (~350 kDa in the case of VAR2CSA) multi-domain extracellular proteins made up of a number of Duffy Binding Like (DBL) subunits anchored by a single transmembrane helix and a cytosolic acidic terminal sequence (ATS). These proteins interact with specific receptors on host cells such as chondroitin sulfate (CSA) decorations on proteoglycans on placental cells. Because it is unknown whether or not VAR2CSA domains **(a)** interact independently and modularly or **(b)** in collaboration as part of a large, globular structure, it is imperative that selections targeting VAR2CSA-expressing iRBCs be performed with whole proteins in their native context. Figure adapted from Dahlback *et al.*[130]

The extracellular domain consists of a variable array of three distinct protein domains: Duffy-Binding Like (DBL) domains, of which there are six classes (DBL-α through DBL-ε, and a small subset that do not fall into these categories denoted DBL-X); Cysteine-rich Interdomain Regions (CIDR) of two classes (α and non-α); and Constant2 (C2) domains[17,34,115]. Even among classes that share a common domain family, there is very little sequence homology, which, coupled with the switching of *var* gene expression, has proved to be a major challenge for vaccine development.

### *3.1.4 Identification and study of the parasite surface proteome*

While parasite-induced changes in the variety of ligands displayed on the surface of infected RBCs is recognized as an important mechanism mediating severe malaria, a detailed characterization has been impeded by limitations in the technologies available for interrogating the infected RBC surface proteome. Bioinformatics approaches based on detecting signature 'PEXEL' motifs involved in trafficking proteins to the RBC compartment have been used to predict a relatively large number of putatively exported proteins[133-135]. However, not all exported proteins are captured by this analysis, as some PEXEL-negative proteins (PNEPs) are also trafficked to the RBC[136,137]. Furthermore, it is not possible to determine *a priori* which of these parasite-exported proteins will be displayed on the infected RBC surface[136,137]. Mass spectrometry-based proteomics intended to selectively and directly interrogate the *P. falciparum* infected RBC surface have revealed a limited number of candidates, but surface localization for the majority of these has not been established[138]. However, many non-exported protein contaminants were present within the putatively surface protein enriched fraction, thus compromising how confidently surface localization can be assigned. Furthermore, known surface-expressed proteins, such as PfEMP1, while detectable by Western blot are under-represented in the dataset. Thus, this approach likely underestimates and in some instances, misrepresents the repertoire of parasite proteins present on the parasite-infected RBC surface.

Specific affinity reagents such as antibodies can be powerful tools for determining the cell surface localization and, through pull-down approaches coupled with mass spectrometry, the identity of target proteins. Only a limited number of antibody reagents–

mostly to a subset of PfEMP1 proteins–are available. However, even when robust antibody reagents are identified, these are available in limited quantities and relatively costly to replenish. We have sought to address this challenge by establishing a new strategy for increasing access to diverse sets of nucleic acid aptamer affinity reagents capable of recognizing distinct epitopes on the surface of parasite-infected RBCs. We reason that aptamers could be ideal affinity reagents to develop as they can: (1) bind their targets with similarly high affinities and specificities as antibodies; (2) be produced inexpensively *in vitro*; and (3) be identified through an *in vitro* selection process (SELEX)[50,51] using live, whole parasite-infected RBCs as targets. Importantly, the latter ensures that recovered aptamers inherently recognize their diverse binding partners when expressed in their native context and natural abundance on the complex parasite-infected RBC surface.

Some attempts have been made to identify smaller adhesion epitopes by limiting targeting assays to individual recombinant PfEMP1 domains[130]. In the case of the VAR2CSA PfEMP1 variant and its CSA placental receptor—perhaps the most direct and best understood association found between iRBC and host cell—several studies have reported CSA binding in many *in vitro* systems to the DBL2X[139] and DBL3X[140] domains. More recent evidence refuted specific binding claims by demonstrating that these domains can bind a number of negatively charged glycosaminoglycans, favoring an electrostatics-dependent explanation of the observed interaction.[141] In total, three of the six DBL domains of VAR2CSA (DBL2X, DBL3X, and DBL6ε) show significant *in vitro* binding of CSA and the remaining three (DBL1X, DBL4ε, and DBL5ε) do not. It is anti-DBL4ε antibodies, however, that appear to have the greatest inhibitory effects of CSA-

mediated adhesion of whole-iRBCs from clinical isolates, despite having no measurable CSA affinity *in vitro*[142]. In addition, while it is known that VAR2CSA is the *exclusive* PfEMP1 protein expressed by iRBCs competent for CSA-dependent sequestration, recombinantly expressed domains from other PfEMP1 variants have shown CSA binding *in vitro*.[141] These conflicting studies highlight the limitations of working with single PfEMP1 domains *in lieu* of live, intact iRBCs and demonstrate that it is not possible to predict iRBC adhesion phenotypes from only single domains. Therefore it is imperative that iRBC targeting efforts, specifically those aimed at studying or interfering with sequestration, preserve the targeted protein in its native cell surface context.

A single study used recombinant polyhistidine- and glutathione *S*-transferase (GST-) tagged DBL1α, a PfEMP1 domain indicated in rosetting phenotypes, as targets for enriching RNA aptamers[143]. Their work aimed to demonstrate specific aptamer binding to DBL1α but failed to rule out aptamer binding to the recombinant protein's GST-tag. Additionally, Barfod and colleagues intended to show aptamer binding to DBL1α-expressing *P. falciparum* cultured iRBCs, but had no alternative means to verify DBL1α presence on the surface of iRBCs nor did they rule out aptamer binding to endogenous RBC surface moieties (i.e. no negative selections were performed on uninfected RBCs). Finally, disruption of rosettes was statistically significant only at near-micromolar levels, a concentration of aptamer they did not reach when testing their negative control. While this study remains the only published aptamer-based probe of *P. falciparum* iRBC-derived targets, it is unsuitable for further development as either a diagnostic or therapeutic agent.

## 3.2 Overview

By targeting live whole iRBCs, we enable selection of probes that bind surface-exposed parasite-derived proteins in their native context. This is essential for capturing true adhesion phenotypes that are characteristic of *in vivo* infections. An important challenge inherent to this approach, however, is that many distinct targets will be present on the cell surface during selection, and these will drive enrichment of diverse aptamer solutions. Therefore, to prevent high false discovery rates that would compromise efficient recovery of high affinity aptamers, our proposed strategy demands a sufficiently stringent selection process to minimize enrichment of non-binding sequences. Because of its stringent partitioning while permitting recovery of diverse sequence solutions, I-SELEX represents an ideal strategy for creating a broad set of aptamer affinity reagents that can be used to more finely map the surface proteome of *P. falciparum* infected RBCs. Here, we use I-SELEX with unmodified, live parasite-infected RBCs to identify a rich pool of aptamers that preferentially and selectively bind parasite-infected RBCs. We demonstrate that aptamer solutions interact with distinct protein surface targets, including VAR2CSA, the PfEMP1 protein variant that mediates binding to CSA in placental malaria.

## 3.3 Results

### *3.3.1 Selecting aptamers against the surface of malaria parasite-infected red blood cells using I-SELEX*

We used the same library (with ~$10^{14}$ diversity) as in Chapter 2 in a *de novo* I-SELEX experiment in which RBCs infected with the *P. falciparum* CS2 strain were used as whole cell targets (*Figure 14*).

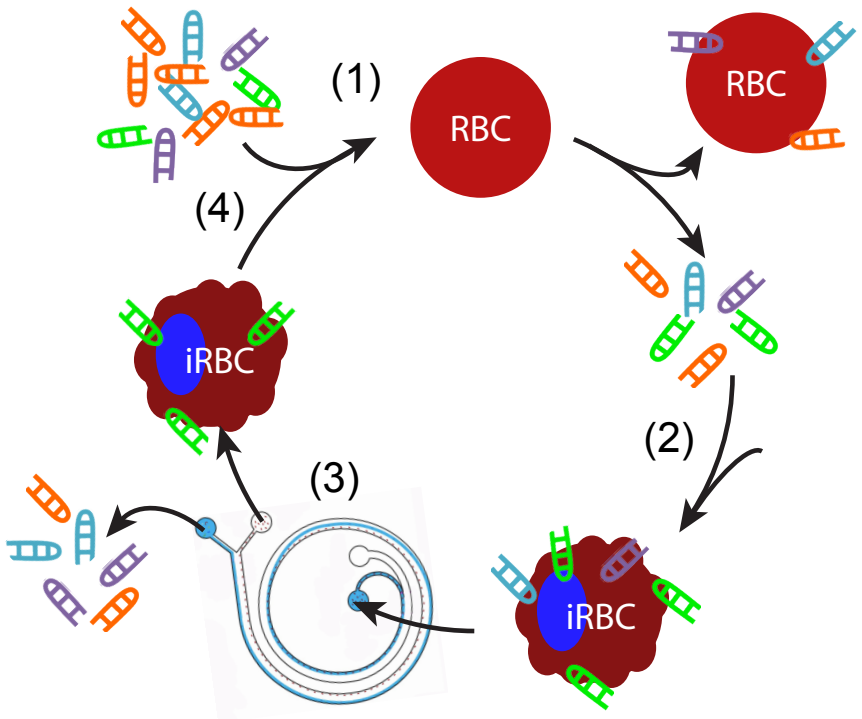


*Figure 14. I-SELEX with malaria-infected red blood cells.* (1) A random RNA library is first incubated with uninfected, mock-cultured red blood cells (RBCs) as a negative selection step. Sequences that bind RBCs are removed and (2) surviving sequences are incubated with MACS-enriched late stage infected red blood cells (iRBCs) in a positive selection step. (3) The reaction mixture is partitioned with a single pass through the I-SELEX microfluidic device, where nonbinding sequences are removed in the waste and binding aptamers are recovered from the cell surface. (4) Surviving sequences are eluted from the cell surface and amplified *in vitro* prior to the next round of selection. In both selection schemes 1 (consistent stringency) and 2 (increasing stringency), eight rounds of selection are performed.

The CS2 strain stably expresses a single PfEMP1 variant, VAR2CSA, which is associated with placental malaria, and does not undergo the normal process of switching which *var* gene is expressed[119,144-146]. We designed our selections to recover aptamers capable of preferentially interacting with any molecular feature(s) present on CS2-infected but not uninfected RBCs. This was achieved by negatively selecting the library on uninfected RBCs and positively on parasite-infected RBCs during each round. In I-SELEX Rounds 6-8, we pursued two selection schemes in parallel. In scheme 1, we increased selection stringency through a 5-fold dilution of the positive selection mixture relative to earlier rounds, while in scheme 2, we maintained the same level of stringency as in Rounds 1-5.

After eight rounds of selection, we determined a limited number of sequences from the enriched pools (16 and 17 from schemes 1 and 2, respectively). Approximately two-thirds of the sampled sequences were unique, and no strongly conserved motifs amongst these could be detected by MEME[93]. However, several sequences were represented multiple times (*Table 3*). From scheme 1, **8.1-1** and **8.1-2** were represented four and two times, respectively, while in scheme 2, **8.2-1** and **8.2-2** were each represented three times.

| Clone ID | Copy # | ΔΔCp | P value | Sequence of variable region |
|---|---|---|---|---|
| | | | | **Selection 1** |
| **8.1-1** | 4 | 3.115 | 0.0002 | CAACGGATCACACGCAAGCGAATCTATGTCCTTCGGGTCTAAGGGTCGCT |
| **8.1-2** | 2 | 3.405 | 0.027 | GTCAGAGTATGGGTACTGCAAGCTGCATGTGTTGCTCCGCTTAGACCCTA |
| **8.1-3** | 1 | 1.476 | > 0.1 | TCCCGCGGCCATGGCGGCCGGGAGCATGCGACGTCGGGCCCAATTCGCCC |
| **8.1-4** | 1 | 1.965 | > 0.1 | GTCCGGGTAGCGAGAGGACTTGCGACGTTTGGTGAGCATAAGCTGTAGAC |
| **8.1-5** | 1 | 3.18 | 0.0378 | GTAAGCGGACGATGGTGCGTGGGCGAATTGATCAGTACTTACTGTGCGAA |
| 8.1-6 | 1 | - | - | GTGGAATACAACCCCGACTTAAAAACCTAACCGGATTCCGTTTGGCGCAA |
| 8.1-7 | 1 | - | - | GGCATCGATTGTATTACTCATGTCCTCCGAGTACTCCGAATGGCCGGCGT |
| 8.1-8 | 1 | - | - | GTGAGTGTCGTTTGACAATCGGAGCTAAGATGATGGCCGTGGTCAACGGA |
| 8.1-9 | 1 | - | - | TGTTAGAGATTTCTTGGAGCGTCGAAAGTAGGATGCCAAGATCGGTTGGA |
| 8.1-10 | 1 | - | - | GAGTGGTATCGGATCGGACGAATAGATTGCCGCGTTAGGATCGTACCTGA |
| 8.1-11 | 1 | - | - | TTTGGAGCGATATGCGATATATCGATTGTAGATGAAGTCATGCAGTGGAA |
| 8.1-12 | 1 | - | - | GACAAAGATCCTAAAACATGCGCGTAACCGGACAGTATTGTAGCTTTGTG |
| | | | | **Selection 2** |
| **8.2-1** | 3 | 2.631 | 0.0159 | CCAGGGGTAAGTTAGTGTAGGACTTGTTCTACATAGGATCGAATCGGTGG |
| **8.2-2** | 3 | 3.388 | 0.0243 | CTCGGATACTTAATAATAGAATTGGCCCAGACGCATGCATGATCCGCCAG |
| **8.2-3** | 1 | 3.125 | 0.0131 | GGCCTATCTGGGAGGAAAGCAGCCCAATTCGAACAGGTATGTGTGATCTG |
| 8.2-4 | 1 | - | - | AGGAAACTAATGTTGATACAACTGGGTACAATTAGTGATCCCGGTCATCT |
| 8.2-5 | 1 | - | - | CTTTTGTTGTGATCGTTTATCCTTAATGGTTTATCCGCAGCTGGGGATA |
| 8.2-6 | 1 | - | - | GGAGTATCAATATCGGCACAGGTATGAGCAATCAGTTATGCACGTTTCGC |
| 8.2-7 | 1 | - | - | GGGGATTGGGTGTGCAGTCCTGTAGAGTAGGTTCACGTAGTTAGCGTTCA |
| 8.2-8 | 1 | - | - | AATTGGTCCGAATGTACGGAGTTTTCGTCTAGATGCTAGGAAATGGTGCC |
| 8.2-9 | 1 | - | - | GTATAGGGTACTGTTCCTGCTGCATTGGGCAGGTCATATAAGTCAGTTCT |
| 8.2-10 | 1 | - | - | TGGTGGTCGTCCTCAAAAACCGCCTATTTGCGATGGATAGGCGTATTGCTC |
| 8.2-11 | 1 | - | - | GCAATGATTTGCATATCCTTCTGAGCTGTGATCACGCTAACATAACAGTC |
| 8.2-12 | 1 | - | - | TGACTTAAATGCCGAAGCGTTGACGTGATGGAGGATGTTGCGAACATTTC |
| 8.2-13 | 1 | - | - | TGAAAGCACTACATTTATTGGTGATGAAAGTGCGTGATGCTGTGTTCCGC |
| | | | | **Scrambled Sequences** |
| **scr-8.1-1** | n/a | 1.243 | null | ATGTCTCCAGCTCTTGTGGCGAACCCAAGCGGGTTGACCAGAATGCATCA |
| **scr-8.2-1** | n/a | 1.302 | null | GAATGGTGTATATGTTGACAGTCAAGCGTCTCAGGTGCGGTAAGTCAGGT |

*Table 3. Sequences recovered from malaria parasite-infected red blood cell I-SELEX.* Clones are grouped by the stringency of the selection from which they were derived: scheme 1 (increased stringency for Rounds 6-8) and scheme 2 (consistent stringency across all 8 rounds). Tested sequences are shown in bold alongside their enrichment values (ΔΔCp) and the statistical significance (P value) of enrichment over scrambled negative control sequences (**scr8.1-1** and **scr8.2-1**).

### *3.3.2 Enrichment assay development for quantifying aptamer recovery*

In order to quantitatively report and rank recovery of library clones, we developed a robust quantitative polymerase chain reaction (qPCR) based enrichment assay (*Figure 15*). We sampled a small fraction (1% by volume) of the initial reaction mixture ("input" sample) prior to sequence incubation with cells. After a binding period, cells are washed using the I-SELEX device and samples are collected from the waste stream (0.1% by volume; "waste" sample) and eluted off the surface of collected cells (100% of cell elution volume; "output" sample).

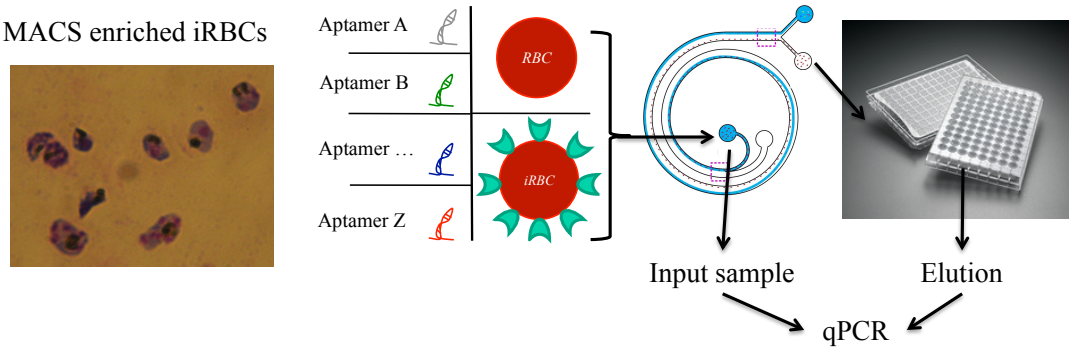


*Figure 15. A schematic of the aptamer enrichment assay.* A single aptamer species is incubated with a target cell type (CS2 iRBCs, protease-treated iRBCs, DC-J iRBCs) or a negative control cell type (uninfected, mock-cultured RBCs). A small fraction of the reaction mixture is measured by qPCR to verify the "input" amount of aptamer. After incubation, the reaction mixture is passed once through the inertial microfluidic device, partitioning unbound aptamers from cells. Aptamers bound to the cell surface are eluted and quantified by qPCR as the "output" amount of aptamer. As measured by qPCR, all input samples have identical Crossing Points (Cp) and output samples are dependent on reaction conditions (e.g. cell type). The difference between input and output Cps (ΔCp) is used to calculate aptamer recovery. Aptamer recovery between target and control cell types (ΔΔCp) is used to establish statistical significance of aptamer enrichment.

By sampling the input, waste, and output streams across samples of constant volumes and concentrations, this allows us to confidently monitor aptamer enrichment. This assay is robust across several logs of RNA recovery concentration and primer concentrations. We independently tested labeling of iRBCs with fluorescently-tagged aptamers. However, we were unable to visualize binding under a variety of conditions. Fluorescent-aptamer labeling of iRBC targets could be limited by the low target abundance or by possible quenching of fluorescent signal at the red cell surface.[147] Ultimately, the qPCR enrichment assay provides a consistent, quantitative method for comparing aptamer recovery across replicates, cell types, and sequences.

### *3.3.3 Malaria iRBC-specific aptamers*

We selected eight sequences total (**8.1-1,2,3,4,5** and **8.2-1,2,3**) and determined that these all selectively bound CS2 parasite-infected RBCs over mock cultured uninfected RBCs (*Figure 16a*). Sequences clustered into high recovery (**8.1-1,2** and **8.2-1,2,3**) and low recovery (**8.1-3,4,5**) groups, with all multiply represented sequences (**8.1-1**, **8.1-2**, **8.2-1** and **8.2-2**) clustering in the high recovery group. To test the sequence specificity of aptamer enrichment, we randomized the variable region of the most highly represented sequence from each selection (***scr*8.1-1** and ***scr*8.2-1**). Both ***scr*8.1-1** and ***scr*8.2-1** were poorly recovered, similar to **8.1-3** and **8.1-4**, and we used these to establish enrichment values ($\Delta\Delta$Cp ~ 1.2-1.3) that define the non-specific binding threshold.

We selected two aptamers from the high recovery group, one from each selection scheme, and calculated apparent $K_d$ values for binding to CS2 parasite-infected RBCs by measuring the amount of recovered aptamer at different concentrations (*Figure 16b*). Using the amount of aptamer recovered from mock cultured uninfected RBCs as the measure of nonspecific binding, we calculate apparent $K_d$ values of 14 ± 10 nM and 84 ± 32 nM for aptamers **8.1-1** and **8.2-1**, respectively.

### *3.3.4 Profiling the interaction of aptamers with the parasite-infected RBC surface*

To understand the nature of the target with which the recovered aptamers interact on the parasite-infected RBC surface, we assessed how recovery of the most represented aptamers from each selection, **8.1-1** and **8.2-1**, is affected by limited trypsin or Proteinase K proteolysis of the parasite-infected RBC surface. We verified successful proteolysis by monitoring loss of glycophorin A from the cell surface, and confirmed that no gross

morphological changes detectable by light microscopy after Giemsa staining had occurred in treated cells (*Figure 16c*).

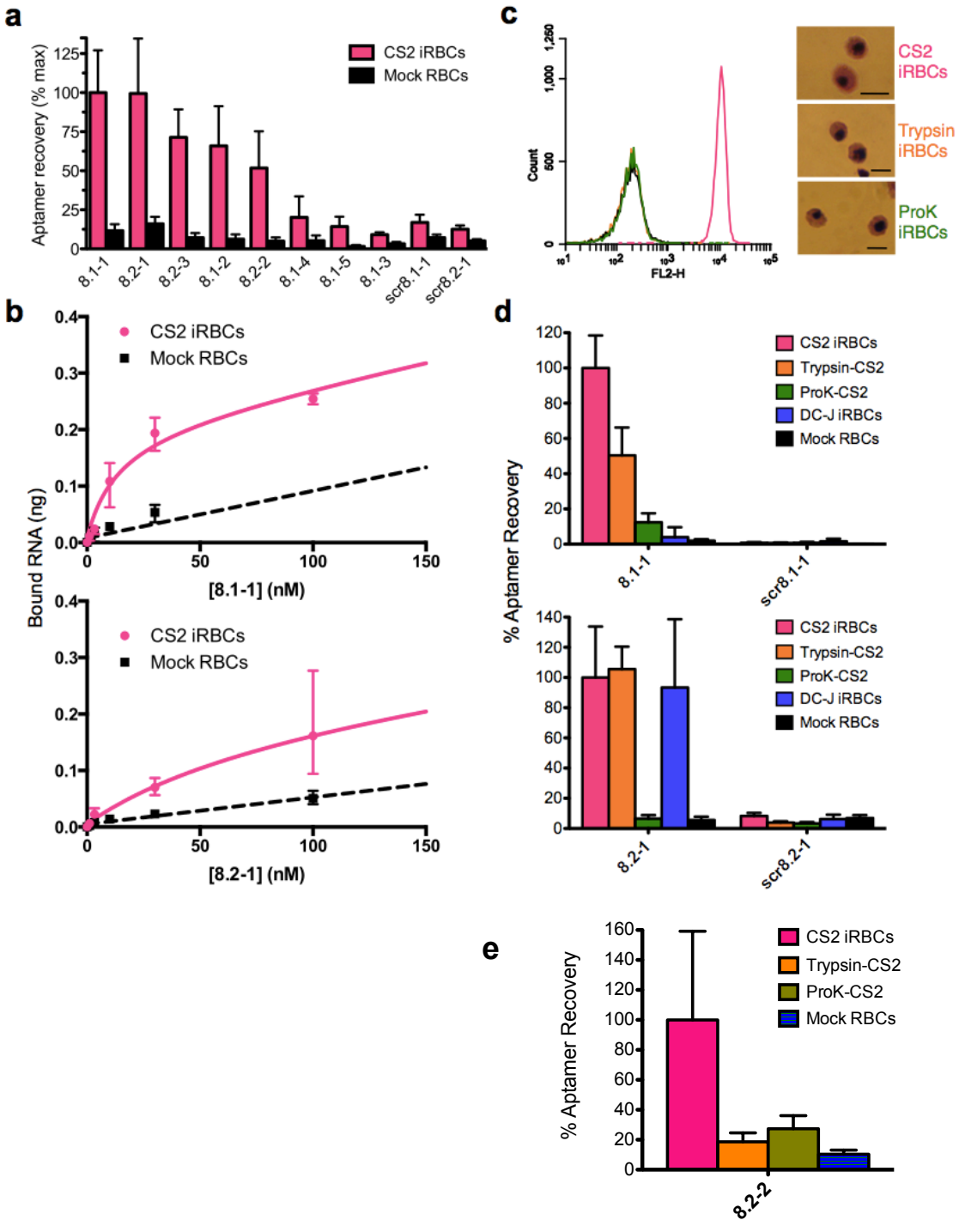


*Figure 16. Characterization of aptamers against malaria-infected red blood cells generated via I-SELEX.* **(a)** Aptamer recovery from CS2 infected RBCs is consistently

greater than recovery from uninfected mock-cultured RBCs (Mock RBCs) for aptamers recovered from Round 8 of selection 1 (8.1-X) or selection 2 (8.2-X). **(b)** Apparent $K_d$ values for the most abundant aptamer from each selection scheme are calculated as 14 ± 10 nM for **8.1-1** and 84 ± 32 nM for **8.2-1**. Aptamer binding to CS2 infected RBCs is fit using linear regression analysis for total binding (specific and nonspecific) while recovery against mock-cultured RBCs is fit as nonspecific binding. **(c)** Glycophorin A (GPA) surface levels present on protease treated or untreated RBCs, and Giemsa-stained light microscopy images of the corresponding cells. Scale bar: 8 μm. **(d)** Profiling of the two most abundant aptamers recovered (**8.1-1** and **8.2-1**) against protease-treated CS2 infected RBCs and the DC-J parasite line that expresses no PfEMP1 surface protein. **(e)** Protease profiling of **8.2-2**, a second aptamer from selection scheme 2, reveals a unique protease sensitivity profile from aptamer **8.2-1**.

Enrichment of **8.1-1, scr8.1-1, 8.2-1 and scr8.2-1** on protease-treated or untreated parasite-infected RBCs target cells was then compared (*Figure 16d*). As expected, basal levels of the non-binding controls **scr8.1-1 and scr8.2-1** were recovered under the various tested conditions. However, **8.1-1** and **8.2-1** exhibited distinct enrichment profiles on the differently treated target cells. Specifically, **8.1-1** binding showed partial trypsin sensitivity (aptamer recovery reduced by ~50%) and high Proteinase K sensitivity (aptamer recovery reduced by ~90%). Conversely, **8.2-1** binding is trypsin resistant but Proteinase K sensitive (aptamer recovery reduced by ~95%). Additional testing of aptamer **8.2-2** yielded a protease sensitivity profile distinct from **8.2-1** as shown in *Figure 16e*, the other major aptamer species recovered in the same selection (scheme 2). These data show that our selection process successfully recovered aptamers that recognize either distinct epitopes on the same protein or distinct proteins present on parasite-infected RBCs.

### *3.3.5 PfEMP1 binding of iRBC aptamers*

Since our I-SELEX protocol was designed to recover aptamers to any target on the parasite- infected RBC surface, we sought to determine whether any of the identified aptamers could interact with the PfEMP1 protein family. To test this, we used the previously reported DC-J line that has been engineered such that expression of all *var* genes is prevented when parasites are grown under blasticidin-S selection pressure[127].

We then compared enrichment levels of **8.1-1** and **8.2-1** on DC-J (no PfEMP1 expression) and CS2 (VAR*2*CSA-expressing) parasite-infected RBCs. Interestingly, while **8.1-1** is enriched on CS2-infected RBCs, we observed no significant enrichment on DC-J-infected RBCs above background (*Figure 16d*). In the case of **8.2-1**, however, enrichment on both CS2- and DC-J–infected RBCs was similarly high. Altogether, these data show that **8.1-1** recognizes VAR*2*CSA on CS2-infected RBCs and its binding to the parasite-infected RBC surface is moderately trypsin sensitive. On the other hand, **8.2-1** interacts with a non-PfEMP1 protein target via an epitope that is resistant to trypsin. Thus, our selection scheme using the I-SELEX strategy facilitates recovery of aptamers capable of recognizing distinct surface epitopes on parasite-infected RBCs.

### *3.3.6 I-SELEX against PfEMP1-switching iRBCs*

Additionally, we conducted an I-SELEX selection experiment against the *Plasmodium falciparum* strain 3D7. This parasite line expresses the diverse repertoire of PfEMP1 proteins across a population of iRBCs as a result of active *var* gene switching. We conducted a total of eight rounds of selection under constant selection pressure and

sequenced small subsets from rounds 3, 5, 7, and 8, the results of which are summarized in *Table 4.*

| Round 3 | Random Region Sequence |
|---|---|
| 3D7-3-1 | TTGATAGTAGGCGATTACACTATGGTAGGGTGGTGCCCCGTTGTGTCGCA |
| 3D7-3-2 | TACGTTTTGACCAGTGTCCGGTGAGCCGAACCGTGTTCGTAATGGGGTCG |
| 3D7-3-3 | TACGAGATTTATGGATGCGGGGGAGGAAAAGTGGTTTACGGACAGGATTT |
| 3D7-3-4 | AGTTCGAGCCGCGCCGCATGAATGGTAGGCTAGTGGTTAAATAGCCCCT |
| 3D7-3-5 | TGGTGTTTGCGTAGTTCGGTGCAACTGGCTGGTCGCAGTGGATAAGAGGG |
| 3D7-3-6 | TCAGAGGTAGCTGGGGTGCCAGCAGTGTTGGCGTAAAGGGCGAGGCTTAG |
| 3D7-3-7t | GCTGTCAGGCGCAGGGTG |
| 3D7-3-8 | GCCATAGGATTGGTCTGTCCATGTCCGTTCTATGAATCTCGCACATGTGA |
| 3D7-3-9 | TAGTAAGGTGCGTGCGAAGCCGGATGGAGGGAGTTAGCGTCCCTTCAAGC |
| 3D7-3-10 | AGGTATTTCTGGGCTGTTGCCTCTAGCAGGTATGCTACCTGAAACCCTTC |
| 3D7-3-11 | AAAGAAGTCATGATATTAATGTCGGGTAAGTGAAATTGATTTGTAAACAGC |
| 3D7-3-12 | TTCGGTACACCTTTGGAGATGGGATATACATAGGGCTAGAAGCGTGGAG |
| Round 5 | Random Region Sequence |
| 3D7-5-1 | CGGTATATCT**AGCCGATACG**ATTCTCACTGCCAGAAGTCTAGGAGTGAGT |
| 3D7-5-2 | TTGGGTGTTACTGAA**TGTCGAGACG**TACGTGAAGGCGATCAAGACTGCTA |
| 3D7-5-3 | AGAAGACTTGGTTATGGAGTAGTTTCAGTGTCGATGC**TGTCGATGCG**TGC |
| 3D7-5-4 | GGCTACATGTGGAATACGGGTCACTTAATGTTACG**TGCCGAGACG**CACCG |
| 3D7-5-5 | CGCATTTTGCTTGGAGCCTCAC**TGCCAAGACG**C***ATGAGATCC***AGCGTACA |
| 3D7-5-6 | CGCGGTATATAAGCAAGGCAAATATGATTATG**ATGTCATCC**GAATTATTC |
| 3D7-5-7 | GGCCGAGTGTTA**ATGTGATCC**AAGCTGCGGCAGTGACTTGGTGCGTTGCA |
| 3D7-5-8 | CATGTTGGTA**TTGTGATCC**ACAGGATAAAGCTAGGTTATCGAAAAGGTCC |
| 3D7-5-9 | GGTGAGTAAAGGACACATCATTCCTTGAGTAAGACT**CCCGCGTTCC**TCAT |
| 3D7-5-10 | TATGAGCCATACTGGCCATGGAAACGGCGCGTTTG**CCGGCGTGCC**AGGTT |
| 3D7-5-11 | GCTTGGTATATTTTGAAGCTGGTGAGACAAGATTACGACGCTGGATTGAA |
| 3D7-5-12 | TGGAGTCTGCAGAGTACGGTGACCAAGGTAGGAGGGTCATAACCGCCTGT |
| 3D7-5-13 | GCTGAGGATAGTGATAGAGCCAGGATCGATATATTGGTTCGGAATAAAGT |
| 3D7-5-14 | ATGGGTACTGGGGGGCACCGACATGATCAGGCAAAACGATTTAGCCTGCT |
| 3D7-5-15 | AGGTCATTGTGGACTATTAGTGAAGGCGGAAAAGGATTATTTAACGATCC |
| 3D7-5-16 | AAGGTAAGTGGCGTAACGCATTCGGGTCGAAGGTATTAAGAGGGAAACGA |
| 3D7-5-17 | CTACCAAGTGTATCATTACGTCCTTGGTGTACAGAGGTAAAGTGTGTAAC |
| 3D7-5-18 | TCTCAAGGCATACTGCAGAGAAGTATCGCCAGACTACCGGTTTTTGGGCT |
| 3D7-5-19 | AGTATACGAGTGGTCAACAGATCGTGCTTTATTTGGTTGACCATGA |
| 3D7-5-20 | GGCATCGATTGTATTACTCAAGTCCTGCGAGTACGCCGAATGGCCAGCGT |
| 3D7-5-21t | GCTTAGGACGGCAATAATGGAAGAGTCGCCCA |
| Round 7 | Random Region Sequence |
| 3D7-7-1 | CGAATGGGAGGAATATAGATTAGAGAACTAATAAAAGACACACGCAGTTT |
| 3D7-7-2 | TTGATTGAGTGGCTTGTTTTTTGTCGCCGTCGGGATAGTTTTAACTCTGC |
| 3D7-7-3 | GCATGAAAATTACTGGACAATTCATCAGGCTGGCAAGTGTTGAAGGTTCA |
| 3D7-7-4t | GTTGGAATGC |
| 3D7-7-5t | TTAGGTTTAGACGTGAACTCGCG |
| 3D7-7-6t | TGTCGATTCCTACGGTGTGACAACCGACT |
| 3D7-7-7t | GATTGATACGTTTCGTATCTGTGT |
| 3D7-7-8t | GAATGGGTGCTTGGGACTTCGC |
| Round 8 | Random Region Sequence |
| 3D7-8-1 | CAACGGATCACACGCAAGCGAATCTATGTCCTTCGGGTCTAAGGGTCGCT |
| 3D7-8-2 | CAACGGATCACACGCAAGCGAATCTATGTCCTTCGGGTCTAAGGGTCGCT |
| 3D7-8-3 | CAACGGATCACACGCAAGCGAATCTATGTCCTTCGGGTCTAAGGGTCGCT |
| 3D7-8-4 | AGTGGACGGATCGTTGAGGGACGGCCCTGGTATTGCCGGTTGCGCCGTTA |
| 3D7-8-5 | TATCACAAAGGGGATATCCCGGACTAAACGTGGTAGGTTTGAACGATGAC |
| 3D7-8-6t | AAGAGGGTGAGAAGATCA |

*Table 4. Sequences recovered from 3D7 I-SELEX rounds 3, 5, 7, and 8.* Truncated sequences are indicated by a "t" after their clone identification number. Putative motifs identified by meme analysis are indicated in bold.

While some sequences shared a poorly conserved motif (indicated in bold), most sequences were unique. In contrast to our CS2 iRBC selections, with which no truncated or concatemer sequences were recovered, the 3D7 iRBC selection pool was plagued by both as early as the third round of selection. Some of these truncation sequences are listed in *Table 4*. Furthermore, no aptamer-labeling of 3D7 iRBCs was observed by flow cytometry when sequences from each round were fluorescently labeled and incubated with enriched iRBCs.

### 3.4 Discussion

Here, we have demonstrated the application of I-SELEX to live malaria parasite-infected RBCs. We show that this approach facilitates recovery of a diverse set of high affinity and specific aptamers to a complex combination of targets natively displayed on whole cells. In applying I-SELEX to malaria parasite-infected RBCs, we show for the first time that this strategy enables discovering novel affinity reagents that recognize distinct surface proteins on infected RBCs. In addition, we believe this is the first report of an anti-VAR2CSA aptamer (**8.1-1**), which demonstrates binding to iRBCs in the presence of *var* expression but not to *var*-silenced iRBCs (DC-J strain) or uninfected RBCs. This is achieved without a requirement for first predicting or otherwise defining relevant surface determinants, while circumventing the challenge of obtaining potentially difficult-to-express and natively folded recombinant proteins for aptamer selection. Thus, I-SELEX addresses several key challenges that have limited access to sufficiently diverse affinity reagents to facilitate defining the *P. falciparum*-infected RBC surface proteome in greater detail.

In our *de novo* selections aimed at establishing proof-of-concept for the I-SELEX strategy, we restricted both sequence and binding analyses to a small fraction of the enriched library. We reasoned that the high partitioning efficiency of the device should favor recovery of pools significantly enriched for binders, thus limiting the requirement to deeply sequence and functionally evaluate our selected pools during our validation phase. It has been previously observed that with very complex targets such as RBC membranes there is a balance to be struck between preserving library diversity – and thus obtaining binders to multiple, unique targets – and driving a selected library to sequence convergence[70]. Therefore, our observation of no shared sequence motifs among the sequenced clones, but rather that approximately a two-third majority of sequences are orphans, is not unexpected given the small number of selection rounds conducted relative to standard cell-SELEX experiments. Our successful proof-of-concept, especially with the malaria parasite-infected RBCs, now strongly indicates that systematically analyzing our archived pools from each round of selection by deep sequencing will likely significantly diversify the pool of aptamers capable of specifically recognizing distinct surface epitopes/antigens on infected RBCs.

We anticipate that subsets of these aptamers will be important for different basic applications, including use as: capture reagents for pull-down and identification of surface antigens; modulators of parasite-infected RBC interactions with host endothelial and other cell types linked to severe disease pathogenesis; and biomarkers of malaria infection. The information gained through studies in these respective areas is broadly expected to enable translational efforts relevant to formulating blood stage vaccines that

include appropriate surface antigens, devising mechanism-based adjuvant therapies to prevent severe malaria disease and developing new malaria diagnostics.

## 3.5 Summary

We have designed, validated and used a simple and broadly applicable inertial microfluidics device as an efficient way of achieving stringent, single pass library partitioning during I-SELEX. Using this strategy, we have identified a diverse set of aptamers, and we have shown that a subset of these specifically interact with distinct epitopes uniquely present on malaria-parasite infected red blood cell surfaces. We envision these aptamer reagents will be useful for characterizing the malaria parasite surface proteome in greater molecular detail, which would in the long-term potentially benefit efforts to develop malaria diagnostics, adjunctive treatment and vaccines to both reduce mortality and prevent the disease.

## 3.6 Methods

### *3.6.1 Device fabrication and flow conditions*

Microfluidic devices were fabricated in polydimethylsiloxane polymer (PDMS, Sylgard 184, Dow Corning, USA) using the double molding process reported previously[105]. Briefly, the patterned silicon wafers were silanized with trichloro(1H,1H,2H,2H-perfluorooctyl)silane (Sigma Aldrich, USA) for 1 hr and PDMS prepolymer mixed in 10:1 (w/w) ratio with curing agent was poured onto the silanized wafer and baked at 80°C for 1 hour. The cured PDMS mold then acted as a template for subsequent PDMS casting (negative replica). The PDMS master template was silanized

for 1 hour before use to aid release of subsequent PDMS microchannels. Finally, holes (1.5 mm) for inlets and outlets were punched and the PDMS microchannels were irreversibly bonded to microscopic glass slides using an air plasma machine (Harrick Plasma Cleaner, USA) and left for 2 hours at 70°C to complete the bonding.

Fluid flow through the microfluidic device was modulated with two NE-300 Just Infusion™ Syringe Pumps, one for sample input (inner inlet) and one for sheath buffer input (outer inlet) (syringepump.com). Micro-tubing (0.86 mm ID (inner diameter) by 1.52 mm OD (outer diameter)) (Scientific Commodities, Inc.) was used to move fluid from the syringes into the device inlets. Using slightly oversized tubing (OD 1.52 mm > device input/exit punch diameter of 1.5 mm) creates enough friction to hold the tubing in place during routine use at the relevant flow rates. Each sample mixture was pumped into the inner inlet at 150 μL $min^{-1}$ while sheath buffer (Thrombin Binding Buffer or TBB = 20 mM HEPES pH 7.4, 150 mM NaCl, 2 mM $CaCl_2$) was pumped through the outer inlet at 1500 μL $min^{-1}$. Sample at the product outlet (cells and aptamers) was collected after 1.5 minutes of run time to allow for establishment of Dean vortices along the channel length.

### *3.6.2 Parasite culture and preparation of* **Plasmodium falciparum** *iRBCs*

*Plasmodium falciparum* CS2 and DC-J parasites were cultured at 10% hematocrit and 1-10% parasitemia in 5% $O_2$ and 5% $CO_2$ in RPMI-1640 media supplemented with 5 g/L Albumax II (Life Technologies), 25 mM HEPES pH 7.4 (pH adjusted with potassium hydroxide), 2 g/L sodium bicarbonate, 1 mM hypoxanthine, and 50 mg/L gentamicin. DC-J parasites were cultured in media with a final concentration of 20 mg/mL

blasticidin-S (Research Products International). Parasites were synchronized by incubation in 300 mM L-alanine, 10 mM HEPES, for 5 minutes at 37°C in order to lyse late-stage parasites. Uninfected human RBCs were mock cultured, "passaged," and "synchronized" identically to iRBCs such that negative selections during I-SELEX also account for cell culturing effects.

### *3.6.3 I-SELEX on malaria parasite-infected RBCs*

Library preparation, amplification, and handling were identical to that of *tRBC* SELEX (Section 2.3.6). Malaria iRBC I-SELEX conditions were identical to those used in *t*RBC I-SELEX, with the exception of cell targets. Uninfected human RBCs ($10^8$ per round) served as negative selection targets and were mock cultured under identical conditions to iRBCs. Late-stage (trophozoite and schizont), highly synchronized *Plasmodium falciparum* CS2 iRBCs were enriched to high (>90%) parasitemia using LD MACS® Columns (Miltenyi Biotec). $10^6$ iRBCs were used as positive selection targets. Five rounds of selection were carried out under conditions identical to *t*RBC I-SELEX. For Rounds 6-8, two selection schemes were carried out in parallel. In scheme 1, incubation of the library with target cells was carried out at a five-fold dilution for rounds 6-8 (5mL TBB reaction volume), while scheme 2 reaction conditions remained consistent through all rounds (1 mL TBB reaction volume). When partitioning Rounds 6-8 of scheme 1, the sheath buffer volume was scaled accordingly from 10 mL to 50 mL to retain the desired 1:10 ratio of reaction:sheath buffer. DNA from selection Rounds 8.1 and 8.2 were cloned into pGEM®-T vectors (Promega), transformed into DH5a cells and mini-prepped plasmid DNA sequenced to identify isolated aptamers (*Table 3*).

### *3.6.4 iRBC protease treatment*

Late-stage CS2 iRBCs were first enriched by MACS® column separation as described above to >90% parasitemia. Cells ($6x10^7$) were incubated with either Trypsin (Sigma) or Proteinase K (Sigma) at 1000 µg/mL in 1 mL of TBB for 30 minutes at 37 °C. Protease-treated cells were then washed 3x with 1 mL TBB with 10 µL protease inhibitor cocktail (Sigma).

Protease digestion of surface-exposed proteins was monitored by loss of anti-glycophorin A (GPA) antibody reactivity. PE-conjugated anti-GPA (25 ng per $10^5$ cells, Life Technologies) was incubated with untreated iRBCs, and trypsin- and proteinase K-treated in 200 µL TBB with gentle agitation for 30 minutes before being washed 3x with 200 µL TBB. Cells were resuspended in 200 µL TBB and analyzed on an Accuri C6 cytometer (BD Biosciences) in the FL2 channel. Fluorescence levels were compared to FL2 channel auto-fluorescence of untreated iRBCs without anti-GPA incubation.

### *3.6.5 iRBC aptamer enrichment quantification and apparent $K_d$ determination*

Sequences from the terminal rounds of iRBC I-SELEX were tested for preferential binding to iRBCs over RBCs using the qPCR-based Enrichment Experiment protocol described above and as illustrated in *Figure 15*. Briefly, 100 nM of a single aptamer species (for enrichment experiments) or a six-point titration of 0-100 nM aptamer (for apparent $K_d$ determination) (*Table 3*) was incubated with either $10^7$ CS2 or DC-J iRBCs (MACS-enriched to >90% parasitemia) or uninfected, mock-cultured RBCs in 1 mL TBB for 60 minutes at room temperature before being passed through an I-SELEX device. 10 µL of the aptamer reaction (before addition of cells) was collected in

order to quantify aptamer "input." Cells were recovered directly from the sample outlet onto a vacuum filter plate membrane (Millipore MSHVS4510). Bound aptamers were eluted (off-vacuum) by a five-minute incubation with 100 µL 1 mM EDTA in TBB, pH 7.4 followed by plate centrifugation. Aptamer "input" (diluted with TBB to equal volume as the elution) and "output" (eluted from the cell surface) were both concentrated by ethanol precipitation and resuspended in 8.5 µL TBB. Aptamer input and output RNA was reverse transcribed using primer CMB183 and SuperScript III (Life Technologies) in accordance with the manufacturer's instructions. Quantitative polymerase chain reaction (qPCR) with SYBR Green was used to determine relative levels of input and output aptamers as described above for different cell types using SELEX Forward and Reverse primers (see Section 3.6.6 List of primers used in this work).

For apparent $K_d$ determination, binding to CS2 infected RBCs is fit to the following model: $Y = B_{max} \times X/(X + K_d) + NS \times X + Background$, and recovery against mock-cultured uninfected RBCs was fit using the nonspecific model $Y = NS \times X + Background$, where Y is bound aptamer RNA, $B_{max}$ is the concentration of binding sites, X is the concentration of aptamer, $K_d$ is the apparent dissociation constant, and NS represents aptamer concentration-dependent nonspecific binding.

All aptamers and scrambled negative control sequences (*Table 3*) were tested in triplicate in two independent experiments with new cell preparations. In the case of our RBC and iRBC targets, the number of output sequences recovered from the cell surface is several orders of magnitude below that of the input or waste samples, such that the number of input sequences is approximately equal to the number of waste sequences. The difference between input and output qPCR crossing points (ΔCp) was calculated for each

iRBC sample and compared to the ΔCp for mock-cultured RBC samples. The resulting difference between cell types (ΔΔCp) is used to quantify preferential aptamer enrichment for CS2 iRBCs over RBCs, protease-treated CS2 iRBCs, or DC-J iRBCs. Error was propagated when taking each difference and statistical significance ($P < 0.05$) was calculated using a Student t test.

### *3.6.6 List of primers used in this work*

| | |
|---|---|
| SELEX Library template | CCGAAGCTTAATACGACTCACTATAGGGAGCTCAGAATAAACGCTCAA-[$N_{50}$]-TTCGACATGAGGCCCGGATCCGGC |
| SELEX Forward Primer | CCGAAGCTTAATACGACTCACTATAGGGAGCTCAGAATAAACGCTCAA |
| SELEX Reverse Primer | GCCGGATCCGGGCCTCATGTCGAA |
| CMB183 | GCGGCTGTCTCCACAAGTCGCCGGATCCGGGCCT |

*Table 5. Primers used in Chapter 3.*

# CHAPTER 4: FUTURE DIRECTIONS OF RESEARCH

## 4.1 Future directions with inertial microfluidics based selections

### *4.1.1 Extension to alternate selection strategies*

While the inertial microfluidics methods presented here discussed only aptamer selections, the underlying fluid dynamic principles are also accommodating of additional selection strategies. For use in its current form, a basic system requirement is that cells/affinity reagents that are collected at the outlet contain all the information necessary to identify themselves, e.g. the binding aptamer is identified by its sequence. For other affinity reagents such as antibodies, the inertial microfluidic device could be used as a stringent washing strategy in selections prior to partitioning (e.g. in yeast surface display prior to FACS-based selection of antigen binding cells). The inertial device is also a rapid, continuous-flow manner in which one can perform buffer exchanges.

In addition to the cellular targets discussed in this work, I-SELEX can be applied to bead-based targets. Traditional SELEX experiments often target recombinantly expressed and/or purified protein targets, which are readily presented on a bead scaffolding by affinity tags. Beads of sufficient diameter (~ 4.5 μm or greater) can be immediately used in the inertial microfluidics chip design described herein. The diverse aptamer library that is recovered from each selection has the potential to produce a large number of aptamer-target solutions relevant to broader applications in disease diagnostics and biomarker development to distinguish different cell types (e.g. in cancer). I-SELEX therefore can be used as a universal partitioning strategy for both whole cell and bead-based targets.

### *4.1.2 Lab on a chip*

While a major advantage of using microfluidics is the small sample volume requirement, one of the challenges of using our current I-SELEX device is that of sample dilution at the outlet. Our inertial microfluidics chip is a continuous flow design, such that the reaction is always moving through the device. In order to achieve our stringent separation of unbound nucleic acid sequences, however, we use a two-inlet design that "pinches" the reaction mixture fluid into a very tight stream using an excess of sheath buffer (*Figure 1)*. At the sample outlet, we capture ~43% of the total volume exiting the device (sample outlet 150 μm; waste outlet 350 μm). This results in a dilution of the recovered particles or cellular targets, unless they are immediately captured (e.g. on a vacuum plate). Sample outlet becomes limiting if one would like to run multiple devices in series as a way to more stringently partition aptamers and large (cellular) targets. The device design could be altered such that the sample outlet dimensions are reduced to capture a smaller percentage of the total flow. Alternatively, the device could be coupled with existing microfluidics chip designs that would effectively concentrate the cells in a capture chamber. However, chip clogging is often a struggle with cell samples. Because the cells themselves are not the desired output of the selection, but rather the aptamers that are bound to them, one could design a microfluidics chip series that captured cells post-partitioning and released aptamers from them by flowing over an elution buffer.

The future of aptamer selection will be automated, where we have complete system integration – from library preparation and amplification, to positive and negative selections, and finally to aptamer elution and sequencing preparation – all occurring on a high-throughput microfluidics platform. Microfluidic technologies have the potential to

be inexpensive, require low sample volumes, and would allow for multiplexing of selections on a single chip. With advances in 3D printing technologies, we now can produce fluidic devices (in the millimeter scale) capable of manipulating and mixing small volumes incredibly inexpensively.[148] While the printing resolution is currently limiting (~0.4 mm),[149] advances in device construction materials and technology will make microfluidics and selection technology widely available, from use in the field to enabling bench top selections in any laboratory.

## 4.2 Future directions with malaria aptamers and selections

### *4.2.1 A broader experimental approach*

Given the complexity of the whole cell surface, a deeper look into the iRBC aptamer pool could identify new or alternative parasite-specific surface epitopes. While we have conducted preliminary characterization of the most *abundant* aptamers in the selection library, retroactively deep-sequencing our aptamer pools from each round would allow us to identify those sequences that are preferentially *enriched* from round to round without requiring those sequences to be the most numerous.

A natural extension of the malaria-infected red blood cell work would be to expand application of I-SELEX against a larger set of *P. falciparum* strains, for instance the commonly used, antigenically variant laboratory strains 3D7, HB3, and Dd2. Furthermore, if one can determine a unique set of aptamer probes that is sufficient to identify each strain of interest, the aptamer panels could potentially be used as an alternative and orthogonal method to PCR-based strain typing whereby strains are classified by their surface proteome.

Targeting iRBCs with aptamers does not need to be limited to the asexual parasitic forms. Interestingly, early-stage *P. falciparum* gametocytes also sequester away from the peripheral circulation similar to late-stage trophozoites and schizonts. Gametocytes are thought to adhere with lower efficiency than the asexual stages, which favors cytoadhesion in areas of reduced blood velocity, such as in the spleen or bone marrow[150]. Late stage gameotocytes are released back into circulation where they can be picked up by a mosquito to complete the transmission cycle. Similar to our proposed asexual stage iRBC aptamer applications, aptamer targeting could potentially be used to disrupt gametocyte sequestration, identify gametocyte surface proteins, and specifically target gametocyte iRBCs for parasite manipulation or monitoring. Gametocytogenesis is an interesting process whereby the cell changes both protein expression and cellular shape and deformity between early and late stage forms. Aptamers could potentially be used to identify differential surface protein expression between early stage, sequestration-capable gametocytes and late-stage "non-sequestering" gametocyte forms, thus providing greater insight into parasite sexual differentiation and transmission mechanisms.

Adaptation of the inertial microfluidic device for use in gametocyte I-SELEX is immediate and the same device specifications can be used for both asexual and sexual stage iRBC I-SELEX. Early stage (Stage II) gametocytes are the smallest of the gametocyte forms at 4.3±0.5 μm across their largest diameter; late stage (Stage IV and V) gametocytes are largest at 11.0±1.2 and 8.7±0.9 μm at their largest diameter, respectively[151]. The larger forms will easily satisfy the required focusing size conditions (*Equation 4)*; the smallest form, Stage II gametocytes, at 4.3 μm will also satisfy the focusing criterion on our 60 μm tall channel: 4.3 μm / 60 μm = 0.072 > 0.07 minimum

focusing ratio. Gametocytes can also be readily purified for aptamer selection using fluorescent sorting of genetically encoded tags, in order to prepare a homogenous cellular population for positive selection targets during I-SELEX. We have conducted preliminary studies confirming the successful focusing and collection of Stage II gametocytes using the I-SELEX device described in this work.

### *4.2.2 A deeper experimental approach*

The iRBC-specific aptamers developed here could be utilized to gain additional insight regarding the contributions the iRBC surface proteome in sequestration and severe disease. First, aptamers identified in this work can be used to identify novel surface proteins or epitopes present on late-stage iRBCs. One could cross-link aptamers to the iRBC surface, pull-down the aptamer binding partner(s), and use mass spectrometry to identify epitopes that are indicative of parasite infection. Our aptamer enrichment studies strongly suggest that aptamer **8.1-1** is able to recognize VAR2CSA, and a mass spectrometry analysis could confirm this conclusion. Furthermore, the binding partner of aptamer **8.2-1** does not appear to be dependent on *var* expression and mass spectrometry analysis could test the hypothesis that **8.2-1** binds a "universal handle" parasite-derived epitope. Identification of novel parasite-derived surface proteins could also give further insight into protein trafficking in the blood stages.

Secondly, the panel of aptamers listed in *Table 3* could be tested for their ability to disrupt cytoadhesion to placental endotheial cells (e.g. BeWo cells) in standard static or flow-based adhesion assays[152]. Aptamers that show significant cytoadhesion disruption

capability could have potential as adjunctive therapies to abate severe disease as they target the molecular mechanisms required for physical sequestration.

Finally, aptamers that show promising iRBC targeting without disrupting iRBC cytoadhesion could be useful for the development of *in vivo* sequestration imaging agents. These aptamers would provide the targeting/specificity portion of an iRBC imaging agent but would require conjugation of contrast agents necessary to visualize sequestration *in vivo* using technologies such as magnetic resonance imaging (MRI). Conjugation of reagents such as SPIONs[153,154] or $^{99m}$Technetium[155] have been successfully used as contrast agents in aptamer-conjugation MRI experiments.

# CHAPTER 5: CONCLUSION

In this thesis work, we have presented a novel method for aptamer selections using inertial microfluidics (I-SELEX). We quantitatively defined the high partitioning efficiency of the device and demonstrated a successful *de novo* I-SELEX experiment using an engineered cell system (*s*RBC/*t*RBC system). Finally, we applied I-SELEX to malaria-infected red blood cells to identify an aptamer panel capable of robustly distinguishing between infected and uninfected cells. We performed protease profiling and enrichment experiments to determine that iRBC aptamers bind to distinct cell surface targets, including VAR2CSA. This is achieved without the need to define, modify, or express potential surface targets or modify the aptamer library. Thus, I-SELEX addresses several key challenges that have limited access to targeting and defining the complex surface proteome of *Plasmodium falciparum* in greater detail.

## BIBLIOGRAPHY


1. WHO | World Malaria Report 2014. *WHO*
2. Sachs, J. & Malaney, P. The economic and social burden of malaria. *Nature* **415,** 680–685 (2002).
3. Life Cycle of the Malaria Parasite. *niaid.nih.gov* at <http://www.niaid.nih.gov/topics/malaria/pages/lifecyce.aspx>
4. Sherman, I. W. *Molecular Approaches to Malaria*. (Amer Society for Microbiology, 2005).
5. Chambers, R. G. UN Envoy's response to estimates of global malaria mortality. *The Lancet* **379,** 707–708 (2012).
6. Kim, Y. & Schneider, K. A. Evolution of Drug Resistance in Malaria Parasite Populations | Learn Science at Scitable. *Nature Education Knowledge* (2013).
7. Crompton, P. D., Pierce, S. K. & Miller, L. H. Advances and challenges in malaria vaccine development. *The Journal of clinical …* (2010).
8. Stoute, J. A. *et al.* A Preliminary Evaluation of a Recombinant Circumsporozoite Protein Vaccine against Plasmodium falciparumMalaria. *N. Engl. J. Med.* **336,** 86–91 (1997).
9. Maitland, K. *et al.* Randomized trial of volume expansion with albumin or saline in children with severe malaria: preliminary evidence of albumin benefit. *Clin. Infect. Dis.* **40,** 538–545 (2005).
10. Guinovart, C. *et al.* Insights into long-lasting protection induced by RTS,S/AS02A malaria vaccine: further results from a phase IIb trial in Mozambican children. *PLoS ONE* **4,** e5165 (2009).
11. Takala, S. L. *et al.* Extreme polymorphism in a vaccine antigen and risk of clinical malaria: implications for vaccine development. *Science Translational Medicine* **1,** 2ra5 (2009).
12. Dolo, A., Diallo, D. A., Doumbo, O. K., Miller, L. H. & Saul, A. A randomized controlled phase 2 trial of the blood stage AMA1-C1/Alhydrogel malaria vaccine in children in Mali. *Vaccine* (2009).
13. Ogutu, B. R. *et al.* Blood stage malaria vaccine eliciting high antigen-specific antibody concentrations confers no protection to young children in Western Kenya. *PLoS ONE* **4,** e4708 (2009).
14. Hoffman, S. L. *et al.* Development of a metabolically active, non-replicating sporozoite vaccine to prevent Plasmodium falciparum malaria. *Hum Vaccin* **6,** 97–106 (2010).
15. Hommel, M., David, P. H. & Oligino, L. D. Surface alterations of erythrocytes in Plasmodium falciparum malaria. Antigenic variation, antigenic diversity, and the role of the spleen. *The Journal of experimental …* (1983).
16. Hänscheid, T. Diagnosis of malaria: a review of alternatives to conventional microscopy. *Clin Lab Haematol* **21,** 235–245 (1999).
17. Cooke, B., Mohandas, N. & Coppel, R. The malaria-infected red blood cell: structural and functional changes. *Advances in Parasitology* (2001).
18. Haase, S. & de Koning-Ward, T. F. New insights into protein export in malaria parasites. *Cell Microbiol* **12,** 580–587 (2010).
19. Goldberg, D. E. & Cowman, A. F. Moving in and renovating: exporting proteins

from Plasmodium into host erythrocytes. *Nature Publishing Group* **8,** 617–621 (2010).
20. Rowe, J. A., Claessens, A., Corrigan, R. A. & Arman, M. Adhesion of Plasmodium falciparum-infected erythrocytes to human cells: molecular mechanisms and therapeutic implications. *Expert Rev Mol Med* **11,** e16 (2009).
21. Buffet, P. A. *et al.* The pathogenesis of Plasmodium falciparum malaria in humans: insights from splenic physiology. *Blood* **117,** 381–392 (2011).
22. Clark, I. A. & Rockett, K. A. The cytokine theory of human cerebral malaria. *Parasitol Today (Regul Ed)* **10,** 410–412 (1994).
23. Hunt, N. & Grau, G. Cytokines: accelerators and brakes in the pathogenesis of cerebral malaria. *Trends in immunology* (2003).
24. Clark, I., Rockett, K. & Cowden, W. Proposed link between cytokines, nitric oxide and human cerebral malaria. *Parasitology Today* (1991).
25. Patankar, T. F., Karnad, D. R., Shetty, P. G., Desai, A. P. & Prasad, S. R. Adult cerebral malaria: prognostic importance of imaging findings and correlation with postmortem findings. *Radiology* **224,** 811–816 (2002).
26. Rogerson, S. J., Chaiyaroj, S. C., Ng, K., Reeder, J. C. & Brown, G. V. Chondroitin sulfate A is a cell surface receptor for Plasmodium falciparum-infected erythrocytes. *J. Exp. Med.* **182,** 15–20 (1995).
27. Turner, G. Cerebral Malaria. *Brain Pathology* **7,** 569–582 (1997).
28. Menendez, C. *et al.* The impact of placental malaria on gestational age and birth weight. *J Infect Dis* **181,** 1740–1745 (2000).
29. Jambou, R. *et al.* Plasmodium falciparum Adhesion on Human Brain Microvascular Endothelial Cells Involves Transmigration-Like Cup Formation and Induces Opening of Intercellular Junctions. *PLoS Pathog* **6,** e1001021 (2010).
30. van Hensbroek, M. B. *et al.* The effect of a monoclonal antibody to tumor necrosis factor on survival from childhood cerebral malaria. *J Infect Dis* **174,** 1091–1097 (1996).
31. Miller, L. H., Baruch, D. I., Marsh, K. & Doumbo, O. K. The pathogenic basis of malaria. *Nature* (2002).
32. Newbold, C., Craig, A., Kyes, S. & Rowe, A. Cytoadherence, pathogenesis and the infected red cell surface in Plasmodium falciparum. *International journal for ...* (1999).
33. Fried, M. & Duffy, P. E. Adherence of Plasmodium falciparum to chondroitin sulfate A in the human placenta. *Science* **272,** 1502–1504 (1996).
34. Haldar, K., Murphy, S. C., Milner, D. A. & Taylor, T. E. Malaria: mechanisms of erythrocytic infection and pathological correlates of severe disease. *Annual review of pathology* **2,** 217–249 (2007).
35. Marsh, K. *et al.* Indicators of life-threatening malaria in African children. *N. Engl. J. Med.* **332,** 1399–1404 (1995).
36. Mishra, S. & Newton, C. Diagnosis and management of the neurological complications of falciparum malaria. *Nature Reviews Neurology* (2009).
37. Thuma, P. E. *et al.* Effect of iron chelation therapy on mortality in Zambian children with cerebral malaria. *Transactions of the Royal Society of Tropical Medicine and Hygiene* **92,** 214–218 (1998).

38. Nosten, F., Rogerson, S. J., Beeson, J. G. & McGready, R. Malaria in pregnancy and the endemicity spectrum: what can we learn? *Trends in …* (2004).
39. Cordoliani, Y. S., Sarrazin, J. L. & Felten, D. MR of cerebral malaria. *American journal …* (1998).
40. Cordoliani, Y. S. *et al.* MR of cerebral malaria. *AJNR Am J Neuroradiol* **19,** 871–874 (1998).
41. John, C. C., Kutamba, E., Mugarura, K. & Opoka, R. O. Adjunctive therapy for cerebral malaria and other severe forms of Plasmodium falciparum malaria. *Expert Rev Anti Infect Ther* **8,** 997–1008 (2010).
42. Warrell, D. A. *et al.* Dexamethasone proves deleterious in cerebral malaria. A double-blind trial in 100 comatose patients. *N. Engl. J. Med.* **306,** 313–319 (1982).
43. Mohanty, D., Ghosh, K., Pathare, A. V. & Karnad, D. Deferiprone (L1) as an adjuvant therapy for Plasmodium falciparum malaria. *Indian J. Med. Res.* **115,** 17–21 (2002).
44. Charunwatthana, P. & Faiz, M. A. N-acetylcysteine as adjunctive treatment in severe malaria: a randomized double blinded placebo controlled clinical trial. *Critical care …* (2009).
45. Kyes, S., Horrocks, P. & Newbold, C. Antigenic variation at the infected red cell surface in malaria. *Annu. Rev. Microbiol.* **55,** 673–707 (2001).
46. Vant-Hull, B., Payano-Baez, A., Davis, R. H. & Gold, L. The mathematics of SELEX against complex targets. *J Mol Biol* **278,** 579–597 (1998).
47. Gupta, S. & Patel, K. Case series: MRI features in cerebral malaria. *Indian J Radiol Imaging* **18,** 224–226 (2008).
48. zur Muhlen, von, C., Sibson, N. R. & Peter, K. A contrast agent recognizing activated platelets reveals murine cerebral malaria pathology undetectable by conventional MRI. *The Journal of clinical …* (2008).
49. McAteer, M. A. *et al.* Magnetic resonance imaging of endothelial adhesion molecules in mouse atherosclerosis using dual-targeted microparticles of iron oxide. *Arterioscler. Thromb. Vasc. Biol.* **28,** 77–83 (2008).
50. Tuerk, C. & Gold, L. Systematic evolution of ligands by exponential enrichment: RNA ligands to bacteriophage 4 DNA polymerase. *Science* **249,** 505–510 (1990).
51. Ellington, A. D. & Szostak, J. W. In vitro selection of RNA molecules that bind specific ligands. *Nature* **346,** 818–822 (1990).
52. Keefe, A. & Cload, S. SELEX with modified nucleotides. *Current Opinion in Chemical Biology* **12,** 448–456 (2008).
53. Ng, E., Shima, D. T. & Calias, P. Pegaptanib, a targeted anti-VEGF aptamer for ocular vascular disease. *Nature reviews drug …* (2006).
54. Famulok, M. & Mayer, G. Aptamers and SELEX in Chemistry & Biology. *Chem Biol* (2014).
55. Daniels, D., Sohal, A. & Rees, S. Generation of RNA aptamers to the G-protein-coupled receptor for neurotensin, NTS-1. *Anal Biochem* (2002).
56. Phillips, J. A., Lopez-Colon, D., Zhu, Z., Xu, Y. & Tan, W. Applications of aptamers in cancer cell biology. *Anal Chim Acta* **621,** 101–108 (2008).
57. Berezovski, M. *et al.* Nonequilibrium Capillary Electrophoresis of Equilibrium Mixtures: A Universal Tool for Development of Aptamers. *Journal of the*

*American Chemical Society* **127,** 3165–3171 (2005).
58. Wong, I. & Lohman, T. M. A double-filter method for nitrocellulose-filter binding: application to protein-nucleic acid interactions. *Proc Natl Acad Sci USA* **90,** 5428–5432 (1993).
59. Ravelet, C., Grosset, C. & Peyrin, E. Liquid chromatography, electrochromatography and capillary electrophoresis applications of DNA and RNA aptamers. *J Chromatogr A* **1117,** 1–10 (2006).
60. Qian, J., Lou, X., Zhang, Y., Xiao, Y. & Soh, H. T. Generation of highly specific aptamers via micromagnetic selection. *Anal Chem* **81,** 5490–5495 (2009).
61. Zimmermann, B., Gesell, T., Chen, D., Lorenz, C. & Schroeder, R. Monitoring genomic sequences during SELEX using high-throughput sequencing: neutral SELEX. *PLoS ONE* **5,** e9169 (2010).
62. Berezovski, M. V., Lechmann, M., Musheev, M. U., Mak, T. W. & Krylov, S. N. Aptamer-Facilitated Biomarker Discovery (AptaBiD). *Journal of the American Chemical Society* **130,** 9137–9143 (2008).
63. Mendonsa, S. D. & Bowser, M. T. In vitro evolution of functional DNA using capillary electrophoresis. *Journal of the American Chemical …* (2004).
64. Lou, X. *et al.* Micromagnetic selection of aptamers in microfluidic channels. *Proc Natl Acad Sci USA* **106,** 2989–2994 (2009).
65. Gold, L., Polisky, B., Uhlenbeck, O. & Yarus, M. Diversity of oligonucleotide functions. *Annual review of biochemistry* **64,** 763–797 (1995).
66. Xu, Y. *et al.* Aptamer-based microfluidic device for enrichment, sorting, and detection of multiple cancer cells. *Anal Chem* **81,** 7436–7442 (2009).
67. Liu, J., Cao, Z. & Lu, Y. Functional nucleic acid sensors. *Chemical reviews* (2009).
68. Lorger, M., Engstler, M. & Homann, M. Targeting the variable surface of African trypanosomes with variant surface glycoprotein- …. *Eukaryotic Cell* (2003).
69. Ulrich, H., Magdesian, M. H., Alves, M. J. M. & Colli, W. In vitro selection of RNA aptamers that bind to cell adhesion receptors of Trypanosoma cruzi and inhibit cell invasion. *J Biol Chem* **277,** 20756–20762 (2002).
70. Morris, K. N., Jensen, K. B. & Julin, C. M. High affinity ligands from in vitro selection: complex targets. in (1998).
71. Shangguan, D. *et al.* Identification of liver cancer-specific aptamers using whole live cells. *Anal Chem* **80,** 721–728 (2008).
72. Tang, Z. *et al.* Selection of aptamers for molecular recognition and characterization of cancer cells. *Anal Chem* **79,** 4900–4907 (2007).
73. Raddatz, M. S. L. *et al.* Enrichment of Cell‐Targeting and Population‐Specific Aptamers by Fluorescence‐Activated Cell Sorting. *Angew. Chem. Int. Ed.* **47,** 5190–5193 (2008).
74. Cerchia, L., Ducongé, F., Pestourie, C. & Boulay, J. Neutralizing aptamers from whole-cell SELEX inhibit the RET receptor tyrosine kinase. *PLoS Biol* (2005).
75. Homann, M. & Göringer, H. U. Combinatorial selection of high affinity RNA ligands to live African trypanosomes. *Nucleic Acids Research* **27,** 2006–2014 (1999).
76. Belmont, B. J. & Niles, J. C. Engineering a direct and inducible protein-RNA

interaction to regulate RNA biology. *ACS Chem Biol* **5,** 851–861 (2010).
77. Shamah, S. M., Healy, J. M. & Cload, S. T. Complex target SELEX. *Accounts of Chemical Research* **41,** 130–138 (2008).
78. Fang, X. & Tan, W. Aptamers generated from cell-SELEX for molecular medicine: a chemical biology approach. *Accounts of Chemical Research* **43,** 48–57 (2010).
79. Di Carlo, D., Edd, J. F., Irimia, D., Tompkins, R. G. & Toner, M. Equilibrium Separation and Filtration of Particles Using Differential Inertial Focusing. *Anal Chem* **80,** 2204–2211 (2008).
80. Bhagat, A. A. S., Hou, H. W., Li, L. D., Lim, C. T. & Han, J. Pinched flow coupled shear-modulated inertial microfluidics for high-throughput rare blood cell separation. *Lab Chip* **11,** 1870–1878 (2011).
81. Lee, W. C. *et al.* High-throughput cell cycle synchronization using inertial forces in spiral microchannels. *Lab Chip* **11,** 1359 (2011).
82. Di Carlo, D. Inertial microfluidics. *Lab Chip* **9,** 3038–3046 (2009).
83. Berger, S. A., Talbot, L. & Yao, L. S. Flow in Curved Pipes. *Annu. Rev. Fluid Mech.* **15,** 461–512 (1983).
84. Ookawara, S., Street, D. & Ogawa, K. Numerical study on development of particle concentration profiles in a curved microchannel. *Chemical engineering science* **61,** 3714–3724 (2006).
85. Martel, J. M. & Toner, M. Inertial focusing dynamics in spiral microchannels. *Phys. Fluids* **24,** 032001 (2012).
86. Di Carlo, D., Irimia, D., Tompkins, R. G. & Toner, M. Continuous inertial focusing, ordering, and separation of particles in microchannels. *Proc Natl Acad Sci USA* **104,** 18892 (2007).
87. Kuntaegowdanahalli, S. S., Bhagat, A. A. S., Kumar, G. & Papautsky, I. Inertial microfluidics for continuous particle separation in spiral microchannels. *Lab Chip* **9,** 2973 (2009).
88. Bhagat, A. A. S., Kuntaegowdanahalli, S. S. & Papautsky, I. Continuous particle separation in spiral microchannels using dean flows and differential migration. *Lab Chip* **8,** 1906 (2008).
89. Chasis, J. A. & Mohandas, N. Red blood cell glycophorins. *Blood* **80,** 1869–1879 (1992).
90. Masud, M. M., Kuwahara, M., Ozaki, H. & Sawai, H. Sialyllactose-binding modified DNA aptamer bearing additional functionality by SELEX. *Bioorg Med Chem* **12,** 1111–1120 (2004).
91. White, R. *et al.* Generation of species cross-reactive aptamers using 'toggle' SELEX. *Mol Ther* **4,** 567–573 (2001).
92. Huang, C.-J., Lin, H.-I., Shiesh, S.-C. & Lee, G.-B. Integrated microfluidic system for rapid screening of CRP aptamers utilizing systematic evolution of ligands by exponential enrichment (SELEX). *Biosensors and Bioelectronics* **25,** 1761–1766 (2010).
93. Bailey, T. L. & Elkan, C. Fitting a mixture model by expectation maximization to discover motifs in bipolymers. (1994).
94. Zuker, M. Mfold web server for nucleic acid folding and hybridization prediction. *Nucleic Acids Research* (2003).

95. Wang, J., Zhan, Y., Ugaz, V. M. & Lu, C. Vortex-assisted DNA delivery. *Lab Chip* **10,** 2057 (2010).
96. Ruff, K. M., Snyder, T. M. & Liu, D. R. Enhanced Functional Potential of Nucleic Acid Aptamer Libraries Patterned to Increase Secondary Structure. *Journal of the American Chemical Society* (2010). doi:10.1021/ja103023m
97. Davis, J. H. & Szostak, J. W. Isolation of high-affinity GTP aptamers from partially structured RNA libraries. *Proc Natl Acad Sci USA* **99,** 11616–11621 (2002).
98. Vaught, J. D., Bock, C., Carter, J. & Fitzwater, T. Expanding the chemistry of DNA for in vitro selection. ... *American Chemical* ... (2010).
99. Gold, L. *et al.* Aptamer-Based Multiplexed Proteomic Technology for Biomarker Discovery. *PLoS ONE* **5,** e15004 (2010).
100. Hoon, S., Zhou, B., Janda, K. D., Brenner, S. & Scolnick, J. Aptamer selection by high-throughput sequencing and informatic analysis. *BioTechniques* **51,** 413–416 (2011).
101. Kupakuwana, G. V., Crill, J. E., McPike, M. P. & Borer, P. N. Acyclic Identification of Aptamers for Human alpha-Thrombin Using Over-Represented Libraries and Deep Sequencing. *PLoS ONE* **6,** e19395 (2011).
102. Singla, N. K. *et al.* A phase 3b, open-label, single-group immunogenicity and safety study of topical recombinant thrombin in surgical hemostasis. *J. Am. Coll. Surg.* **209,** 68–74 (2009).
103. Bock, L. C., Griffin, L. C., Latham, J. A., Vermaas, E. H. & Toole, J. J. Selection of single-stranded DNA molecules that bind and inhibit human thrombin. *Nature* **355,** 564–566 (1992).
104. Kubik, M. F., Stephens, A. W., Schneider, D., Marlar, R. A. & Tasset, D. High-affinity RNA ligands to human alpha-thrombin. *Nucleic Acids Research* **22,** 2619–2626 (1994).
105. Hou, H. W. *et al.* Deformability based cell margination--a simple microfluidic design for malaria-infected erythrocyte separation. *Lab Chip* **10,** 2605–2613 (2010).
106. Li, N. *et al.* Technical and biological issues relevant to cell typing with aptamers. *J. Proteome Res.* **8,** 2438–2448 (2009).
107. Marti, M., Baum, J., Rug, M., Tilley, L. & Cowman, A. F. Signal-mediated export of proteins from the malaria parasite to the host erythrocyte. *J. Cell Biol.* **171,** 587–592 (2005).
108. Rug, M., Prescott, S. W., Fernandez, K. M., Cooke, B. M. & Cowman, A. F. The role of KAHRP domains in knob formation and cytoadherence of P falciparum-infected human erythrocytes. *Blood* **108,** 370–378 (2006).
109. Spillman, N. J., Beck, J. R. & Goldberg, D. E. Protein Export into Malaria Parasite-Infected Erythrocytes: Mechanisms and Functional Consequences. *Annual review of biochemistry* (2015). doi:10.1146/annurev-biochem-060614-034157
110. W Sherman, I., Eda, S. & Winograd, E. Cytoadherence and sequestration in Plasmodium falciparum: defining the ties that bind. *Microbes Infect* **5,** 897–909 (2003).
111. Kyes, S. A., Rowe, J. A., Kriek, N. & Newbold, C. I. Rifins: a second family of

clonally variant proteins expressed on the surface of red cells infected with Plasmodium falciparum. *Proc Natl Acad Sci USA* **96,** 9333–9338 (1999).
112. Cheng, Q. *et al.* stevor and rif are Plasmodium falciparum multicopy gene families which potentially encode variant antigens. *Mol Biochem Parasitol* **97,** 161–176 (1998).
113. Trenholme, K. R. *et al.* clag9: A cytoadherence gene in Plasmodium falciparum essential for binding of parasitized erythrocytes to CD36. *Proc Natl Acad Sci USA* **97,** 4029–4033 (2000).
114. Ockenhouse, C. F., Klotz, F. W., Tandon, N. N. & Jamieson, G. A. Sequestrin, a CD36 recognition protein on Plasmodium falciparum malaria-infected erythrocytes identified by anti-idiotype antibodies. *Proc Natl Acad Sci USA* **88,** 3175–3179 (1991).
115. Gardner, M. J. *et al.* Genome sequence of the human malaria parasite Plasmodium falciparum. *Nature* **419,** 498–511 (2002).
116. Aird, W. C., Mosnier, L. O. & Fairhurst, R. M. Plasmodium falciparum picks (on) EPCR. *Blood* (2014).
117. File:Maternal malaria placenta - cropped - very high mag.jpg - Wikimedia Commons. *commons.wikimedia.org* at <https://commons.wikimedia.org/wiki/File:Maternal_malaria_placenta_-_cropped_-_very_high_mag.jpg>
118. Berendt, A. R., Simmons, D. L., Tansey, J., Newbold, C. I. & Marsh, K. Intercellular adhesion molecule-1 is an endothelial cell adhesion receptor for Plasmodium falciparum. *Nature* **341,** 57–59 (1989).
119. Duffy, M. F. *et al.* VAR2CSA is the principal ligand for chondroitin sulfate A in two allogeneic isolates of Plasmodium falciparum. *Mol Biochem Parasitol* **148,** 117–124 (2006).
120. Li, A. *et al.* Molecular Mechanistic Insights into the Endothelial Receptor Mediated Cytoadherence of Plasmodium falciparum-Infected Erythrocytes. *PLoS ONE* **6,** e16929 (2011).
121. Mazo, I. B. *et al.* Hematopoietic Progenitor Cell Rolling in Bone Marrow Microvessels: Parallel Contributions by Endothelial Selectins and Vascular Cell Adhesion Molecule 1. *Journal of Experimental Medicine* **188,** 465–474 (1998).
122. Wu, Y. & Craig, A. Comparative proteomic analysis of metabolically labelled proteins from Plasmodium falciparum isolates with different adhesion properties. *Malar J* **5,** 67 (2006).
123. Scherf, A. *et al.* Antigenic variation in malaria: in situ switching, relaxed and mutually exclusive transcription of var genes during intra-erythrocytic development in Plasmodium falciparum. *EMBO J* **17,** 5418–5426 (1998).
124. Jiang, L. *et al.* PfSETvs methylation of histone H3K36 represses virulence genes in Plasmodium falciparum. *Nature* **499,** 223–227 (2013).
125. Dzikowski, R. & Deitsch, K. W. Genetics of antigenic variation in Plasmodium falciparum. *Curr Genet* **55,** 103–110 (2009).
126. Voss, T. S. *et al.* A var gene promoter controls allelic exclusion of virulence genes in Plasmodium falciparum malaria. *Nature* (2005). doi:10.1038/nature04407
127. Dzikowski, R., Frank, M. & Deitsch, K. Mutually Exclusive Expression of

Virulence Genes by Malaria Parasites Is Regulated Independently of Antigen Production. *PLoS Pathog* **2,** e22 (2006).
128. Amit-Avraham, I. *et al.* Antisense long noncoding RNAs regulate var gene activation in the malaria parasite Plasmodium falciparum. *Proceedings of the ...* (2015).
129. Horrocks, P., Pinches, R., Christodoulou, Z., Kyes, S. A. & Newbold, C. I. Variable var transition rates underlie antigenic variation in malaria. *Proc Natl Acad Sci USA* **101,** 11129–11134 (2004).
130. Dahlbäck, M., Nielsen, M. A. & Salanti, A. Can any lessons be learned from the ambiguous glycan binding of PfEMP1 domains? *Trends Parasitol* **26,** 230–235 (2010).
131. Janes, J. H. *et al.* Investigating the host binding signature on the Plasmodium falciparum PfEMP1 protein family. *PLoS Pathog* **7,** e1002032 (2011).
132. Smith, J. D. *et al.* Switches in expression of Plasmodium falciparum var genes correlate with changes in antigenic and cytoadherent phenotypes of infected erythrocytes. *Cell* **82,** 101–110 (1995).
133. Sargeant, T. J., Marti, M., Caler, E. & Carlton, J. M. Lineage-specific expansion of proteins exported to erythrocytes in malaria parasites. *Genome ...* (2006).
134. Hiller, N. L. *et al.* A host-targeting signal in virulence proteins reveals a secretome in malarial infection. *Science* **306,** 1934–1937 (2004).
135. Marti, M., Good, R. T., Rug, M., Knuepfer, E. & Cowman, A. F. Targeting malaria virulence and remodeling proteins to the host erythrocyte. *Science* **306,** 1930–1933 (2004).
136. Maier, A. G. *et al.* Exported proteins required for virulence and rigidity of Plasmodium falciparum-infected human erythrocytes. *Cell* **134,** 48–61 (2008).
137. Heiber, A. *et al.* Identification of new PNEPs indicates a substantial non-PEXEL exportome and underpins common features in Plasmodium falciparum protein export. *PLoS Pathog* **9,** e1003546 (2013).
138. Florens, L. *et al.* Proteomics approach reveals novel proteins on the surface of malaria-infected erythrocytes. *Mol Biochem Parasitol* **135,** 1–11 (2004).
139. Resende, M. *et al.* Identification of glycosaminoglycan binding regions in the Plasmodium falciparum encoded placental sequestration ligand, VAR2CSA. *Malar J* **7,** 104 (2008).
140. Singh, K., Gittis, A. G., Nguyen, P. & Gowda, D. C. Structure of the DBL3x domain of pregnancy-associated malaria protein VAR2CSA complexed with chondroitin sulfate A. *Nature structural & ...* (2008).
141. Resende, M. *et al.* Chondroitin sulphate A (CSA)-binding of single recombinant Duffy-binding-like domains is not restricted to Plasmodium falciparum Erythrocyte Membrane Protein 1 expressed by CSA-binding parasites. *Int J Parasitol* **39,** 1195–1204 (2009).
142. Magistrado, P. A. *et al.* High efficacy of anti DBL4ε-VAR2CSA antibodies in inhibition of CSA-binding Plasmodium falciparum-infected erythrocytes from pregnant women. *Vaccine* **29,** 437–443 (2011).
143. Barfod, A., Persson, T. & Lindh, J. In vitro selection of RNA aptamers against a conserved region of the Plasmodium falciparum erythrocyte membrane protein 1. *Parasitol Res* 1557–1566 (2009). doi:10.1007/s00436-009-1583-x

144. Salanti, A. *et al.* Evidence for the involvement of VAR2CSA in pregnancy-associated malaria. *J. Exp. Med.* **200,** 1197–1203 (2004).
145. Viebig, N. K. *et al.* A single member of the Plasmodium falciparum var multigene family determines cytoadhesion to the placental receptor chondroitin sulphate A. *EMBO Rep.* **6,** 775–781 (2005).
146. Reeder, J. C. *et al.* The adhesion of Plasmodium falciparum-infected erythrocytes to chondroitin sulfate A is mediated by P. falciparum erythrocyte membrane protein 1. *Proc Natl Acad Sci USA* **96,** 5198–5202 (1999).
147. Wan, Y. *et al.* Surface-immobilized aptamers for cancer cell isolation and microscopic cytology. *Cancer research* (2010).
148. Kitson, P. J., Rosnes, M. H., Sans, V., Dragone, V. & Cronin, L. Configurable 3D-Printed millifluidic and microfluidic 'lab on a chip' reactionware devices. *Lab Chip* **12,** 3267–3271 (2012).
149. Chia, H. N. & Wu, B. M. High-resolution direct 3D printed PLGA scaffolds: print and shrink. *Biofabrication* **7,** 015002 (2015).
150. Smalley, M. E., Abdalla, S. & Brown, J. The distribution of Plasmodium falciparum in the peripheral blood and bone marrow of Gambian children. *Transactions of the Royal Society of Tropical Medicine and Hygiene* **75,** 103–105 (1981).
151. Hanssen, E. *et al.* Soft X-ray microscopy analysis of cell volume and hemoglobin content in erythrocytes infected with asexual and sexual stages of Plasmodium falciparum. *J. Struct. Biol.* **177,** 224–232 (2012).
152. Viebig, N. K. *et al.* Disruption of var2csa gene impairs placental malaria associated adhesion phenotype. *PLoS ONE* **2,** e910 (2007).
153. Wang, A. Z. *et al.* Superparamagnetic Iron Oxide Nanoparticle-Aptamer Bioconjugates for Combined Prostate Cancer Imaging and Therapy. *ChemMedChem* **3,** 1311–1315 (2008).
154. Yigit, M. V., Mazumdar, D. & Lu, Y. MRI detection of thrombin with aptamer functionalized superparamagnetic iron oxide nanoparticles. *Bioconjugate Chemistry* **19,** 412–417 (2008).
155. Charlton, J. & Sennello, J. In vivo imaging of inflammation using an aptamer inhibitor of human neutrophil elastase. *Chem Biol* (1997).